Observing the impact of soils on local urban climate

DISSERTATION

ZUR ERLANGUNG DES DOKTORGRADES

DER NATURWISSENSCHAFTEN IM FACHBEREICH

GEOWISSENSCHAFTEN

DER UNIVERSITÄT HAMBURG

vorgelegt von

SARAH WIESNER

aus

KAISERSLAUTERN

HAMBURG

2013

Als Dissertation angenommen vom Fachbereich Geowissenschaften der Universität Hamburg

auf Grund der Gutachten von Prof. Dr. Annette Eschenbach
und Prof. Dr. Felix Ament

Hamburg, den 29. Mai 2013

Prof. Dr. Jürgen Oßenbrügge
(Leiter des Fachbereichs Geowissenschaften)

Contents

List of Tables

List of Figures

List of Abbreviations and Nomenclature

AWC	available water capacity
BSU	Behörde für Stadtentwicklung und Umwelt
DGD	deep groundwater district
EF	evaporative fraction
ET	evapotranspiration
H	sensible heat flux
HUSCO	Hamburg Urban Soil Climate Observatory
LCZ	local climate zone
LE	latent heat flux
RR	precipitation sum
SGD	shallow groundwater district
q	specific humidity
SWT	soil water tension
T_a	air temperature
topsoil	5 cm depth
UHI	urban heat island
upper layers	5 and 10 cm depth
VWC	volumetric water content
WRB	World Reference Base
Θ	normalized volumetric water content

Variables in italic font were calculated or used for calculation.

Abstract

The investigations in this study reveal that soils and shallow groundwater tables contribute to the formation of a specific local urban climate.

The climate in cities differs from that in surrounding areas, as the natural energy and moisture balances are influenced by the modified surfaces. Furthermore, urban soils are highly variable within small spatial scales and feature anthropogenic alterations. Whether this variability contributes to the formation of the distinct local urban climate at the micro scale was to be observed within this study. Focus lay on soil hydrology and groundwater table depth and their contribution to evapotranspiration. This issue was approached by designing and operating a measurement network which provided long-term data on urban pedological and meteorological parameters. It covered three distinct land use types: the suburban types "green space" and "housing area", located within two districts with different mean groundwater table depths and characteristic urban soil properties, and the inner city type “sealed surface”.

It is found for the years 2011 and 2012 that the temporal evolution of water content and soil water tension for the sites is very distinct, related to soil substrate, organic matter content and groundwater table depth. Impacts of different vegetation types on the soil water dynamics can be identified, while the influence of urban land use is not found to be definite. The effect of intensive precipitation events on soil water content and tension varies in temporal endurance, infiltration and percolation depth. Three types of seasonal topsoil moisture trends are identified, for which a close relation to soil characteristics is ascertained. On shorter timescales, during a three-week dry phase the upper 40 cm of soils at the suburban district with a deep groundwater table lose 35 % of the plant-available water capacity, while at the shallow groundwater table district this amount decreases by only 10 %. This signifies an impact of groundwater table depth on the water content of the upper soil layers during low precipitation periods.

The observed average nocturnal urban heat island is +1.7 K at the city core, +0.7 K at the deep groundwater table suburban housing area and +0.3 K at the nearby green

space. The effect is most prominent when wind speed is low and sky is only partly cloudy. In mean daytime air temperature for the inner city sites positive differences arise in the order of less than a fifth of the observed nighttime urban heat island effect. No evidence for a significant impact of topsoil moisture on the nighttime urban heat island is found. For the daytime span of air temperature 11 to 17 % of its variance is found to be explained by topsoil water content for selected relevant days.

The magnitude of turbulent latent heat fluxes above a suburban district with housing development shows major differences within the vegetation period. The phenological cycle is mirrored in the annual progression of the evaporative fraction. Near-surface flux measurements at a green space show a less defined amplitude and less scatter. Differences in the share of latent heat fluxes on the evaporative fraction can, to some part, be attributed to the surface characteristics and land use of source areas.

Zusammenfassung

Die Untersuchungen in dieser Arbeit zeigen, dass Böden und geringer Grundwasserflurabstand zur Ausformung eines spezifischen lokalen Stadtklimas beitragen.

Das Klima in Städten unterscheidet sich von dem in den umliegenden Gebieten, da die natürlichen Energie- und Feuchtebilanzen von den modifizierten Oberflächen beeinflusst werden. Darüber hinaus sind städtische Böden kleinräumig stark unterschiedlich und weisen anthropogene Überprägungen auf. Ob diese Variabilität zur Formierung des lokal unterschiedlichen Stadtklimas auf der Mikroskala beiträgt, war in dieser Arbeit zu untersuchen. Der Fokus lag auf der Bodenhydrologie und dem Grundwasserflurabstand sowie deren Beitrag zur Evapotranspiration. Diesem Thema wurde sich mittels der Konzipierung und des Betriebs eines Messnetzwerks angenähert, welches Langzeitmessungen zu städtischen bodenkundlichen und meteorologischen Parametern lieferte. Es umfasste drei verschieden Landnutzungstypen: die randstädtischen Typen „Grünfläche“ und „Wohngebiet“, gelegen innerhalb zweier Stadtteile mit unterschiedlichen Grundwasserflurabständen und stadtcharakteristischen Bodeneigenschaften, sowie den innerstädtischen Typ „versiegelte Oberfläche“.

Für die Jahre 2011 und 2012 wird festgestellt, dass der zeitliche Verlauf von Wassergehalt und Bodenwasserspannung für die Standorte sehr unterschiedlich ist, abhängig von Bodensubstrat, Gehalt an organischer Substanz und Grundwassertiefe. Einflüsse von verschiedenen Vegetationsarten auf den Verlauf des Bodenwasserhaushalts können beobachtet werden, während eine Beeinflussung durch städtische Landnutzung nicht deutlich wird. Der Effekt von Starkregenereignissen auf den Bodenwassergehalt und die Wasserspannung variiert in zeitlicher Dauer, Infiltration und Tiefe der Perkolation. Drei Arten von saisonalen Verläufen der Oberbodenfeuchte werden ermittelt, für welche ein enger Zusammenhang zu Bodencharakteristika festgestellt wird. Für einen kürzeren Zeitraum, während einer dreiwöchigen Trockenphase, betrachtet, verlieren die oberen 40 cm der Böden im Stadtteil mit einem tiefen Grundwasserstand 35 % der pflanzenverfügbaren Wasserkapazität, während dieser Anteil im Stadtteil mit einem

hohen Grundwasserstand nur um 10 % sinkt. Dies weist auf einen Einfluss von Grundwasserflurabstand auf den Wassergehalt der oberen Bodenbereiche während Phasen mit geringem Niederschlag hin.

Die beobachtete mittlere nächtliche städtische Überwärmung beträgt +1.7 K im Stadtkern, +0.7 K im Wohngebiet des Stadtteils mit tiefen Grundwasser und +0.3 K auf der nahegelegenen Grünfläche. Der Effekt ist am deutlichsten, wenn die Windgeschwindigkeit gering und der Himmel nur teilweise bewölkt ist. An den innerstädtischen Standorten treten positive Abweichungen der mittleren Tagestemperatur in Höhe von weniger als einem Fünftel des beobachteten nächtlichen Wärmeinseleffekts auf. Es findet sich kein Hinweis auf einen signifikanten Einfluss von Oberbodenfeuchte auf die nächtliche Wärmeinsel. Für die Spannweite der Lufttemperatur während des Tages wird eine Erklärbarkeit ihrer Varianz durch den Oberbodenwassergehalt von 11 bis 17 % für ausgewählte relevante Tage gefunden.

Die Größenordnung der turbulenten latenten Wärmeflüsse über einem randstädtischen Gebiet mit Wohnbebauung zeigt innerhalb der Vegetationsperiode wesentliche Unterschiede. Der phänologische Zyklus der Vegetation spiegelt sich im Jahresverlauf der Evaporative Fraction (Verdunstungsanteil) wieder. Bodennahe Flussmessungen auf einer Grünfläche zeigen eine weniger deutlich ausgeprägte Amplitude und weniger Streuung. Unterschiede im Anteil der latenten Wärmeflüsse an der Evaporative Fraction können teilweise den Oberflächencharakteristika und der Landnutzung der Ursprungsgebiete zugeschrieben werden.

1 Introduction

The heterogeneous surface of urban areas is able to influence and modify the local atmospheric conditions by enhancing or attenuating the greater atmospheric forcing. On the relevance of urban land use for atmospheric properties, profound knowledge has been gained in the past decades (see e.g. Arnfield, 2003). Modifications of the natural surface lead to transformation of the radiative, thermal and moisture characteristics of the surface itself and the overlying atmospheric boundary layer at the micro and meso scale (e.g. Delleur, 2003; Grimmond and Oke, 1986). As a consequence, the natural energy and moisture balances are influenced, leading to the formation of a distinct urban climate, its intensity depending on the severity of the human impacts (Morris et al., 2001). One of the best-known effects in this context is the urban heat island (UHI) effect, the nocturnal urban-rural temperature difference as described by Oke (1982). In addition to research on the impact of urban surfaces, the number of studies focusing on urban vegetation increased in the last years, dealing with the air temperature-reducing effects of urban parks and unsealed vegetated areas on nearby surroundings and on human comfort (e.g. Jansson et al., 2007; Lee et al., 2009), or their impact depending on the large-scale climate (e.g. Spronken-Smith and Oke, 1998).

In addition to vegetation transpiration effects, water transmission by soil and exchange with the atmosphere through evaporation are important influencing and modifying factors for the local climate in natural environments (Brubaker and Entekhabi, 1996; Seneviratne and Stöckli, 2008). In simulations, the soil surface-atmosphere interactions in terms of evapotranspiration were found to significantly influence ambient air temperature (e.g. Jaeger and Seneviratne, 2011). Thus, they can be of importance within an urban environment as well, as they presumably contribute to a locally reduced warming of air temperature. In contrast to natural undisturbed or agriculturally used soils of rural areas, urban soils are highly variable within small spatial scales, featuring anthropogenic land use typical characteristics, e.g. different bulk densities due to soil compaction, varying contents of organic matter or coarse

material in soils such as large gravel, or the occurrence of construction waste (Pickett et al., 2001).

However, these features are important controlling factors for soil functions (Burghardt, 1994) and, in combination with groundwater managing and surface water discharge, for soil water dynamics. Model calculations show that even slight differences in soil characteristics like fraction of clay or field capacity result in local changes of the near-surface meteorological parameters (e.g. Anders and Rockel, 2009). It was shown in simulations that groundwater acts as a source for soil water in near-surface layers when the water depth lies within a critical zone. Furthermore, surface energy flux partitioning, latent heat fluxes respectively, are dependent on groundwater table depth as well (Maxwell and Kollet, 2008). However, neither the climate impact of soil specific properties, influencing water dynamics, nor groundwater level and capillary rise versus percolation has been in the focus of research for urban areas, yet.

In this study, the impact of soils and their properties on the local urban climate is observed. The prior aim is to gain deeper knowledge on the processes and influencing factors of the interactions between pedosphere and atmosphere in the urban environment at the micro scale. For this purpose the relevance of soil hydrology on local urban climate is to be estimated. The effectiveness of soil as a storage and transmitter for water is mainly depending on soil properties, local groundwater table, land use and, as transpiration has a substantial share on this effect, vegetation cover. Thus, the local air temperature-reducing benefit of soils through evapotranspiration is certainly affected by its ratio of sealing on the one hand, and the water availability at the surface on the other hand. To find out to which extend these two parameters limit the local climate effectiveness of soils within the urban environment, measurement data derived from the project HUSCO (Hamburg Urban Soil Climate Observatory) is used. The present knowledge on the relevance of soils for the local urban climate is described in Chapter 2, followed by an introduction into the concept of the project HUSCO in this context. A detailed description of the measurement network itself and the methods applied are provided in Chapter 3.

The targets of the study are approached in particular by, first, quantifying the heterogeneity of water dynamics in urban soils and the range of their hydrological characteristics as a function of soil properties, groundwater table depth and urban land use in Chapter 4. Particular attention will be paid to the following questions:

- How variable are soil moisture contents and water tension at the studied urban sites?
- What role do soil properties and urban land use play in controlling soil water dynamics?
- To which extent does the groundwater table depth have an impact on soil moisture of the upper layers?

Second, the spatial variability of urban local air temperature and humidity in the city of Hamburg will be analyzed in Chapter 5. A quantification of the UHI in suburban areas and the identification of the impact of topsoil moisture is aimed at and discussed in this chapter. However, the closest relation between soil moisture and air temperature is due to evapotranspiration, which is mainly active during daytime. Thus, specific questions to be answered are:

- How variable are the meteorological parameters in Hamburg in spatial terms, as observed with the measurement network?
- How pronounced is the nocturnal urban heat island effect observed within the network? Which conditions have an impact on its intensity? Which spatial peculiarities can be made out?
- Do significant daytime temperature differences occur? If yes, which circumstances lead to their occurrence and which impacting factors on their intensity can be identified?
- Is soil moisture a significant impacting factor for local air temperature?

This analysis allows an assessment of the relevance of the various influencing factors, like e.g. soil moisture and surface sealing, on the daytime temperature evolution and air temperature anomalies in urban areas.

These two separately considered urban characteristics, namely soil hydrology and local air temperature, are linked via turbulent heat fluxes. These fluxes are controlled by the availability of soil water and their divergence affects the change in air temperature. Chapter 6 provides a preliminary analysis of the fluxes, as measured by two eddy covariance systems, calculating turbulent fluxes of sensible heat (i.e. change of air temperature) and latent heat (i.e. evapotranspiration). A question that will be discussed on the results of this data evaluation is:

- Which trends of latent and sensible heat fluxes can be observed at the annual and the diurnal scale and by which parameters are they presumably induced?

In Chapter 7 a synthesis of the results provides possible answers to the question:

- To which extend do soil parameters and groundwater table depth have an impact on urban local climate?

The discussion of this issue and concluding remarks are provided, followed by an outlook to further research aims and focuses in Chapter 8.

2 Soils in the urban climate system

2.1 Present research on soil-atmosphere interactions

The heterogeneous urban land use leads to distinct characteristics of the local meteorological parameters near the surface. Well known effects which are prominent within the research field of urban climatology (Arnfield, 2003), are the nocturnal urban heat island effect (Oke, 1973) and the specific urban atmospheric turbulence within the urban canopy layer and the urban roughness layer, affecting the exchanges of energy and water (a review can be found in Roth, 2000). These urban climatic effects result from processes at different spatial scales, from microclimatic scale within a few centimeters to meso scale. Local site-specific characteristics and elements (e.g. trees, buildings, and roads) control airflow and energy exchange at the micro scale and thereby build their own microclimate. Greater structures and patterns, like parks or districts, result in effects at more extensive local scales. In combination, these characteristics contribute to the formation of a meso scale climate, forming the boundary layer of a whole city.

Within this interaction of parameters and processes, the single elements can either intensify or attenuate the greater atmospheric conditions. Man-made buildings and surfaces (asphalt, concrete, brick) are known to mainly lead to an increase of air temperature during nighttime, owing to their high thermal capacity (e.g. Henry and Dicks, 1987). In contrast, open vegetated spaces in urban areas, first and foremost green spaces, contribute to a local reduction of air temperature. They do so by increasing the evaporative fraction[1] (*EF*), i.e. the percentage of latent heat flux on the total heat flux including sensible heat, due to higher water availability at the surface and the transpiration of plants (e.g. Givoni, 1991). The inherent cooling effect of urban green spaces and water bodies, mainly through evapotranspiration (ET), has been identified in field studies, indicating a positive effect not only within the structure itself but also for

[1] The term „evaporative fraction“ includes both components of the evapotranspiration, the evaporation as well as the transpiration. Yet, in literature the notation „evaporative“ instead of the more complicated “evapotranspirative” is common and thereby this convention is used in this study as well.

adjacent built-up areas (e.g. Lee et al., 2009; Upmanis et al., 1998). A high percentage of green space measured by the total urban area also reduces the general UHI significantly (Kuttler, 2011).

Grimmond and Oke (1999) highlight the importance of knowledge on ET in cities for several urban microclimatological and hydrological issues, illustrating the clear differences in its intensity according to land use - mainly between downtown, light industrial and residential areas - and land cover, i.e. fractions of the surface vegetated. In accordance, Arnfield (2003) also emphasizes, that studies on the water budgets in urban areas of different types are needed because they will clarify the role of ET, in particular its interaction with surface water availability and micro scale advection.

Alongside with urban parks, also vegetated backyards, lawns and certainly open water bodies contribute to an increased evaporation and ET, respectively. These urban structures can therefore be assumed to also attenuate local air temperature. At a superior level, the patchy structure of residential areas, including open vegetated and unsealed areas, leads to a less pronounced heat island effect during night time (e.g. Voogt, 2003) as well, due to a higher percentage of area contributing to an increased ET. Moreover, according to a study of Grimmond and Oke (1999) in residential areas ET constitutes an energy sink of 22-37 % of the daytime, and 28-46 % of the daily (24h) net all-wave radiation, while in downtown and light industrial areas this flux is much less important. The study of Balogun et al. (2009), dealing with the surface energy balance of residential areas at the exurban fringe of Kansas City, USA, showed that newly developed areas feature a latent heat flux more similar to rural areas than to city core structures. For Melbourne, Australia, Coutts et al. (2007) found an impact of increasing housing density on the energy balance, evaporative fraction respectively, and especially greater nocturnal differences. An oasis effect of residential areas in Tokyo, Japan, was shown by Moriwaki and Kanda (2004) in terms of an increased latent heat flux during summer months. However, the intensity of energy fluxes over areas with similar land use can vary significantly: Over “homogeneous” suburban residential areas Schmid et al. (1991) found a variability of energy fluxes by up to 25-40 % within scales of 100 to 1000 m. They ascribe this range of different surface energy balances at large scales to

micro advective interactions between surface types at small scales, e.g. increased ET from irrigated suburban lawns.

While the general cooling effect[2], of green spaces and vegetated areas within the urban environment is well researched, specific knowledge on the relevance of soils and soil properties within this system is rare. This is despite soils, in their function as a storage and transmitter for water, contribute to evaporation by providing water at the surface as well as to vegetation transpiration by supplying the roots of plants.

The intensity of mere evaporation from the soil surface is controlled by factors within the atmosphere on the one hand, and soil specific properties on the other hand: As e.g. Lemon (1956) and Idso et al. (1974) described in their studies on the stages of evaporation, in the case of unlimited water supply within the very near-surface soil the atmospheric conditions control the evaporation rate. These conditions are mainly vapor pressure of the air near the surface, as well as wind velocity. But this situation, often referred to as stage I after a precipitation event, is transient in most cases and followed by stage II and III. In these situations, soil properties increasingly control the rate of evaporation, while the atmospheric conditions' impact remains valid. Additionally, plant transpiration also depends to a major part on soil water availability (Daly and Porporato, 2005). One main determining soil specific factor regarding the evaporation rate from the soil surface is the ratio of its sealing. Like Pearlmutter et al. (2009) showed in the open-air scaled urban surface (OASUS) model experiment, the daily total latent heat flux increases consistently with increasing vegetated and unsealed fractions of the surface. Studies on the impact on surface sealing ratios on ET (e.g. Wessolek and Facklam, 1997) also point out, that ET rates are reduced with an increase in the ratio of sealing. Thus, soils influence the local climate in urban areas as well by means of higher latent and lower sensible heat fluxes, their intensities depending to some extend on the ratio of unsealed soil surface.

[2] As evapotranspiration is an energy intensive process, it leads to an air temperature reduction by diminishing the energy amount transformed into sensible heat. In the following this relation is designated as a "cooling effect" of areas, soils or surfaces.

As a second soil specific factor influencing the water dynamics and thereby the water supply at the soil surface through capillary rise is certainly the distribution of pores, determined by soil texture, bulk density and organic matter content (Burghardt, 1994). Previous research on the effect of natural soil heterogeneities on the ET rates indicated that the observed variability of soil moisture resulting from these heterogeneities seriously influences the regional ET (Wetzel and Chang, 1987).

A third factor conditioning the intensity of the climate relevance of soils is the water availability, the soil water content of the topsoil respectively, determined by soil physical properties (e.g. Kondo et al., 1990). It is given either through stored precipitation in the topsoil (Krakauer et al., 2010) or provided by capillary rise of groundwater (as described by e.g. Nachabe et al., 2005). For agricultural rural areas, groundwater capillary rise and evapotranspiration from soil surface has been investigated in field work at a local and regional scale (e.g. Logsdon et al., 2009; Yeh and Famiglietti, 2009). In models it was shown that groundwater acts as a source for soil water near the surface when the water depth lies within a critical zone (Maxwell and Kollet, 2008), i.e. the zone where water table depth variations have a strong impact on surface ET. The location of this zone is depending mainly on the soil texture: For loam and loamy sand soil textures Maxwell and Kollet (2008) simulated a critical zone of about 2 m below surface. Soylu et al. (2011) distinguished the depth of critical zones and the sensitivity of modeled ET to water table depth by soil textures, using soil hydraulic parameter values from two different sources: Their results indicated a strong influence of soil texture as well as of water table depth on the groundwater contributions to ET. For both soil parameter datasets the thickest and deepest critical zone was found for silt loam, the shallowest for clay and silty clay loam, with a range from 0.5 m to 3.5 m for one dataset, and 3 to 15 m for the second one.

These field measurements and model simulations indicate that groundwater may supply water for surface water flux and ET in natural environments. A spatial variability in groundwater table depth can therefore additionally create spatial differences in soil moisture and thus in surface water fluxes as well (e.g. Chen and Hu, 2004). This in turn

allows the assumption that groundwater table depth and spatial variability of it lead to distinct contributions to ET from the soil surface in urban areas as well.

To sum up, water availability is an import factor controlling the rate of ET and thereby directly influencing the air temperature increase. This also applies in particular to urban areas, entirely unsealed urban parks as well as gardens and backyards within partly sealed residential areas. Thereby water availability signifies the potential for surface evaporation as well as the water supply for plant transpiration. Model surveys on the importance of topsoil moisture have verified the necessity of adequate water supply to ensure cooling effectiveness of soils in urban parks (e.g. Goldbach and Kuttler, 2013). In the special case of urban vegetated areas, water availability, soil water content respectively, can also be influenced by irrigation (Givoni, 1991).

The relevance of the research on soil impact on local urban climate is manifold: As many studies show, intra-urban air temperature variations due to heterogeneous urban land use influence the health and comfort of the inhabitants, as well as the energy consumption and air quality (e.g. Eliasson and Svensson, 2003). In particular, the lower air temperature within green spaces and vegetated areas is perceived as more comfortable during hot summer periods, especially at night, in comparison to densely built-up inner city structures or suburbs with a high sealing ratio (e.g. Mayer and Hoppe, 1987; Spronken-Smith and Oke, 1998). These different effects of urban-land use in general, and of open vegetated areas in particular, are certainly relevant for application in urban planning. The integration of climate within town planning has been an issue of concern for decades (e.g. Givoni, 1991; Oke, 1984), and different kinds of greenery are prominent to be relevant due to their general cooling function (Matzarakis et al., 1999) and therefore are regarded in recent town planning. However, the special relevance of soil properties, water availability within the topsoil, and in particular groundwater table depth - as it is often lowered in urban areas by water management - contributing to this climatic effect of unsealed urban soils, has not been under research, yet. Furthermore, results increasing the knowledge on the importance of urban soils for the local climate can contribute to decision-making regarding urban soil protection (e.g. Oechtering and Däumling, 2012).

2.2 The HUSCO approach

The data used in this study was collected by the measurement network of the research project “Hamburg Urban Soil Climate Observatory” (HUSCO). This project aims at the experimental quantification of the heterogeneity of the urban climate depending on the impact of soils. It investigates the exchange processes of water and energy from urban soils to the near-surface atmosphere and vice versa. The effects on urban micro and meso climate resulting from these climate controlling processes are to be detected. Thereby, different urban structural units are considered, with regard to local soil properties, groundwater table depth and land use characteristics. In addition to the detection of the local scale processes, the greater meteorological conditions and the cumulative effect of the city structure itself are taken into account.

HUSCO thereby examines some up to now barely considered aspects within the urban climate research landscape:

- the impact of soils under different urban land use on the local climate,
- the observation of different groundwater table depths in urban areas and their impact on topsoil water content and availability,
- the fluxes of latent and sensible heat over different urban areas, residential and green space, observed in long-term measurements.

Hence, HUSCO aligns into a row of other measurement networks which focus on adjacent research questions. The spatial variability of soil moisture and evapotranspiration is observed mainly in studies on agricultural and rural areas: The surface soil moisture mapping project SGP97 and follow ups (Famiglietti et al., 1999) found consistencies in differences in mean moisture content and variations in soil type, vegetation cover, and rainfall gradient. A wireless soil moisture network in Eastern Washington within the ARS Long-Term Agro-Ecosystem Research Program (Robinson et al., 2008) addresses the spatial variability of soil hydrology. Seasonal to interannual variations of soil moisture at 60 stations across Oklahoma State, USA, are measured within the meteorological observing network Oklahoma MesoNet (Illston et al., 2004). The Environment and Climate Observing Network ECONet provides information about

soil physical parameters and soil moisture at two sites in North Carolina, USA, since 1999 (Pan et al., 2012). Analysis of the highly variable soil water content progress at the sites indicated that information on few specific soil properties could provide an understanding of differences at the sites. The large-field experiment REMEDHUS in Spain analyzed the temporal stability of soil moisture for a period of 36 months (Martinez-Fernandez and Ceballos, 2003). Results of forty-five years of soil water content measurements within the upper 1 m of 141 stations in the Ukraine are presented by Robock et al. (2005). To collect the pedohydrological data of numerous networks and single stations worldwide, a data hosting facility for world wide in situ soil moisture measurements was build up by the Vienna University of Technology (Dorigo et al., 2011), named “International Soil Moisture Network” (ISMN).

The combination of soil measurements in meteorological networks is realized in projects like COPS in Southwest Germany (Krauss et al., 2010), showing that soil texture controls the vertical soil moisture gradient relative to the near surface soil moisture, and TRANSREGIO’s SoilNet in Western Germany (Bogena et al., 2009), investigating the spatial variability of soil moisture at different depths with a wireless soil moisture sensor network. Within the network of Terrestrial Environmental Observatories (TERENO) in Germany, also the soil-vegetation and atmosphere feedbacks are monitored at multiple temporal and spatial scales (Zacharias et al., 2011).

To observe the variability of atmospheric parameters within urban areas, numerous meteorological networks exist throughout the world, located within diverse types and sizes of cities, from small towns to megacities. The main focuses of these observations, however, differ at the spatial and temporal scale as well as in the considered parameters itself. The results obtained from urban meteorological networks operated in the temperate latitudes can be a valuable supplementation of the HUSCO network measurements: The Oklahoma City Micronet operates 40 stations, spanning a land use gradient from rural to urban with high spatial temporal density (Basara et al., 2011). Basel’s urban boundary layer project BUBBLE, investigates the boundary layer structure in the City of Basel, Switzerland, over different surface types, including turbulence measurements (Rotach et al., 2005). Flux and turbulence measurements have

been realized e.g. within the project ESCOMPTE at a densely built-up site in Marseille, France, for a limited time during summer (Grimmond et al., 2004), as well as at four urban locations Łódz, Poland for a single summer month (Offerle et al., 2006a) and a single month for a two year period (Offerle et al., 2006b). A detailed overview on the progress in measuring and observing the urban atmosphere can be found in Arnfield (2003) and Grimmond (2006) .

The measurement network HUSCO aims at contributing to this so far gained knowledge, broadening the insights on soil-atmosphere interactions in the urban environment according to land use and soil hydrological properties. This issue is addressed by running an urban meteorological and pedological measurement network. It provides high-temporal-resolution data on water and energy budgets of diverse soils under different urban land use and with contrasting groundwater levels as well as on meteorological conditions of corresponding urban sites.

The research sites of the project are located in the city of Hamburg, Germany. This city is located in northern Germany (53° 33′ N, 10° 0′ E), situated on the river Elbe 110 km southeast of the North Sea coast. With 1.8 million inhabitants it is the second largest German city, covering an area of 755 km^2. The climate is dominated by marine meteorological effects, characterized by a moderate air temperature amplitude, mild winters and moderately warm summers, and high wind speeds (von Storch and Claussen, 2010). One main point that can be examined in Hamburg especially well is the impact of groundwater table depth on the soil-atmosphere interaction: Hamburg's location in the North German Plain and its average altitude of 6 m above sea level allow very shallow groundwater tables, mainly within the marshlands near the river Elbe, but also in areas with peat supplied by tributary rivers. Besides also areas with a deeper groundwater table, dominant in geest areas from Pleistocene moraines and sandurs, constitute considerable percentage of the city area.

Additionally, the city area features many different urban structures (e.g. Bechtel and Daneke, 2012), ranging from densely built-up inner city modern core to extensive green space areas and water bodies. Human settlements and transport infrastructure account for 60 % of the total area, 25 % are under agricultural use, while the remaining 15 % are

near-natural areas, e.g. forests, water bodies. Residential areas, as part of the settlement, constitute 21.3 % (data valid for 2010, Statistisches Amt für Hamburg und Schleswig-Holstein, 2011). A diverse composition of buildings, regarding height, density, arrangement, as well as material of façades can be found at the different housing districts (Lafrenz, 2001). Furthermore, Hamburg is known as the “green city” as 7.1 % of its area are green spaces and recreation areas (Statistisches Amt für Hamburg und Schleswig-Holstein, 2011). These diverse structures qualify Hamburg accessorily for the observation of urban land use impacts on the spatial variability of local climate. A typology of the urban surfaces in Hamburg, following the Local Climate Zone (LCZ) classification scheme, a system of thermally homogenous urban structures introduced by Stewart and Oke (2012), can be found in Bechtel and Daneke (2012). This LCZ classification indicates, that outside of the dense inner city areas (“modern core” and “old core” class), wide spaces are covered with a morphology matching the “regular housing” LCZ class, with many inclusions of “park” and “garden” class areas. This characteristic structure lead to the selection of the HUSCO measurement sites, as it is described in Chapter 3.1.

3 Measurement Sites, Material and Methods

3.1 Concept of the measurement network and site description

With the start-up of the project HUSCO, the measurement network concept and design had to be developed. Regarding the aims of the project, the following questions had to be covered with the setup to best effect:

- Which qualitative and quantitative impact does the soil hydrology have on local climate, with regard to urban land use?
- Which effect do distinct soil properties have?
- Does the groundwater table depth of a district have local climate relevance? And if so, to which extent?

To tackle these issues, a combination of meteorological and pedological measurement stations was chosen: For the detection of the local climate effects, particularly the heterogeneity of temperature and humidity in urban areas, meteorological stations, called “MeteoStations”, were planned to be set up to analyze the core atmospheric parameters. To record the processes and seasonal variations of the soil water balance and soil thermal properties, so-called “SoilStations”, equipped with pedological sensors in different depths, were conceived. Complementing these measurements, eddy covariance systems were planned to quantify the climate-controlling processes, like turbulent fluxes of energy and water. An integration of existing meteorological measurement stations was planned to supply information on the greater climatic conditions, on the atmospheric conditions outside of Hamburg, as well as on parameters that could not be covered, e.g. wind speeds at greater heights and cloud coverage.

These three types of measurement stations provided the framework conditions to develop a network setup concept that covered as many of the mentioned topics as possible. The approach selected was intended to cover several issues by combining specific characteristics of the urban areas and Hamburg, respectively, at the sites instead

of setting up different station for each topic. Thus, the location of the HUSCO sites and measurement stations was selected based on the following criteria. First, the types of urban development, i.e. local land use, surface cover, size and spacing of buildings and vegetation stock, that would be considered, were chosen. After the evaluation of land use data provided by the Behörde für Stadtentwicklung und Umwelt (BSU) concerning building densities, surface coverage and sealing ratios, three types of urban development were chosen to be monitored. They can be classified into the categories “inner city sealed surface” (modern core / old core according to Bechtel and Daneke, 2012), “single housing development” (regular housing) and “urban green space” (field). These categories have large shares on the city area and therefore can be considered as three distinct typical urban land use types for Hamburg. By choosing sites within the inner city featuring an entirely sealed surface, the situation of virtually no soil-atmosphere interaction was given with a sealing ratio of more than 90 % in average in this area. Entirely to the contrary the category of urban green spaces practically features no surface sealing (less than 5 % at average), allowing an undisturbed exchange between soil and overlying atmosphere and an entirely vegetation coverage. The single housing development areas constitute an intermediate category with an average sealed surface of about 50 %, one to two-storey buildings and patchy vegetation, especially within the backyards. With these three categories a broad range of surface sealing ratios and urban development types typical for Hamburg is covered.

For the locations of the categories “housing” and “green space”, two suburban districts were selected according to their mean overall groundwater level, derived from geological information (Appendix Figure A.1) provided by Behörde für Stadtentwicklung und Umwelt (2010a). To ensure comparability of the groundwater impact observations the main criteria for the districts was their resemblance in structure, i.e. size and vegetation of the green space and characteristics of the housing area. These districts thus had to be similar in the proportions of the two land use types, but one district needed to feature a shallow (< 2.5 m below surface), the other one a deep mean groundwater table depth (> 5 m below surface). A detailed analysis of the urban land use classes in Hamburg and the mean groundwater table depth, evaluating data with a

geographical information system (GIS), led to a selection of seven possible districts. On-site visits ultimately verified the best suitable districts. The concept that evolved from this selection progress provides for six different measurement locations within three districts. The nomenclature of the station includes information on their urban land use type and regional groundwater mean water table depth: C stands for inner city, SGD stands for shallow mean groundwater district, DGD for deep mean groundwater district. The suffixes indicate the location within the districts: G stands for stations within green spaces, H for stations within housing areas .The district with a shallow mean groundwater table per definition (SGD) is Hamburg-Langenhorn, the one with a deep mean groundwater table (DGD) Hamburg-Stellingen. The inner city sites (C) are located at Hamburg-Neustadt and Hamburg-HafenCity (Figure 3.1).

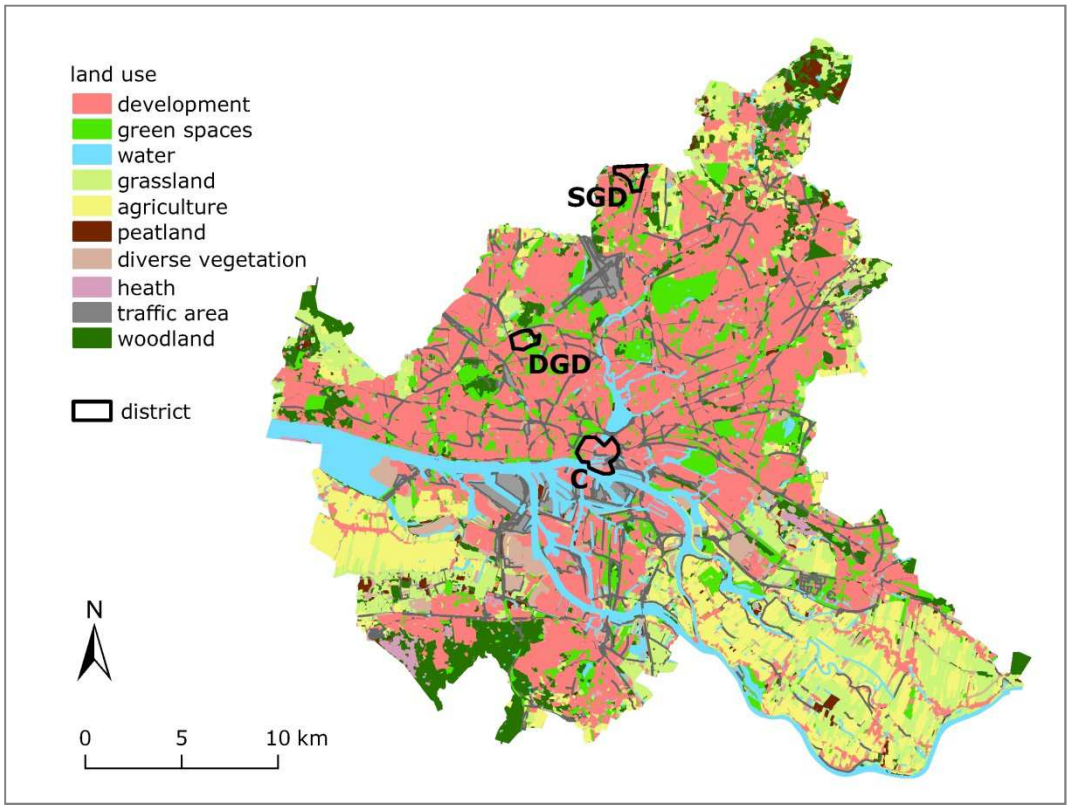

Figure 3.1 Urban land use in Hamburg (Freie und Hansestadt Hamburg, 2010c) and location of observed districts. SGD = shallow groundwater table district, DGD = deep groundwater table district, C = inner city.

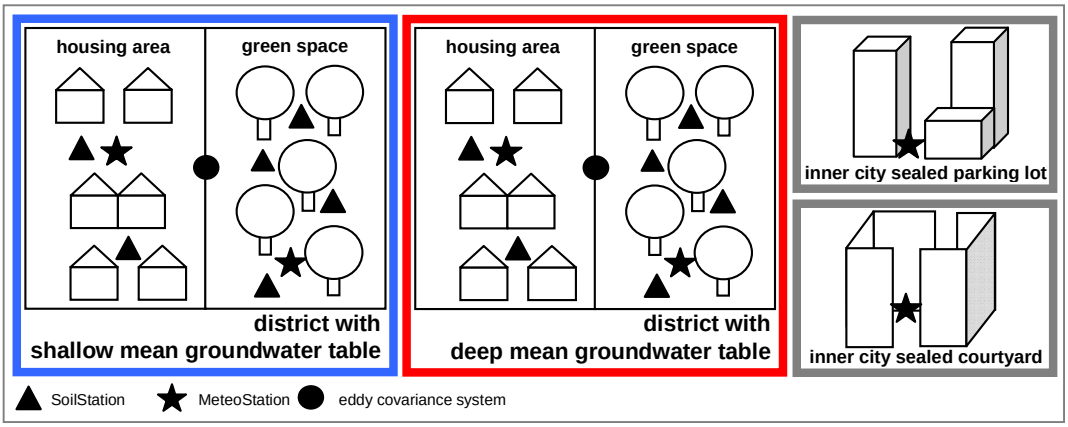

Figure 3.2 Concept of the HUSCO measurement network setup within three categories of urban land use and two districts with distinct mean groundwater table depth.

Based on this concept of the measurement network setup, the exact site locations of the MeteoStations, SoilStations and eddy covariance systems within these districts were chosen (Figure 3.2). The MeteoStations' location had to be representative for the surrounding area. In addition they had to fulfill as many of the criteria as possible for obtaining representative meteorological observations at urban sites, listed by Oke (2004), e.g. the location at the site and measurement height of the sensors. Each suburban area thus owns one MeteoStation within a green space area and a second one in the backyard of a single family house, the sites resembling in spatial structure and vegetation, as well as being representative for distinct degrees of surface sealing (5 % at green space sites, 50 % at housing developments). The inner city stations were chosen within business districts featuring a mean surface sealing ratio of 90 %. In addition to the scientific requirements that had to be fulfilled, several administrative, logistic and applicatory circumstances had to be regarded while choosing the final setup location, e.g. approval of the land owners, energy supply, accessibility and security from vandalism. The selected MeteoStation locations for each land use type resemble well in their site specific properties as surface and vegetation, surrounding and degree of surface sealing (Table 3.1). The deployment location of the MeteoStations is illustrated in Appendix Figure A.2 including information on the surface sealing ratios of Hamburg. The MeteoStation C_1 was mounted in June 2010, the stations in SGD and DGD in September 2010. MeteoStation C_2 was put into operation in August 2011.

Table 3.1 MeteoStations within HUSCO: nomenclature, and site specific properties.

district	site	land use	surface / vegetation	surrounding	degree of surface sealing at district[3]	local climate zone[4]
inner city	**C_1**	sealed surface (courtyard)	asphalt concrete	buildings (7 to 9 storeys)	90 %	old core / compact midrise
	C_2	sealed surface (parking lot)	asphalt concrete	buildings (> 5 storeys)	90 %	modern core / compact midrise
shallow mean groundwater	**SGD_G**	urban green space	high pasture grass	adjacent wood with deciduous trees	5 %	field / low plants
	SGD_H	single housing development	lawn	single family house, row of bushes, compost pile, adjacent wood with deciduous trees	50 %	regular housing / open low rise
deep mean groundwater	**DGD_G**	urban green space	high pasture grass	adjacent row of single trees (> 10 m)	5 %	field / low plants
	DGD_H	single housing development	lawn	single family houses, single deciduous trees, row of bushes, small garden shed	50 %	regular housing / open low rise

For the location of the SoilStations additional criteria had to be considered. As the pedosphere intrinsically is a heterogeneous sphere, the representativeness of the measurements had to be increased by a greater number of measurement stations. At each district six sites were selected according to urban land use characteristics and regarding their prevailing soil texture: Four sites at the green spaces, vegetated with high pasture grass, short grass or deciduous trees, and two sites within the backyards of single-family houses. This increased quantity of pedological stations allows retrieving information about the small scale variability of the soil water balance within the areas. To ensure representativeness of the SoilStations' profiles, prior to the final selection of their location a consideration to geological and pedological information provided by BSU was given. Additionally, a field investigation including a pedological mapping of

[3] The degree was estimated according to maps provided by Freie und Hansestadt Hamburg (2008).
[4] according to Stewart and Oke (2009) / Stewart and Oke (2012), compared with results from Bechtel and Daneke (2012).

the green spaces at selected points along transects was carried out (Appendix Figure A.3 and Figure A.4). For the exact choice of the SoilStations' location, additional restrictions applied, given by the need to consider piping lines, the results from the investigations of bomb disposal teams, as well as the necessity for protection against vandalism. A complete pedological description, i.e. data recorded at time of installation, is provided in Appendix B. The nomenclature of the SoilStations includes, in analogy to the MeteoStations, information on their regional mean groundwater table depth and urban land use type: SGD and DGD name the mean groundwater table, the suffixes G1-4 stand for profiles at green spaces, H1 and H2 for profiles within housing areas. The installation of the SoilStations was performed in November 2010 (G1, G2 and H1) and March 2011 (G3, G4 and H2).

The SoilStation sites are characterized as follows (Table 3.2): At the deep groundwater district DGD the prevailing soil textures are loamy sand and sand, in northern areas also peat covered with sand. At all stations, construction waste is present to different degrees. Two green space stations of DGD are located beneath the canopy of trees, the two other stations on open grassland. Within the housing areas the soil surface is vegetated with short grass. At the shallow groundwater district SGD more sandy substrates appear within the housing areas. The green spaces are dominated by peat, often covered with a sand layer which was presumably added anthropogenically. One green space SoilStation is located within a stock of trees, as the other stations are covered with high pasture grass and short grass respectively. Within the housing area short grass vegetation is present. High organic matter contents within the upper 40 cm of soil were found at two green space sites, concurrently with high groundwater table (< 0.4 m) as detected during field work. The two other green space stations feature a groundwater table depth of 0.9 and 1.2 m, respectively. For additional information on the location of the SoilStations at the two districts, including information on the prevailing soil textures, as given by information provided by BSU, see Appendix Figure A.5 and Figure A.6.

Table 3.2 SoilStations within HUSCO: nomenclature, and site specific properties. Approximate groundwater table depth as detected during field work in November 2010 and March 2011 (water surface / influx of water).

district and land use		profile	approx. water table depth	dominant soil texture	WRB soil group[5]	organic matter content (5 cm depth)	type of vegetation / observed rooting depth	construction waste[6] (depth)
shallow mean groundwater table	**green space**	**SGD_G1**	0.4 m	peat / loamy sand	Histic Gleysol	30 %	high pasture grass / > 40 cm	no
		SGD_G2	0.4 m	peat / loamy sand	Eutric Histosol	17 %	no grass, deciduous trees / > 40 cm	no
		SGD_G3	1.2 m	sand	Gleyic Regosol	6 %	short grass / > 155 cm	no
		SGD_G4	0.9 m	loamy sand	Gleyic Regosol	8 %	high pasture grass / 30 cm	no
	housing area	**SGD_H1**	> 1.6 m	sand	Terric Anthrosol	10 %	short grass / > 155 cm	yes (0.5m)
		SGD_H2	> 1.6 m	loamy sand	Terric Anthrosol	8 %	short grass / 155 cm	no
deep mean groundwater table	**green space**	**DGD_G1**	1.6 m	sandy loam	Stagni-Gleyic Cambisol	12 %	high pasture grass / 95 cm	yes (0.3m)
		DGD_G2	> 1.6 m	loamy sand	Terric Anthrosol	7 %	row of deciduous trees, ground-cover plants / > 110 cm	yes (1.1m)
		DGD_G3	> 1.6 m	loam	Stagnic Regosol	8 %	stock of deciduous trees, ground-cover plants / 45 cm	yes (0.7m)
		DGD_G4	> 1.6 m	sand	Lamellic Luvisol	7 %	short grass / 40 cm	yes (0.4m)
	housing area	**DGD_H1**	> 1.6 m	loamy sand	Gleyic Cambisol	4 %	short grass / 70 cm	yes (0.4m)
		DGD_H2	> 1.6 m	sand / sandy clay loam	Stagni-Terric Anthrosol	11 %	short grass / 15 cm	yes (0.6m)

[5] Reference soil groups of the World Reference Base (WRB) for soil resources (IUSS Working Group WRB, 2006).
[6] relevant amounts of construction waste observed (> 1 %)

The measurement of turbulent fluxes of energy and water using the eddy covariance technique were planned to merge and link the information provided by the MeteoStations and SoilStations. Therefore the eddy covariance systems needed to be deployed at strategically favorable locations (maps are provided in Appendix Figure A.7 and Figure A.8). Several scientific and technical requirements regarding the setup of flux measurements within urban boundary layer, i.e. the location within the constant flux layer but far enough above individual surface elements (Schmid, 1997), had to be taken into account. Thus, an appropriate height of more than two times the height of the roughness elements and a location downwind of a fairly homogeneous land use (e.g. Grimmond and Oke, 1999) needed to be ensured for integrated flux measurements of the whole districts. At the shallow groundwater district SGD, a setup matching these conditions could be realized in August 2011, mounting the measurement system onto a mobile phone mast at 30 m height above ground. The surrounding trees have an approximate height of 10 to 15 m and the single houses nearby are up to two storeys high. An estimation of the source areas of the fluxes measured with an eddy covariance system mounted this way resulted in a flux source area prediction based on the footprint calculation method by Kljun et al. (2004). Depending on the wind direction, the source area of the recorded fluxes is either lying westward of the mast, providing information emerging from the housing area, or lying eastward with its origin in a more heterogeneous area featuring higher buildings as well as the green space area of this district. However, at the deep groundwater district a similar instrumentation at greater heights could not be realized. As an alternative, the measurement of fluxes directly above the green space surface appeared to be appropriate to provide valuable information on the exchange processes between soil and atmosphere as well. A complementary eddy covariance system was therefore deployed at the DGD green space in September 2011, considering local conditions and guidelines provided by Campbell Sci. Inc. (2006b). Here, the source area of the fluxes recorded by the system is nearly homogeneous grassland with high pasture grass vegetation.

In addition to the HUSCO measurements, data of other meteorological stations is used for the analysis of the network data. Three reference sites provide data for the

meteorological analyses carried out within this study: The rural reference station is situated 43 km east of Hamburg, operated by the German Meteorological Service (in the following designated as station WD_G). It features a mainly agricultural and undisturbed surrounding. In previous studies this station proved to be a reasonable reference for observation on the climate of Hamburg (Schlünzen et al., 2009). In addition, data of two other meteorological stations were used: one operated by the German Meteorological Service (designated as WD_F), providing data on cloud coverage, the other one by the Meteorological Institute of the University of Hamburg (labeled as WM), providing data on wind speed in 10 m height (Table 3.3).

Table 3.3 Reference stations with location and measured parameters used for data evaluation in this study. T_a = air temperature, *rH* = relative humidity, *FF* = wind speed in 10 m height, *DD* = wind direction in 10 m height, *nm* = total cloud coverage [eighths], *so* = hours of sunshine [h], *RR* = precipitation sum, T_s = surface temperature.

reference station	initial	latitude / longitude	height (above sea level)	parameters used (interval)
Hamburg-Fuhlsbüttel (German Meteorological Service)	WD_F	53°38'24"N / 9°58'58"E	11 m	T_a, *rH*, *FF*, *DD* (10 minutes) *nm*, *so* (1 hour)
Grambek (German Meteorological Service)	WD_G	53°34'10"N / 10°40'57"E	27 m	T_a, *rH* (10 minutes)
Weather Mast Hamburg-Billwerder (Meteorological Institute, University of Hamburg)	WM	53°31''9"N / 10°06'10"E	0.3 m	T_a, *rH*, *RR*, T_s, *FF*, *DD* (1 minute)

With this concept of the HUSCO measurement network the main issues and questions of the present study can be addressed. A comparison of the variability of meteorological parameters between different land uses is possible via an inner-district comparison, where the greater climatic effects can be assumed to be alike. The impact of different groundwater tables can be compared by the contrast of mean groundwater tables of the two suburban districts. And as an extreme example for sites without natural surfaces, the inner city sites provide meteorological information. In addition, reference

stations outside Hamburg are included into the data evaluation, giving information on the atmospheric parameters of nearly rural sites. Complementary to the measurements of atmospheric and pedological parameters, flux measurements above one urban district and within the green space provide information on the exchange processes at two different scales - integrated over an entire district as well as near surface.

3.2 Measurement techniques

All MeteoStations (Figure 3.3) were equipped with sensors for measuring air temperature, relative humidity, surface temperature, wind speed and direction, and precipitation (Table 3.4). The sensors at the suburban sites were attached to a tripod. At inner city sites they were mounted at a solid metal rod attached to a street lamp. One station in each district was additionally equipped with a barometric pressure sensor. Data of all sensors were collected continuously every minute since September 2010 using CR1000 data loggers (Campbell Scientific Inc., 2009c). Power supply was provided by rechargeable batteries charged by solar panel power.

Figure 3.3 MeteoStations at C_1, DGD_G and SGD_H (from left).

Table 3.4 Meteorological measurement sensors used in HUSCO.

measurement	instrument	model	accuracy	mounting height	delivering company	reference
air temperature (T_a)	temperature and relative humidity probe, shielded	Vaisala HMP45C	±0.2°C (20°C), ±0.3°C (0°C / 40°C)	2 m	Campbell Scientific, Ltd.	Campbell Scientific Inc. (2009b)
relative humidity (*rH*)	temperature and relative humidity probe	Vaisala HMP45C	±2% (0%-90% RH) ±3% (90%-100% RH) (at 20°C)	2 m	Campbell Scientific, Ltd.	Campbell Scientific Inc. (2009b)
wind speed / direction (*FF*, *DD*)	two dimensional sonic anemometer	Gill Instruments WindSonic	±2% / ±3°	2.3 to 3 m	Campbell Scientific, Ltd.	Campbell Scientific Inc. (2010c)
surface temperature (T_s)	infra-red remote temperature sensor	IR120	±0.2°C	1.2 to 1.6 m	Campbell Scientific, Ltd.	Campbell Scientific Ltd. (2011)
precipitation (*RR*)	tipping bucket raingauge, unheated	Young 52203	2% up to 25 mm/h 3% up to 50 mm/h	1.1 to 1.7 m	Campbell Scientific, Ltd.	Campbell Scientific Ltd. (2010)
barometric pressure (*P*)	barometric pressure sensor	CS106	±0.3mb (20°C) ±0.6mb (0°C/40°C)	0.7 to 1.5 m	Campbell Scientific, Ltd.	Campbell Scientific Inc. (2009a)

The SoilStations (Figure 3.4) were instrumented with devices for soil water and temperature monitoring. Depending on their location, the stations were equipped with different types of sensors, either with separate probes measuring soil temperature and volumetric water content (*VWC*), or a combined probe for both parameters (Table 3.5). At SoilStations located next to the MeteoStations, thermistor temperature probes for soil temperature and water content reflectometers for *VWC* were used, while the other SoilStations were equipped with sensors which measure both temperature and *VWC* (combined probe with a thermistor and an oscillator measuring dielectric permittivity). All SoilStations were equipped with the same tensiometer probes to measure soil water tension (*SWT*).

Table 3.5 Soil measurement sensors used in HUSCO.

Measurement	Sensor type	Data logger	Delivering company	Reference	profiles
volumetric water content (*VWC*)	CS616 water content reflectometer	Campbell CR1000	Campbell Scientific Ltd., Bremen Germany	Campbell Scientific Inc. (2006a)	SGD_G1,SGD_G2, SGD_H1 DGD_G1,DGD_G2, DGD_H1
soil temperature (T_{soil})	T107 thermistor	Campbell CR1000	Campbell Scientific Ltd. Bremen Germany	Campbell Scientific Inc. (2010b)	SGD_G1,SGD_G2, SGD_H1 DGD_G1,DGD_G2, DGD_H1
volumetric water content / soil temperature (combined)	Decagon 5TM	ECH$_2$O EM50	UMS GmbH Munich, Germany	Decagon Devices Inc. (2010)	SGD_G3,SGD_G4, SGD_H2 DGD_G3,DGD_G4, DGD_H2
soil water tension (*SWT*)	T4e tensiometer	Campbell CR1000/ Delta-T DL6-te	UMS GmbH Munich, Germany	UMS GmbH (2009)	all soil profiles

Figure 3.4 SoilStations and soil profiles at DGD_G1, SGD_G1 and DGD_H2 (from left).

The sensors were installed in the undisturbed soil profile at 5, 10, 40, 80 and 160 cm depths below the surface (unless limited by shallow groundwater table or regulatory restrictions). Data collection was carried out automatically by data loggers with a measurement interval of 30 minutes (Table 3.5), starting in March 2011. The

investigation time of this study includes data from 01 April to 31 October 2012 for *VWC* and *SWT*, topsoil moisture data in Chapter 4.2 additionally includes data from November 2011 and 2012. All station setups included a pedological description (Appendix B, considering Ad-hoc-Arbeitsgruppe Boden, 2005) and sampling of disturbed and undisturbed soil samples for subsequent laboratory analysis. Laboratory analyses of the soil samples were carried out according to standard procedures (Table 3.6). The core physical soil properties were determined and the saturated hydraulic conductivity was estimated according to Renger et al. (2009) for all SoilStation profiles (Table 4.2 and Table 4.3), including the available water capacity (*AWC*) and the field capacity. For additional information on the analysis results of the disturbed samples see Appendix Table B.1 and Table B.2.

Table 3.6 Methods and instruments used for soil sample laboratory analyses.

parameter	method	instrument	instruction
bulk density (ρ_b)	undisturbed core method		Klute and Dirksen (1986)
drainage branch of retention curve	gravimetric technique of a porous plate apparatus		Hartge and Horn (2009), Richards (1948)
particle density	helium pycnometer	AccuPyc II 1340, Micromeritics Instrument Corporation, Norcross, GA	
particle size distribution	sieving /sedimentation method in accordance with the Köhn analysis method	Sedimat 4-12, UGT GmbH, Müncheberg, Germany	DIN-ISO11277 (2002)
organic matter content[7] / total C	laboratory analyzer for the determination of carbon, nitrogen and sulfur	vario MAX CNS, Elementar Analysensysteme GmbH, Hanau, Germany	DIN-ISO10694 (1996)
pH	determination of pH		DIN-ISO10390 (2005)
electrical conductivity	determination of the specific electrical conductivity		DIN-ISO11265 (1994)

[7] The organic matter content was calculated by multiplying the organic carbon content by the factor 1,724 (Scheffer, 2002).

The eddy covariance systems (Figure 3.5, Table 3.7) measure sensible heat flux, momentum flux and the fluxes of water and CO_2 between the atmosphere and the earth's surface. They consist of a fast response three-dimensional sonic anemometer, a fast response gas analyzer and a slow response air temperature/relative humidity sensor. The high frequency measurement data was recorded by a CR3000 datalogger. All components of these systems were provided by Campbell Scientific, Inc. as an open path eddy covariance system. In addition, Kipp & Zonen pyranometers sampled data on solar radiation.

Table 3.7 Eddy covariance system sensors used in HUSCO.

Measurement	Sensor type	Delivering company	Reference
three-dimensional sonic anemometer	CSAT3	Campbell Scientific Ltd., Bremen Germany	Campbell Scientific Inc. (2010a)
open path infrared gas analyzer	LI-7500(A)	Campbell Scientific Ltd. Bremen Germany	LI-COR Inc. (2004)
temperature and humidity probe	HMP45C	Campbell Scientific Ltd., Bremen Germany	Campbell Scientific Inc. (2009b)
Pyranometer (ventilated)	CMP11	Kipp & Zonen, Delft	Kipp & Zonen (2010)

Figure 3.5 Eddy covariance systems at SGD (left) and DGD (right).

3.3 Data correction

An appropriate quality of the measurement data prior to evaluation was ensured by an automated as well as manual quality control (Table 3.8). Implausible values and leaps as well as data collected during maintenance work at the stations were removed from the series of measurements. All sensors used within the measurement network have been calibrated by the manufacturer, providing an appropriate accuracy. However, within networks a main issue is the comparability between the observations at the different stations. The measurement values provided by the probes therefore need to be as accurate as possible.

Table 3.8 Criteria of the raw data quality control. If criteria are valid, data is disregarded for evaluation. T_a = air temperature, *rH* = relative humidity, *RR* = precipitation sum [mm], T_s = surface temperature, *P* = barometric pressure, *VWC* = volumetric water content [%], *SWT* = soil water tension [hPa], T_{soil} = soil temperature, Δ_{abs}.= change of absolute parameter value.

station	parameter	criterion 1: Δ_{abs}	criterion 2: value
MeteoStation	T_a	> 5 K/min	
	rH	> 20 %/min	> 100 % or < 0 %
	RR	> 10 mm/min	< 0 mm
	T_s	> 20 K/min	
	P	> 10 mbar/min	> 1100 mbar or < 900 mbar
SoilStation	*VWC*	> 10 %/10 min	> 100 % or < 0 %
	SWT	> 400 hPa/30 min	
	T_{soil}	> 2.5 K/10 min	
eddy covariance system	*H*	> 300 W m^{-2}/30 min	
	LE	> 300 W m^{-2}/30 min	
	T_a	> 5 K/min	

a) MeteoStations

To ensure comparability of the air temperature measurements at the MeteoStations, data on air temperature was height corrected with the US standard atmosphere (Dutton, 1986) to 0 m above sea level for all MeteoStations and reference stations. No further correction of the meteorological measurement data was performed.

b) SoilStations

At the SoilStations, different types of sensors were used due to practical reasons. The used water content probes CS616 (Campbell Scientific Inc.) are sensitive to changes in soil temperature (Seyfried and Murdock, 2001). Therefore, a temperature-correction was carried out in accordance with the user manual's calibration equation (Campbell Scientific Inc., 2006a). According to the manufacturer, the water content sensors ECH_2O by Decagon are only weakly sensitive to temperature fluctuations and do not need a temperature correction (Campbell, 2001). Other studies found a slight sensitivity for soil temperatures above 20 °C (Czarnomski et al., 2005) or stated little or no noticeable temperature sensitivity below 15 cm measurement depth or under a full vegetative canopy (Cobos and Campbell, 2007). The electrical conductivity of all soils observed was significantly lower than 1 dS m^{-1}. Thus, no specific calibration for site-specific salinity was necessary according to past research findings (e.g. Starr and Palineanu, 2002).

However, as reported in the literature (Campbell, 2001; Czarnomski et al., 2005; Ventura et al., 2010), considerable differences between soil moisture readings of the two sensor types operated for *VWC* measurements have been observed. To achieve an improvement in the comparability of the measurement data, the two sensor types were parallel instrumented at one site (DGD_G1). Here, CS616, T107 and ECH_2O 5TM were installed at the five measurement depths with about 20 cm horizontal distances from each other. The temperature measurements, collected during the vegetation period 2011, show good conformity between the different sensor types as depicted in Figure 3.6. The slight deviations between the data of the sensor types at 5 cm depth are to be expected due to the typical natural inhomogeneities within the humus rich upper soil layers. The coefficients of determination R^2 for linear regression functions between the temperature values measured by the sensor types are higher than 0.98 at all depths within this timeframe selected for calibration calculations. The slopes of the linear regression functions lie between 0.98 and 1.03, and the intercept ranges between -0.28 °C to -0.71 °C, which lies within the measurement accuracy of 5TM sensors. Thus, no need for calibration was seen.

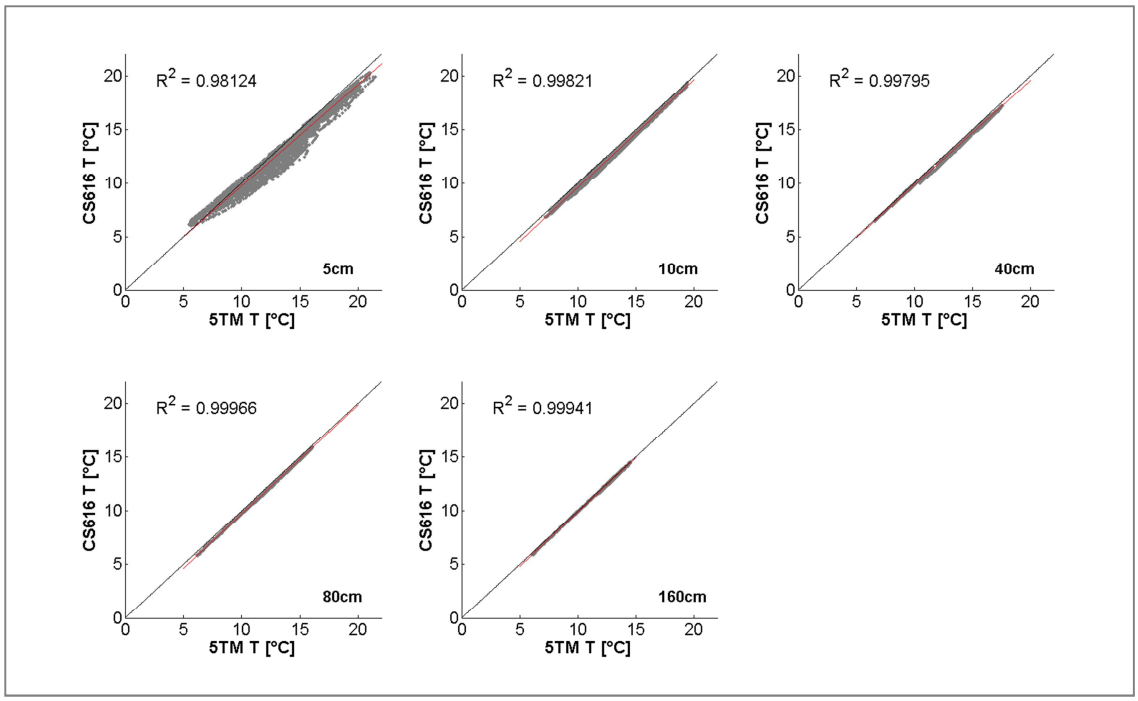

Figure 3.6 Relation of soil temperature measurements at parallel instrumented SoilStation DGD_G1 (x-axis: ECH$_2$O 5TM, y-axis: Campbell T107) for the five measurement depths.

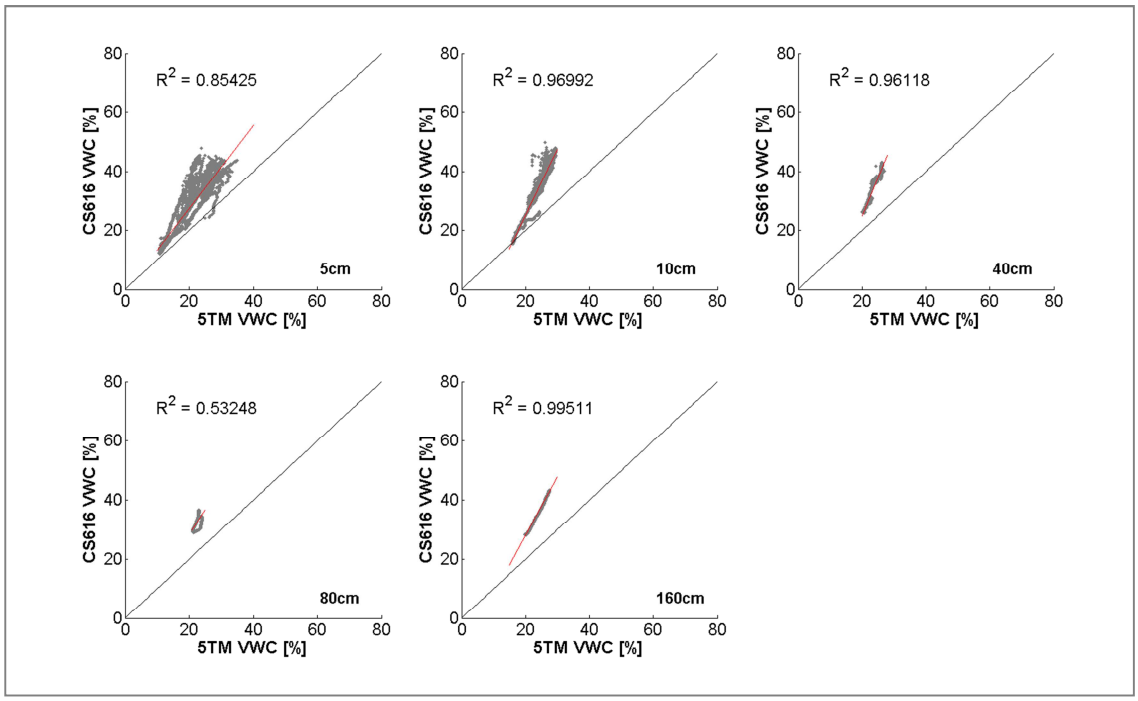

Figure 3.7 Relation of volumetric water content (*VWC*) measurements at parallel instrumented SoilStation DGD_G1 (x-axis: uncorrected ECH$_2$O 5TM, y-axis: Campbell CS616) for the five measurement depths.

Yet the *VWC* measurements deviate much stronger between the sensor types within this period (Figure 3.7): the smallest R^2 for linear regression function is 0.69, slope values are up to 3.16 and intercepts lie between -4.7 % and -39.4 %.

Findings of previous studies and comparisons between different water content sensors (Campbell, 2001; Czarnomski et al., 2005; Mittelbach et al., 2012; Ventura et al., 2010) indicate that a field-specific calibration is necessary, especially when data of different sensor types are compared. To get a clue which sensor provides more realistic soil water content, first a validation of total water content in the upper soil layers, i.e. 5 and 10 cm depth, through water balance calculations from field data was carried out. Therefore, the difference between the precipitation sum during two heavy rain events was compared to the measured increase of water content within the upper 10 cm of the soil column during the following two days (Table 3.9).

The ΔVWC_{top} in the upper 10 cm was defined as a weighted mean of the measured *VWC* of the upper (0 - 7.5 cm, $\Delta VWC_{5\text{cm}}$) and the second sensor (7.5 - 10.0 cm, $\Delta VWC_{10\text{cm}}$):

$$\Delta VWC_{top} = 0.75 \cdot \Delta VWC_{5cm} + 0.25 \cdot \Delta VWC_{10cm} \qquad \text{(Equation 1)}$$

The measured *VWC* of the ECH$_2$O 5TM sensors deviate stronger from the expected water content than the values provided by the CS616 sensors after a rain event with known amount of precipitation. While at stations with CS616 sensors the mean difference between precipitation sum and increase in volumetric water content of the upper 10 cm is 9.3 mm for the rain event in August and 2.5 mm in January, for the ECH$_2$O probes the differences result in 13.9 mm and 12.5 mm, respectively. As a consequence, it was assumed that the ECH$_2$O 5TM data needed to be corrected to fit the data of the CS616 sensors. The correction is based on a linear regression of the data of the parallel instrumented soil profile.

The linear regression (R^2 = 0.90) between the 5TM and the CS616 data, using a joint dataset of all depths (Figure 3.8a), provided the correction function:

$$y = 1.52 \cdot x \qquad \text{(Equation 2)}$$

with y = *VWC* ECH_2O 5TM corrected and x = *VWC* ECH_2O 5TM original reading. Equation (2) was used to correct all data collected by the ECH_2O 5TM sensors. No offset was added because this would lead to implausible very low (< 10 %) and negative values of *VWC* in the corrected data. For example, an alternative linear regression function would provide an intercept value of -22.5 %. Thus, a simple linear regression function without the intercept term is appropriate. A standardized correction for all SoilStations instrumented with ECH_2O 5TM was feasible here, because soil textures of these HUSCO soil profiles are mainly sand or loamy sand. Therefore they are comparable with each other, as studies and information on the differences in calibration depending on soil substrate show: Campbell et al. (2009) found no differences for a calibration of ECH_2O probes between sand and silt loam, and the CS616 probes' accuracy is given by the manufacturer for sandy loam and coarser textures (Campbell Scientific Inc., 2006a).

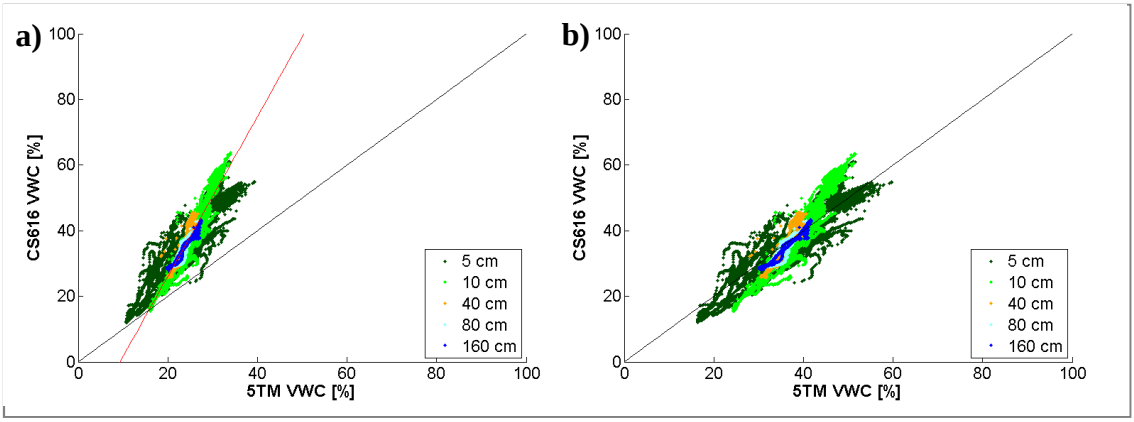

Figure 3.8 Relation of volumetric water content (*VWC*) measurement data at parallel instrumented SoilStation profile DGD_G1, joint data of all measurement depths. **a)** uncorrected data, **b)** with a factor of 1.52 corrected ECH_2O 5TM data.

Table 3.9 Soil moisture variance within two days after heavy rain events. Difference between precipitation sum ΣRR [mm] at the MeteoStation next to the SoilStation, and weighted ΔVWC_{top} = $0.75 \cdot \Delta VWC_{5cm} + 0.25 \cdot \Delta VWC_{10cm}$ [mm], for CS616 sensor data and ECH_2O 5TM data (before and after correction). *VWC* = volumetric water content.

			before correction		after correction	
variable	11.08.11	04.01.12	11.08.12	04.01.12	11.08.12	04.01.12
	CS616		**ECH_2O 5TM**			
	SGD_G1		*SGD_G3*			
ΣRR	21.9	18.0	21.9	18.0	21.9	18.0
ΔVWC_{top}	6.9	27.1	4.6	6.3	10.9	13.0
$\Sigma RR - \Delta VWC_{top}$	15.0	-9.1	17.4	11.7	11.0	3.0
	SGD_H1		*SGD_G4*			
ΣRR	21.9	18.0	21.9	18.0	21.9	18.0
ΔVWC_{top}	6.9	9.3	9.5	6.5	22.6	15.6
$\Sigma RR - \Delta VWC_{top}$	15.0	8.7	12.4	11.5	-0.7	2.5
	DGD_G1		*SGD_H2*			
ΣRR	19.4	22.2	21.9		21.9	
ΔVWC_{top}	15.8	19.8	6.9		16.4	
$\Sigma RR - \Delta VWC_{top}$	3.6	2.4	15.1		4.9	
	DGD_G2		*DGD_G1 parallel*			
ΣRR	19.4	22.2	19.4	22.2	19.4	22.2
ΔVWC_{top}	14.7	14.7	7.1	7.9	17.0	18.9
$\Sigma RR - \Delta VWC_{top}$	4.8	7.5	12.3	14.3	2.4	3.3
	DGD_H1		*DGD_G3*			
ΣRR	18.4	15.4	19.4		19.4	
ΔVWC_{top}	10.4	12.4	6.9		16.5	
$\Sigma RR - \Delta VWC_{top}$	8.0	3.0	12.5		3.0	

The water budget calculations after heavy rain events (Table 3.9) are significantly better with the correction applied, with average deviations from the precipitation amount of only 4.1 mm and 2.9 mm, respectively. Also the correlations between the measurement data of the sensor types at the parallel instrumented profile (Figure 3.8b) and the water retention curve fits show distinctly better agreements after this correction.

To measure soil water tension at all SoilStations, tensiometers were used. The used sensor type provides a measuring range of +1000 hPa (pressure) to -850 hPa (tension)[8]. However, higher tensions at the SoilStations occurred, resulting in missing *SWT* data during these stages. The data loss between 0 and 850 hPa in relation to the measured data is individually different for each SoilStation and measurement depth (Table 3.10).

[8] To simplify matters, in the following *SWT* data are stated as absolute values, because tension equals negative pressure.

To the most part the percentage of missing data within the two vegetation periods 2011 and 2012 is little (< 5 %). However, the depths of some soil profiles are prone to have higher *SWT* values and thus tensiometers reached their measurement range more often. Of the 53 monitored measurement depths only seven show data losses of more than 20 %, distributed amongst three profiles in DGD district. In eight measurement depths 10 to 20 % of the data was not collected. An immediate refilling of these tensiometers, which is necessary to ensure their subsequent functionality, was not always feasible. Also missing data resulted from temporary sensor failure. Thus, data gaps occurred which needed to be closed within the measurement range.

To fill these data gaps of *SWT* within the measurement range up to -850 hPa the measured field retention data of each depth interval were fitted to the Mualem-van Genuchten hydraulic model function (van Genuchten, 1980). It describes the nonlinear relations in soil and porous media between the normalized dimensionless water content (Θ) and soil water tension *SWT* as:

$$\Theta = \frac{\theta - \theta_r}{\theta_s - \theta_r} \qquad \text{(Equation 3)}$$

$$\Theta = \left[\frac{1}{1 + (\alpha \cdot h)^n} \right]^m \qquad \text{(Equation 4)}$$

with θ, θ_r and θ_s are the actual *VWC*, residual *VWC* and saturated *VWC*, *h* is the *SWT*, α, m and *n* are soil specific hydraulic parameters. Data on *SWT* was converted to a logarithmic value prior to the calculation of the nonlinear fit.

As the water retention curves of the field data at DGD_H1 exemplarily show (Figure 3.9), best conformity between the measured field data of *VWC* and *SWT* and the water retention curve resulting from fitting the Mualem-van Genuchten hydraulic model function is found in lower depths (40 cm and deeper). Gap-filling of *SWT* data (highlighted) was necessary mainly in the upper areas (5 and 10 cm) due to the increased ratio of exceeding the measurement range of the tensiometers. The fitted water retention curves for all twelve SoilStations are provided in Appendix C.

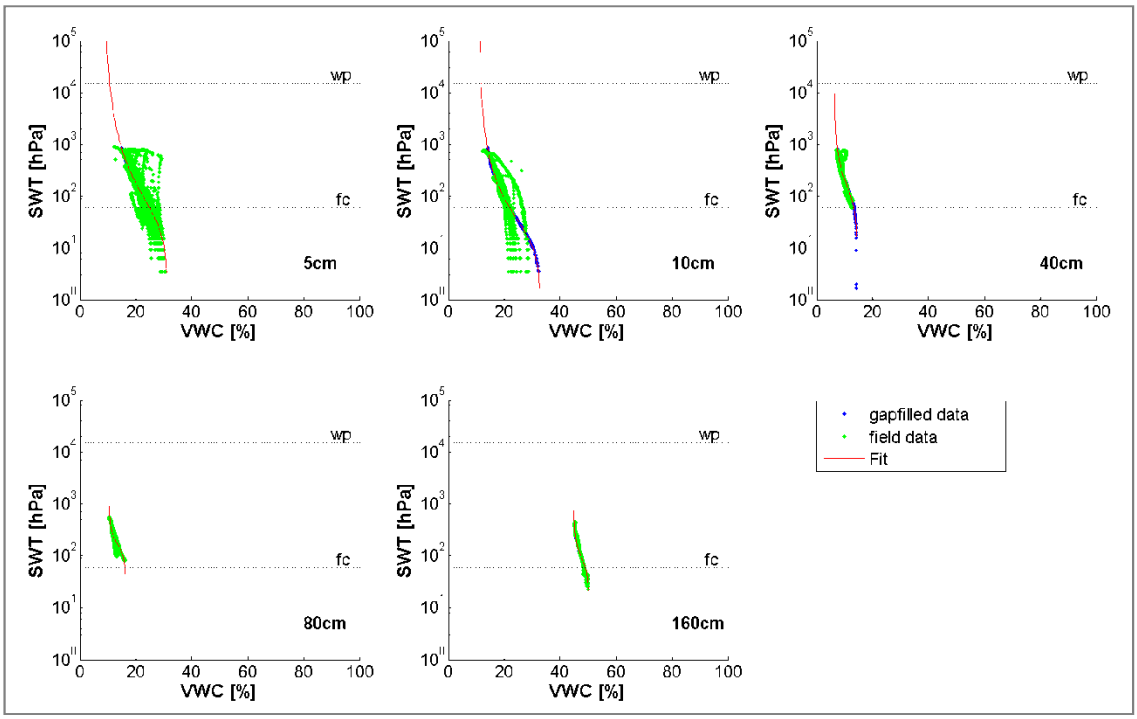

Figure 3.9 Water retention curves of field data of 2011 and fitted (van Genuchten, 1980) curve for the DGD_H1 profile, including reconstructed soil water tension (*SWT*) data. Reconstructed data is depicted as blue data points, *VWC* = volumetric water content, wp = permanent wilting point, fc = field capacity.

As a measure for the goodness-of-fit of the Mualem-van Genuchten hydraulic model curve, the root-mean-square error factor (F_{rmse}) was calculated (Table 3.10), taking into consideration that the hydraulic curve is plotted as a logarithmic function. The factor F_{rmse} is derived as the exponential function of the root-mean-square error calculated from the residuals around the fit. A perfect match between measured data and fit would result in an F_{rmse} of 1. The higher the factor, the larger is the deviation of the measurement from the fit. It is well apparent that the best matches ($F_{rmse} < 1.5$) between measurement and fit are found for lower depths, mainly 40 cm or deeper. Within the upper layers at 10 cm depth and above, to the most part the F_{rmse} is larger compared to the values within the single soil profiles. It even attains values of 2 or higher at four sites. A reasonable explanation for this effect is the high organic matter content within the upper soil layers, providing high water retention in general, which leads to pronounced hysteresis effects. Only DGD_G3 and DGD_H2 exhibit these high F_{rmse}

values also for depths of 80 cm and below. Here, the remarkably high bulk densities in these depths lead to almost no observed variations in *VWC* in the field. Apart from the organic matter content a dependence of the F_{rmse} on soil texture, substrate or land use is not obvious here.

Table 3.10 Percentage (%) of gap-filled soil water tension (*SWT*) data and root-mean-square error factor (F_{rmse}). Gap-fill was conducted for missing values between 0 and 850 hPa, percentage given relative to the total amount of measurement data for vegetation periods 2011 and 2012. Root-mean-square error factor (F_{rmse}) of the Mualem-van-Genuchten hydraulic model fit of field measurements 2011.

depth	**SGD_G1**		**SGD_G2**		**SGD_G3**		**SGD_G4**		**SGD_H1**		**SGD_H2**	
	%	F_{rmse}	%	F_{rmse}	%	F_{rmse}	%	F_{rmse}	%	F_{rmse}	%	F_{rmse}
5 cm	0.4	1.82	0.4	1.81	3.7	1.67	18.4	1.70	0.3	2.25	9.5	1.58
10 cm	0.4	1.74	0.4	1.84	3.6	1.47	14.4	1.63	0.3	1.44	8.6	1.64
40 cm	0.4	1.90	0.4	1.86	3.3	1.23	3.3	1.14	0.3	1.31	5.3	1.35
80 cm					3.3	1.45	3.3	1.38	0.3	1.51	4.0	1.25
160 cm									0.3	1.34	4.0	1.10

depth	**DGD_G1**		**DGD_G2**		**DGD_G3**		**DGD_G4**		**DGD_H1**		**DGD_H2**	
	%	F_{rmse}	%	F_{rmse}	%	F_{rmse}	%	F_{rmse}	%	F_{rmse}	%	F_{rmse}
5 cm	3.1	1.66	29.8	2.11	20.1	2.10	8.2	1.72	2.1	1.73	27.8	1.83
10 cm	2.9	1.87	15.6	1.98	20.5	1.60	13.0	1.54	5.0	2.67	21.7	1.52
40 cm	19.5	1.92	39.5	1.32	15.8	2.00	5.7	1.46	7.8	1.42	9.6	1.95
80 cm	0.5	1.25	39.2	1.44	8.5	1.83	5.7	1.15	0.0	1.27	13.3	2.14
160 cm	0.1	1.66	0.7	1.13	12.6	2.19	5.7	1.32	0.0	1.25		

c) Eddy covariance system

The eddy covariance system collected high frequency data (20 Hz) of three-dimensional wind and H_2O measurements, and slow frequency data (every 5 seconds) of air temperature, humidity and solar irradiance. This raw data was processed with the LI-COR software Eddy Pro 3.0 to obtain 30 minutes averaged data on fluxes of sensible and latent heat. The basic data processing includes all necessary correction steps, e.g. coordinate rotation, de-spiking, time delay removal and WPL correction (Webb-Pearman-Leuning correction, as introduced in Webb et al., 1980). In addition to the

calculated fluxes it provided statistical information, quality flags and estimated footprints (LI-COR Inc., 2012).

The eddy covariance method is used to calculate turbulent fluxes[9] of latent heat (i.e. evapotranspiration ET) and sensible heat (i.e. change of air temperature T_a). It is only valid if certain major assumptions are made (see e.g. Burba and Anderson, 2007). For example, density fluctuations and the mean vertical flow are assumed negligible. The terrain is assumed to be horizontal and uniformed, and as measurements at a point are assumed to represent the upwind area of interest, the wind direction and speed needs to be taken into account for the data interpretation of the fluxes' source area. Wind directions from areas that are not suitable for the measurement technique, as they do not comply with the conditions, must not be interpreted. Apart from that, also predominantly low winds do not provide valuable data (Burba and Anderson, 2007), as the fluxes' source area is very close to measurement station and biased by the measurement construction. Data of wind speeds below 1 m s^{-1} therefore is not regarded as well. Thus, the collected data provides only information for limited area and time, namely when the conditions match the requirements on the origin of fluxes. For the installations within the HUSCO network, the two eddy covariance systems provided information on fluxes from areas with very distinct surface characteristics and spatial extend. At the SGD district's eddy covariance system, mounted in great height and thus owning a wide footprint, two different source areas can be defined: During easterly air flow (80° to 180°) the footprint lay within a mixed land use area of detached houses and green space (named SGD_EC1 in the following), while with prevailing westerly air flow (230° to 330°) the source area was located within the housing area (SGD_EC2). For a map of the footprints, including information on the percentage of fluxes originating from these areas compare Appendix Figure A.7. At the DGD district site, the eddy covariance system at 2.5 m height above the ground covered a comparably small source area, yet more homogenous in its land use (named DGD_EC). Here, with westerly air flow from 180° to 360° the source of the fluxes was located on the grass

[9] The term „flux" is used in this study as a synonym for the more precise term „flux density", as, to be strictly accurate, the eddy covariance technique calculates the density of fluxes in Watt per square meter [W m^{-2}]. However, the term "flux" is commonly used in literature.

land (see Appendix Figure A.8). Depending on the source area's location and the wind speed, the percentage of the valuable measurement data on the total collected data varies for the two operated eddy covariance systems (Table 3.11). At SGD district a total of 72 % of the data is useful, distributed to 25 % for the evaluation of the heterogeneous area and 47 % for the consideration of the housing area. At DGD only 31 % of the data can be used to interpret fluxes originating from the green space, due to the constrained wind directions. Only in westerly direction of the measurement station the green space area is wide enough to match the requirements for applying the eddy covariance technique at 2.5 m height. For the evaluation of the eddy covariance measurements, in addition to the quality control during the raw data procession, only data from the valuable wind directions was used.

Table 3.11 Percentage of valuable data on total collected data. Data derived from eddy covariance method measurements.

district	name	valuable wind direction	wrong wind direction	low wind speed (< 1 m s^{-1})	ideal conditions
SGD	SGD_EC1	80° - 180° (green space)	73 %	2 %	25 %
	SGD_EC2	230° - 330° (housing area)	51 %	2 %	47 %
DGD	DGD_EC	180° - 360° (open grassland)	43 %	26 %	31 %

As latent and sensible heat flux intensities predominantly depend on the amount of solar radiation, different approaches to evaluate and interpret data can be chosen to make measurements from different seasons and meteorological situations better comparable. One common method is the calculation of the Bowen ratio, i.e. the ratio of sensible heat *(H)* to latent heat (*LE*). It is useful for many analyses concerning the energy conversion into latent heat (e.g. Stull, 1988). However, when absolute flux values are small, Bowen ratios becomes unbounded, potentially leading to ambiguous and misleading interpretations. Another quotient which regards also the absolute values by normalizing the ratio is the evaporative fraction (*EF*). It is a relative measure for the

contributions of turbulent latent heat fluxes to the available energy at the land surface, i.e. the net radiations' energy that is not conducted downwards into the ground as soil heat flux. It is defined as:

$$EF = \frac{LE}{H + LE} \qquad \text{(Equation 5)}$$

Thereby it reaches values within the range of 0 (no partitioning into latent heat fluxes) to 1 (available energy is completely converted into latent heat fluxes). The *EF* thus is a diagnostic of the surface energy balance that is self-preserved or constant during daytime by isolating surface control, i.e. soil moisture and vegetation, from radiation and turbulent factors (Gentine et al., 2011). Thus, it is the parameter of choice for the evaluation of the eddy covariance measurement data within the present study. However, with very small absolute fluxes the *EF* can also be calculated, yet not meaningful to interpret and prone to large errors due to limited measurement accuracy of the eddy covariance system sensors. To avoid misinterpretation only *EF* derived from latent and sensible heat fluxes larger than the measurement accuracy were taken into consideration. According to Mauder et al. (2006) the uncertainty in the measured turbulent heat fluxes amounts to at least 10 W m^{-2} or 5 % for sensible heat flux *H* and to 20 W m^{-2} or 10 % for latent heat flux *LE*. Fluxes below these thresholds are not regarded for the calculation of *EF* within the data evaluation of the present study. For the calculation of daily averages of the fluxes only days are included that provided data for all 30 minute intervals between 10:00 and 15:00 CET. The calculation of daily averages of *EF* is a good way to relate it to the less fluctuating soil water contents at average without the risk of over interpreting temporal peculiarities which are inherent in the hourly or 30 minute data. Using the average *EF* is feasible because it shows a strong linear relation to the midday *EF*, as found by e.g. Farah et al. (2004) and Nichols and Cuenca (1993).

4 Variability of urban soils and soil water dynamics

The soil profiles studied within HUSCO differ distinctly from each other in substrate, soil physical properties and organic matter content (see Chapter 3.1 for details). Thus, considerable differences among their water budget and dynamics can be expected. Their characteristics are described and discussed in this chapter in relation to urban land use and groundwater table depth. After a detailed description and discussion of the variability during the vegetation period 2011 for the whole profile (Chapter 4.1) and in particular for their topsoil moisture trends (Chapter 4.2), a comparison to the vegetation period of 2012 is made in Chapter 4.3. A discussion of the results with regard to the possible impact of urban soil hydrology differences on local climate is given in Chapter 4.4.

4.1 Spatial and temporal variability of soil moisture and water tension in the year 2011

Measurements of *VWC* and *SWT* within the vegetation period of 2011 are given for selected sites in Figure 4.1 and Figure 4.2 respectively. This time period (01 April to 31 October 2011) was characterized by a mean air temperature of 14.7 °C (maximum: 30.2 °C, minimum -0.9 °C, average observations at MeteoStations) and a total amount of precipitation of 378 mm (measured at reference WM, Figure 4.1a. The total amount of precipitation during the vegetation period was very similar at all studied sites (±7 %), whereas high daily deviations occurred due to the spatial inhomogeneity of precipitation. While spring was exceptionally dry (39.9 mm total during April and May, with a 30 year mean for Hamburg of 100 mm at WD_F), the second part of the vegetation period was comparatively wet. The differences in temporal evolution of the *VWC* profiles between sites, both during the course of the study period and within shorter periods (a few days), are clearly identifiable (Figure 4.1). In particular, rare events like heavy rainfall or long periods of low precipitation are reflected in the *VWC* of the upper soil layers and, in some cases, even in greater depths.

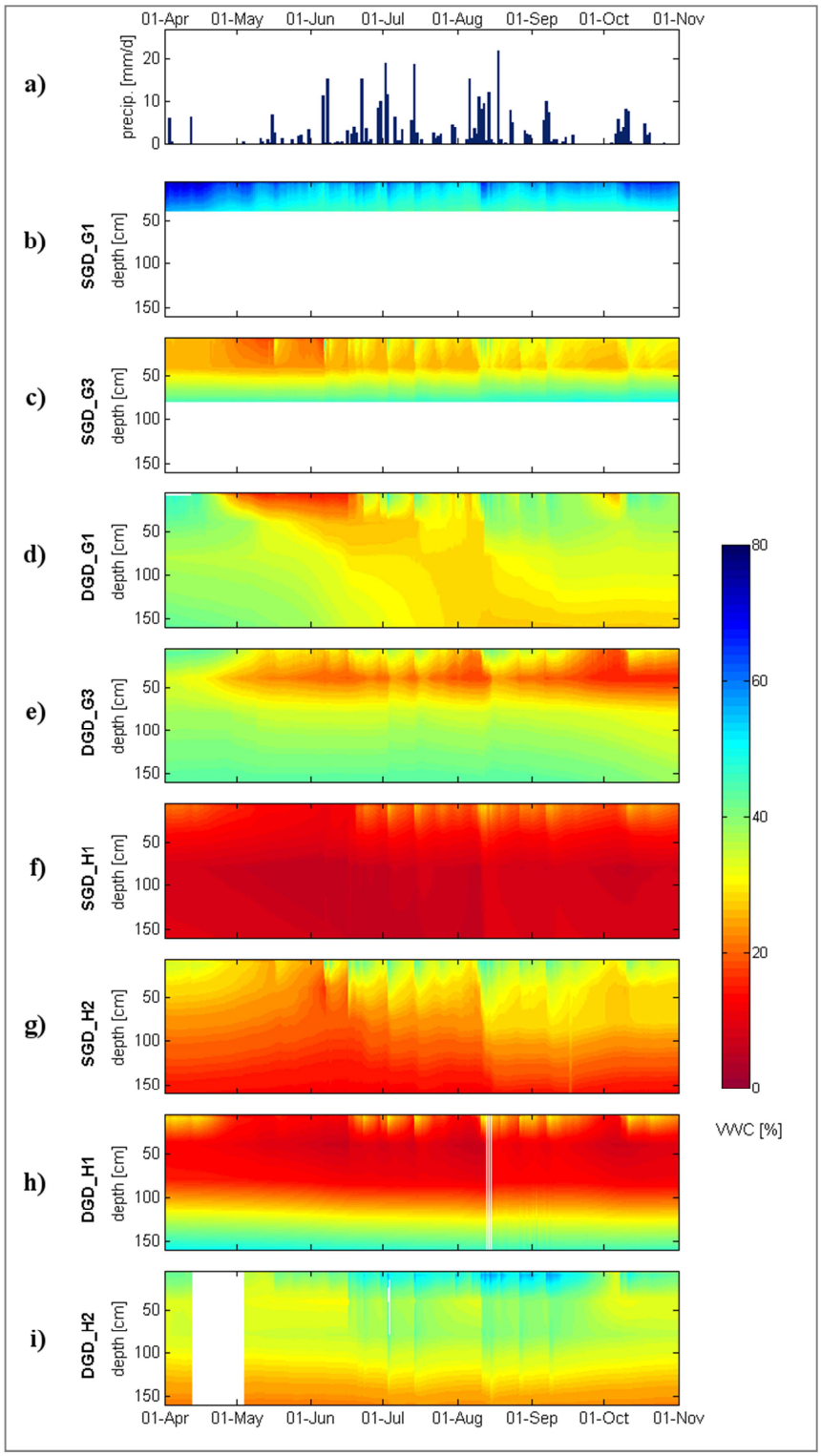

Figure 4.1 Precipitation at reference station WM (a, upper row) and 2D time-depth evolution of volumetric water content (*VWC*) at eight exemplary soil profiles in 2011 (linear interpolation between measurement depths).

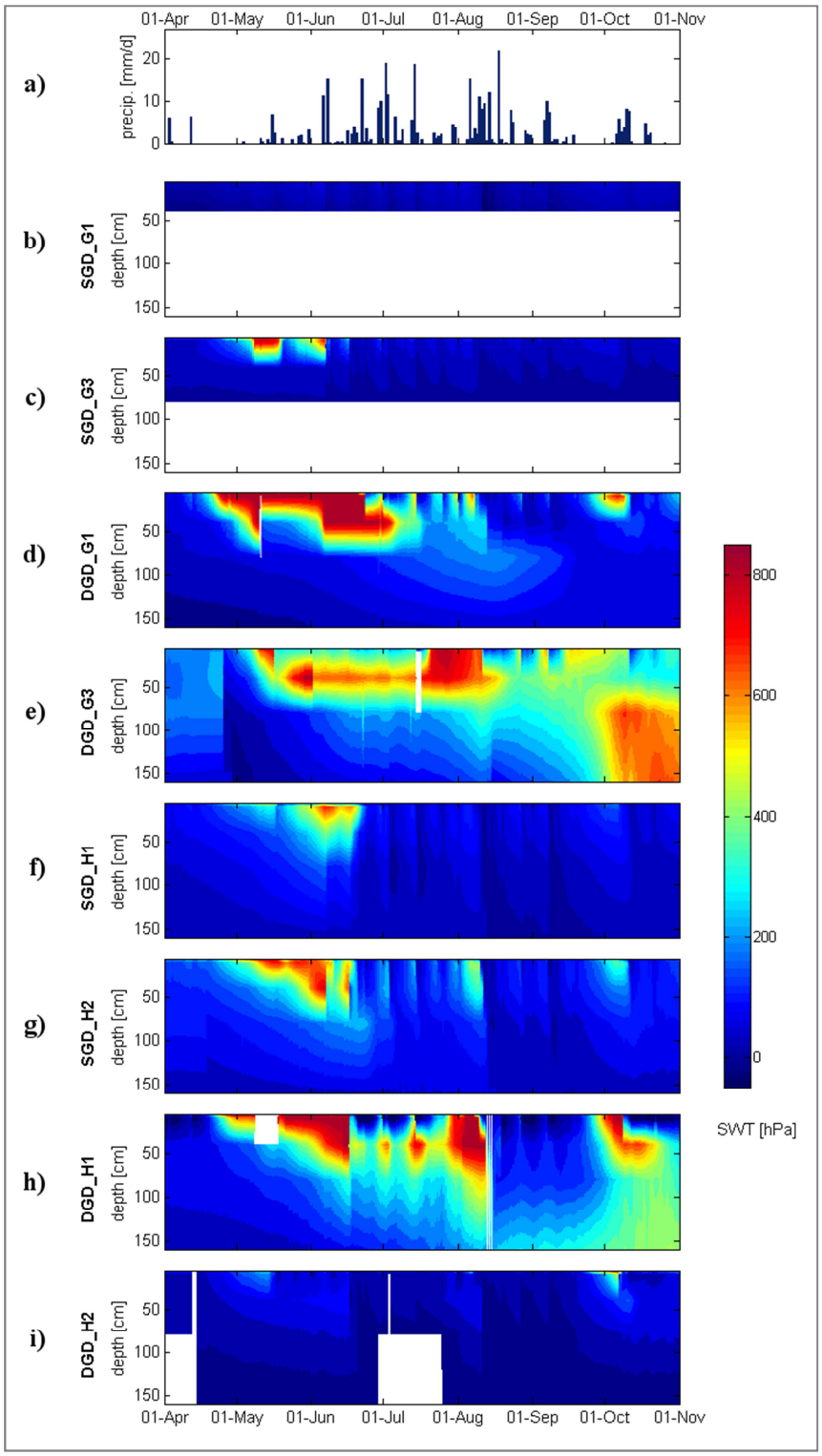

Figure 4.2 Precipitation at reference station WM (a, upper row) and 2D time-depth evolution of soil water tension (*SWT*) at eight exemplary soil profiles in 2011 (linear interpolation between measurement depths). Values of *SWT* estimated to be > 850 hPa are depicted in the dark red color, white spaces indicate non-gap-filled missing data.

Characteristic soil-hydrological features for the vegetation period in the temperate latitudes are a high initial *VWC* in spring due to residual water from winter precipitation (snow and ice melt), a comparably dry summer season and rewetting of soil in fall (Illston et al., 2004). Even though 2011 was an untypical year in terms of the temporal distribution of precipitation, this sinusoidal annual cycle of change in *VWC* can be identified at most of the HUSCO stations (Figure 4.1). However, a shift of maximum drying towards early summer months (May/June) is evident, caused by a dry spring period with a sequence of three weeks without precipitation (12 April to 02 May 2011) and followed by single days with intensive rainfall (up to 10 mm per day, Figure 4.1a). This period allows to illustrate the hydrological characteristics of the soil profiles particularly well and thus to draw conclusions on their potential effects on local climate. Therefore a special focus lies on this three-week dry phase and the relative decrease in *VWC* of the available water capacity *AWC* within the following analysis of the measurements (Table 4.1).

Table 4.1 Decrease of volumetric water content (Δ*VWC*) during dry phase (12 April to 03 May 2011), available water capacity (*AWC*) within the upper 40 cm of soil, and relative change [%] of the decrease on the *AWC*.

upper 40 cm	**SGD_G1**	**SGD_G2**	**SGD_G3**	**SGD_G4**	**SGD_H1**	**SGD_H2**
Δ*VWC* [mm]	12.04	2.03	14.3	41.3	12.5	13.9
AWC [mm]	151.8	156.9	107.4	128.0	103.0	87.5
relative change [%]	7.9	1.3	13.3	32.3	12.1	15.9
	DGD_G1	**DGD_G2**	**DGD_G3**	**DGD_G4**	**DGD_H1**	**DGD_H2**
Δ*VWC* [mm]	37.4	33.09	27.6	30.3	28.5	-
AWC [mm]	100.5	85.8	92.4	80.6	83.2	78.6
relative change [%]	37.2	38.5	29.8	37.5	34.3	-

a) Green spaces with shallow groundwater table

The SoilStations at the green spaces within the district featuring a shallow average groundwater table (SGD_G1, Figure 4.1b, as well as SGD_G2, not shown) show high *VWC* values throughout the whole investigation period. Here, the local shallow

groundwater table depth (approximately 40 cm below surface) is considered to be the dominant controlling factor on soil water dynamics. The water content of the upper soil at this site is controlled by this near-surface groundwater level as well as by the high content of organic matter (> 10 % content of carbon), which determines a high pore volume (> 65 %, Table 4.2) and very low bulk density (0.7 g cm^{-3}). This combination of characteristics leads to high rates in potential capillary rise of the groundwater, estimated at 2.5 to 5 mm per day (according to Ad-hoc-Arbeitsgruppe Boden, 2005). Additionally the high organic content allows for prolonged water holding, as visible in the high field capacity of more than 50 %.

Table 4.2 Laboratory analysis results for undisturbed soil samples at SGD. kf = saturated hydraulic conductivity estimated according to Renger et al. (2009), *AWC* = available water capacity, fc = field capacity.

profile	depth [cm]	pore volume [%]	*AWC* [%]	fc [%]	soil texture[10]	bulk density [g cm^{-3}]	kf[11] [cm d^{-1}]
SGD_G1	5	69.5	28.9	55.1	Sl3	0.7	-
	10	70.4	40.3	58.6	Sl2	0.7	-
	40	65.8	39.8	55.5	Us	0.8	45
SGD_G2	5	69.4	40.6	62.6	Su3	0.7	-
	10	65.8	24.7	54.3	Sl2	0.8	-
	40	73.0	55.5	66.5	Su4	0.6	-
SGD_G3	5	58.4	34.3	41.6	mSgs	1.1	-
	10	45.4	30.7	37.4	mSgs	1.4	312
	40	40.5	18.6	22.3	gSms	1.6	315
	80	38.9	22.8	26.4	gSms	1.6	315
SGD_G4	5	58.9	35.4	45.8	Sl2	1.0	-
	10	56.8	29.8	40.9	Su2	1.1	-
	40	47.7	32.8	39.9	mSgs	1.3	375
	80	41.2	23.2	25.0	gSms	1.6	315
SGD_H1	5	54.7	23.4	35.7	Su2	1.1	> 185
	10	56.0	24.8	34.1	mSfs	1.1	> 375
	40	54.7	28.1	41.1	Su2	1.1	-
	80	38.9	6.2	9.8	Su2	1.6	85
	160	37.2	8.1	8.7	mSgs	1.7	150
SGD_H2	5	55.5	28.9	42.3	Su2	1.1	-
	10	55.4	23.0	35.1	Su2	1.1	> 185
	40	56.2	17.1	25.0	Su2	1.1	> 185
	80	38.3	12.7	15.7	Su2	1.6	85
	160	42.0	18.8	20.8	mSgs	1.5	250

[10] soil texture according to Ad-hoc-Arbeitsgruppe Boden (2005)
[11] "-" indicates no specification

Nevertheless, a slightly sinusoidal cycle can be identified in this profile as well, with an initial water content of 70 % in April, which represents almost saturation, and the lowest *VWC* in 40 cm depth with 55 % *VWC* in August. Consequently, *SWT* remains at low levels (< 200 hPa) throughout the study period (Figure 4.2b). The lack of precipitation in spring leads to a slow but steady decrease of the generally high *VWC* at greater depths. Within the selected three-week dry phase in April and May (Table 4.1), a total decrease of 12 mm water (SGD_G1), respectively 2 mm (SGD_G2), within the upper 40 cm is measured. Considering that the *AWC* of the soil column down to this depth is > 150 mm at both profiles, this loss of water equals less than 10 % of the total available water. Meanwhile, *SWT* in 40 cm depth increases only very slightly (8.6 hPa). Thus, a considerably drying does not occur at these sites.

Measurements at the nearby site SGD_G3 (Figure 4.1c) reveal a different picture. This site is located in 500 m distance from SGD_G1, also within a short grass green space area, but it features a soil texture of pure sand with more than 30 % macro pores, less organic matter content (only up to 3 % total carbon content) and a deeper mean groundwater table (1.2 m below surface). The initial *VWC* here is substantially lower (< 30 %) and spring drying of soil reaches down to 40 cm depth with a decrease of 13 % of *AWC* for the upper 40 cm (Table 4.1). This drying is also visible in an increasing *SWT* (Figure 4.2c). Down to this depth the effects of precipitation and subsequent drying periods can be clearly identified. Water percolation proceeds faster into depth but water remains within the soil column for shorter periods of time (Figure 4.1c). *SWT* reaches increased values after periods with little precipitation. In the sand layer below 40 cm depth, rain water percolation does not lead to a considerable increase of *VWC*, nor to a change in *SWT*. The subsoil (below 40 cm depth), featuring a higher bulk density compared to layers above (1.0 to 1.4 g cm^{-3} in the upper layers, 1.6 g cm^{-3} in 80 cm depth, Table 4.2), remains at almost constant *VWC* (40-45 %) and only moderately varying *SWT* during the whole season. The soil water dynamics at the nearby located site SGD_G4 is comparable due to rather similar soil-physical characteristics, with only a 6 to 8 % higher percentage of silt and 2 % less macro pores in the upper 10 cm. A slightly deeper water percolation and a more intensive drying in

spring can be observed, most likely due to high root water uptake by pasture grass vegetation (not shown). These findings depict that at these sites precipitation has a greater short-term impact on *VWC* of the upper soil than the high groundwater table due to substrate characteristics. Thus, an incomplete refilling of soil layers down to 40 cm depth by capillary rise of groundwater can be attributed to these two sites (Figure 4.2c). This effect is considered to be promoted by the pore size distribution at the site SGD_G4 with 17 to 25 % medium sized pores within the upper 40 cm, and to a reduced extend at the site SGD_G3 with 6 to 20 % medium-sized pores.

b) Green spaces with deep groundwater table

The temporal variability of *VWC* and *SWT* within the deep groundwater district's green space follows the general annual course described above. Soil profile DGD_G1 is characterized by a soil profile of mostly sandy loam, a decreasing pore volume with increasing depth, a humus rich topsoil layer (6.2 % total carbon content) and coverage with high pasture grass. Here, an intensive spring drying of the upper 40 cm can be observed, indicated by a *VWC* decrease (Figure 4.1d). Concurrently, *SWT* increases throughout the profile down to 80 cm, exceeding the measurement range (850 hPa tension) of the tensiometers in early May (Figure 4.2d). Within three weeks of no precipitation, a loss of 37 mm of water occurs within the upper 40 cm, equaling 37 % of the available water capacity *AWC* (Table 4.1). Until the end of June the impact of this reduced precipitation is detectable down to the lowest measurement depth (160 cm). Summer precipitation percolates in deep soil layers starting in mid-August so that a refilling of the profile below 40 cm measurement depths is detected in late summer and fall. The 30 m apart located profile DGD_G2 (not shown) shows a similar temporal evolution with higher remaining *VWC* in 80 cm depth. The decrease of *VWC* at both stations proceeds to greater depths during summer and early fall, while the upper layers (5 and 10 cm) are rewetted by intensive summer precipitation events. This effect is, to this extent, only detectable at the profiles DGD_G1 and DGD_G2 (the latter not shown). Probably, this pronounced reduction of *VWC* in deeper soil layers is caused by a combination of intensive percolation due to a high saturated hydraulic conductivity of more than 100 cm d^{-1} in the inferior layers (80 cm) at DGD_G2 and the sandy soil

texture in 160 cm at DGD_G1 (Table 4.3), respectively, as well as root uptake by grass and tree vegetation, and a missing refilling by percolation water from the layers above.

The profile DGD_G3 (Figure 4.1e), located in a slightly elevated area nearby, features a loamy sand texture with a high percentage of construction waste (15-20 %) within the upper half meter, high bulk density (1.8 g cm^{-3}, Table 4.3) below this layer and a vegetation of deciduous trees and ground-cover plants. This soil profile also very noticeably depicts the reduction in *VWC* starting in spring. Within the three-week dry phase in April, *VWC* of the upper 40 cm is reduced by 30 % of the *AWC* (Table 4.1). The depth of around 40 cm shows major drying starting in late spring with only slight temporary gains after intensive precipitation events. The increase of *SWT* up to 850 hPa (detection threshold) or more (Figure 4.2e) indicates intensive drying at this time. Upper soil layers show fluctuations of *VWC* with higher frequency and a less distinct decrease in the course of the year. However, root water uptake in general is best visible at this site DGD_G3. The reduction of *VWC* by water uptake by deciduous trees and ground-cover plants at 40 cm depth is more distinct with increasing intensity in the course of the vegetation period, compared to the other sites (Figure 4.1e). Below the observed rooting depth of 50 cm at this site - presumably due to construction waste below 50 cm depth and a high content of loamy substrate roots do not grow deeper but more horizontally than vertically (Appendix B) - *VWC* remains almost at constant values with only a minor annual decline (44 % down to 39 %). An interesting phenomenon can be observed starting in September 2011: Below 40 cm depth *VWC* decreases slowly associated with a simultaneous increase in *SWT* up to 700 hPa in depths below 80 cm. This seems to result from slow percolation in these depths, because no roots were found in these layers.

Table 4.3 Laboratory analysis results for undisturbed soil samples at DGD. kf = saturated hydraulic conductivity estimated according to Renger et al. (2009), *AWC* = available water capacity, fc = field capacity.

profile	depth [cm]	pore volume [%]	*AWC* [%]	fc [%]	soil texture[12]	bulk density [g cm^{-3}]	kf[13] [cm d^{-1}]
DGD_G1	5	68.2	35.1	48.2	Sl3	0.8	-
	10	54.8	28.6	46.6	Sl3	1.1	> 100
	40	37.8	16.1	36.9	Ls4	1.6	32
	80	30.9	8.7	27.8	Sl3	1.8	30
	160	27.9	24.0	26.0	mSfs	1.9	-
DGD_G2	5	54.6	29.9	43.1	Sl3	1.2	> 100
	10	41.4	21.2	33.5	Sl3	1.5	70
	40	43.9	17.5	29.9	Sl3	1.4	85
	80	51.0	20.6	33.6	Sl3	1.2	> 100
	160	27.5	13.5	22.7	Sl3	1.9	30
DGD_G3	5	58.4	31.8	46.6	Sl2	1.1	-
	10	57.7	29.3	42.2	Sl3	1.1	-
	40	39.0	11.5	30.9	Sl3	1.6	55
	80	32.8	3.6	23.6	Ls4	1.8	17
DGD_G4	5	59.3	30.0	39.0	mSgs	1.0	-
	10	56.2	19.6	26.8	Sl3	1.1	> 100
	40	42.1	15.9	21.1	gSms	1.5	380
	80	40.6	11.1	13.4	mSfs	1.6	200
	160	47.7	16.0	18.0	mSfs	1.4	312
DGD_H1	5	47.7	24.1	36.9	Su2	1.4	185
	10	48.8	21.7	34.0	Sl2	1.3	160
	40	45.9	18.1	27.6	Sl2	1.4	130
	80	40.0	12.0	18.5	Su2	1.6	95
	160	36.3	5.7	34.0	Ls3	1.7	20
DGD_H2	5	53.4	24.8	42.0	mSfs	1.1	> 375
	10	54.3	23.5	40.0	mSfs	1.1	-
	40	36.5	12.6	25.9	Sl2	1.7	50
	80	32.7	1.6	32.4	Lts	1.8	< 5
	160	48.1	28.8	33.2	Su2	1.4	155

One conclusion that can be drawn from these observations at the green spaces (sections 4.1a and b) is that at these sites the groundwater table depth, and thus the capillary rise in the unsaturated zone, is most likely to be the major controlling factor for soil hydrology and for the water dynamics within the soil column. At sites with permanently shallow groundwater table of about 40 cm depth only minor low frequency fluctuations of *VWC* and *SWT* can be identified within the entire soil profile. Measurement data at nearby sites with lower groundwater table (0.9 to 1.2 m) indicates

[12] soil texture according to Ad-hoc-Arbeitsgruppe Boden (2005)
[13] "-" indicates no specification

an insufficient refilling to the upper layers during phases with little precipitation, while *SWT* remains at low values in greater depth and during periods with regular precipitation. However, at sites with a groundwater table below 1.6 m (the instrumented depth), the variation in soil water content depends predominantly on soil texture. The observation indicate that the SGD district green spaces shows a decrease of only about 10 % of *AWC* within the upper 40 cm whereas at the DGD district sites about 35 % of *AWC* are lost through evapotranspiration and percolation.

c) Housing areas

Within the housing areas, the soil substrates at the SoilStations in general feature coarse particle sizes, which are associated with higher saturated hydraulic conductivities of commonly more than 100 cm d^{-1} in the upper soil layers (Table 3.2 and Table 4.2). Thus, *VWC* values (Figure 4.1f-i) are lower in general and less variable in absolute values as well as relative to *AWC* (Table 4.2) throughout the measurement period. Percolation appears to take place more rapidly and with only short-time effect on *VWC* at deeper layers.

At the housing area sites in the shallow groundwater level-district SGD_H1 and SGD_H2, soil water dynamics are considerably different to the nearby green space sites (section 4.1a), as well as in comparison with each other. In contrast to previous findings, here the dominant controlling factor on soil water dynamics is most likely the soil texture and substrate. Direct effects of groundwater level fluctuations are diminished by a drawdown of the groundwater table from drainage measures at this housing area (Table 3.2, information from personal communication).

The backyard's soil profile SGD_H1, featuring an entirely sandy soil texture, a low bulk density due to high organic matter content up to 40 cm depth and short grass vegetation, depicts *VWC* within the range of 10 % to 30 % in the upper soil (5 and 10 cm depth) throughout the vegetation period (Figure 4.1f). Spring drying is visible in a *VWC* decrease for depths down to 80 cm, with a loss of about 12 % of *AWC* during the three week dry period in April (Table 4.1). Concurrently, *SWT* increases steadily during the dry phase, penetrating into depth (Figure 4.2f). Thus, in this profile the

drying of near surface layers is, in addition to evapotranspiration, influenced by percolation. Only heavy summer rainfall events result in short-time peaks of moisture in the upper soil with relative increases of up to 15 % within a few days. The saturated hydraulic conductivities of > 185 cm d^{-1} and the pore volume of about 55 % in the upper layers (Table 4.2) indicate rapid infiltration and percolation of water within hours after intensive precipitation events in this sandy substrate.

At the second backyard soil profile in this district (SGD_H2, Figure 4.1g) the upper soil layers consist of loamy sand (5 % clay down to 10 cm) without coarse particles, e.g. construction waste or gravel. Thus, soil moisture from precipitation remains within the soil column for an extended time and is therefore detectable down to 80 cm depth, showing a retarded decrease of *VWC* after precipitation events. Deeper soil layers consist of sandy material and remain at a low *VWC* level throughout the year, even though a slight increase in late summer is measured, presumably as a result of prior continuous high precipitation over several days and slow percolation of soil water.

The two profiles within the housing area in the district with a deep groundwater table (DGD_H1 and DGD_H2) also differ clearly from each other, although located only 150 m apart from each other. The loamy sand profile DGD_H1 (Figure 4.1h) is characterized by a low *VWC* in general (< 16 %) and especially at the depths 40 and 80 cm throughout the whole studied period. Despite the little fluctuation of absolute water content *VWC, SWT* clearly varies in these depths from spring (up to 300 hPa in 40 cm / 100 hPa in 80 cm depth) to early summer (> 850 / 300 hPa) and in early August (> 850 / 500 hPa) (Figure 4.2h). During the dry phase in April, *VWC* within the upper 40 cm is reduced by nearly 35 % of *AWC* (Table 4.1), and *SWT* increases significantly. Subsequently, the water supplied by precipitation in early summer does not lead to a significant rise of *VWC* deeper than 10 cm depth. While at 80 cm and below *VWC* remains at nearly constant levels, in late summer and fall signs of slow percolation are found in *SWT* measurements (Figure 4.2h).

At the second backyard's soil profile (DGD_H2, Figure 4.1i) soil water dynamics expose distinct characteristics. This profile features a sandy soil texture with construction waste up to 50 cm depth, covered by a soil layer with high organic matter

content (bulk densities < 1.2 g cm^{-3} and high saturated hydraulic conductivity > 375 cm d^{-1}, Table 4.2) and a sandy clay loam with a high percentage of natural gravel below. *VWC* remains at nearly constant levels throughout the measurement period at all depths. Only heavy precipitation events (> 15 mm rain sum) lead to a short-time increase of *VWC* records, which are even detected at the lower measurement depths with a *VWC* increase of up to 10 % in 80 cm and 4 % in 160 cm depth. The impact of these events on soil moisture within the upper layers is only slightly more intense with about 15 % increases. After this distinct rise of *VWC*, nearly initial values are obtained after a comparably short period of about five days. Likewise, *SWT* alterations are observed only within the upper 10 cm and very slight ones down to 40 cm (Figure 4.2i). The sandy clay loam layer in about 80 cm depth of DGD_H2 with high bulk densities (1.8 g cm^{-3}) and a very low saturated hydraulic conductivity of < 5 cm d^{-1} (Table 4.2) seems to constitute the upper limit of an impermeable layer. This leads to nearly constant values in *VWC* and *SWT* throughout the measurement period.

To conclude, the housing area's soil profile water dynamics seem to be influenced mainly by soil substrate and specific soil layering, apart from groundwater management. It is noteworthy that, however, in analogy to the green space site's decrease of water in the upper 40 cm during the three-week dry phase in April (Table 4.1) a comparable percentual decrease of *VWC* on the *AWC* is found according to the prevailing groundwater table depth within the housing areas: At the SGD district backyards a decrease of only about 15 % of *AWC* is found, whereas *VWC* at the DGD district site shows a diminishing of about 35 % of *AWC*, as well.

4.2 Variability of topsoil moisture in the year 2011

Regarding the climate effectiveness of soils, the water availability at the soil surface is one important factor by controlling evaporation, alongside the water availability within the rooting depth which determines vegetation transpiration processes. Therefore, topsoil moisture, here this term is defined as the *VWC* within the upper five centimeters of the soil profile, is discussed in detail in the following. Local precipitation is the main input factor for topsoil water contents, and its percolation is controlled by

soil properties and of course the intensity of root water uptake in that depth and below due to the gradient of hydrostatic tension. As the mean precipitation amount is almost similar at all stations, the role of texture and substrate for controlling topsoil water dynamics is analyzed by the observation of seasonal trends in *VWC* and is discussed in relation to vegetation structures. Figure 4.3 depicts the variability of mean *VWC* in 5 cm depth for spring, summer and fall 2011 for each station. The observed seasons featured the following precipitation sums (observations at WD_F, fall data including November): spring (AM) 40 mm, summer (JJA) 287 mm, fall (SON) 88 mm.

Three different regimes of seasonal *VWC* dynamics can be identified, which are independent from vegetation coverage. The first type (label "1" in Figure 4.3) shows a rise in mean *VWC* from spring to fall 2011. This is the dominant type within HUSCO SoilStations, prominent at soil profiles with sandy to loamy sand topsoil substrates. This increase is caused by untypical high summer precipitation rates (123 % of the 30-year-average at WD_F) during this investigation period. Characteristic for this type of topsoil water regime is the location of measured field *VWC*s within the lower range of the *VWC*, determined by laboratory analyses (Figure 4.3, grey bars). These type 1 topsoil moisture trends are observed independent from vegetation, since short grass, high pasture grass as well as deciduous tree vegetation appear at these soil profiles.

The second type (label "2") of seasonal trends can be described as a curve-type form. Spring and fall *VWC*s are at a comparable level, while summer *VWC* differs. Type 2a comprises two sites with very high content of organic matter and a groundwater table in about 40 cm depth. Their level of *VWC* is the highest measured within the HUSCO sites during the whole period. However, under summer conditions mean topsoil *VWC* is significantly lowered. Conversely, the type 2b site DGD_H2 shows a relative increase in summer months' mean *VWC* and a subsequent decrease in fall. Probably this trend type is caused by the high water holding capacity of the sandy clay loam substrate below the organic upper layer. Type 2 trends arose under tree canopy as well as under grass covering. The sites have in common, that their mean field *VWC*s are within the upper range of the pore volume close to the saturated water content θ_s. Profile DGD_G3 shows a decrease in mean *VWC* for the studied period, and therefore it is labeled as

type “3”. This soil features a high content of loamy and clay-rich soil substrate, but it distinguished itself from the other profiles with loamy substrates by its location beneath a tight canopy of oak trees and the ground-coverage of herbs (Table 3.2). Here, a constant interception loss during rainfall events is most likely to have prevented a refilling of topsoil water by summer precipitation, as it is observed at other SoilStations of the HUSCO monitoring network. Studies on interception loss observed a loss of 29.3 % of gross rainfall for leafed canopy (deciduous trees in summer) (Herbst et al., 2008), or season-long loss of 18.8 % with single events ranging 9.4 % to 89.0 % (Price and Carlyle-Moses, 2003).

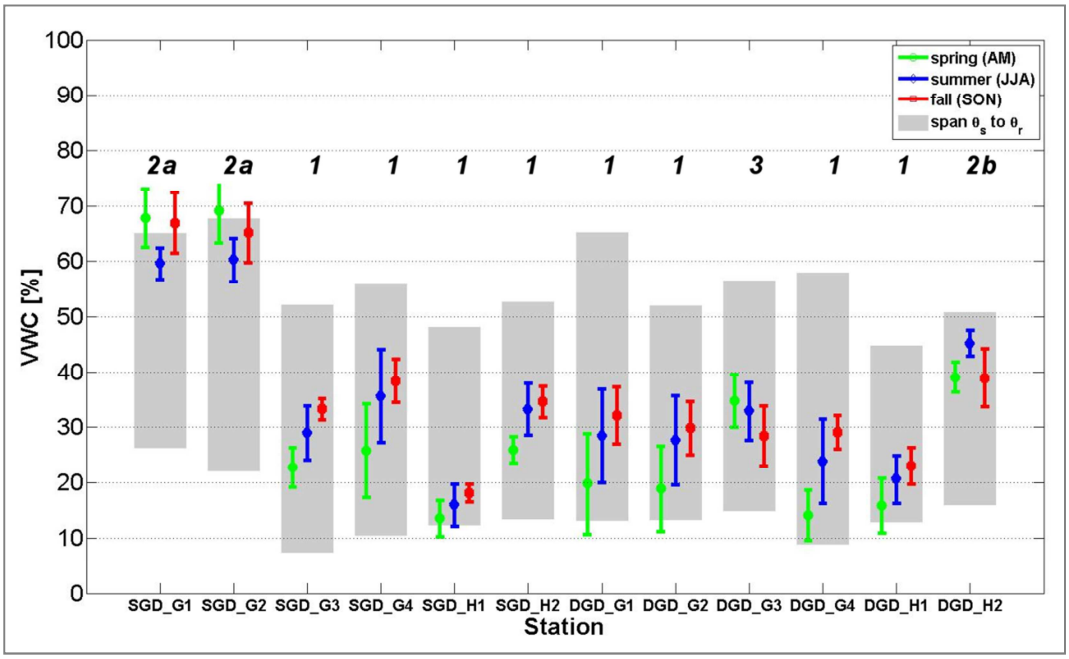

Figure 4.3 Seasonal variability of mean topsoil volumetric water content (*VWC*) (5 cm depth) at soil profiles in 2011. The standard deviation is illustrated as thin bars, grey boxes indicate the span between θ_r (residual volumetric water content) and θ_s (saturated volumetric water content) provided by laboratory analyses. Numbers above the bars name the type of seasonal trend.

Considering the standard deviation of the mean seasonal *VWC*, spring and summer water contents show a greater spread at most of the profiles, while fall measurements has a smaller range at all profiles of type 1. The housing area profiles show less fluctuation in all seasons, compared to green space soils. This circumstance is most

likely resulting from the rather sandy substrate found at the observed backyards and the short grass vegetation, while profiles with high grass vegetation (DGD_G1 and SGD_G4) feature a wider range.

From this analysis, the potential range of topsoil water contents within urban areas becomes well apparent. For all seasons the soil profiles SGD_G1 and SGD_G2 feature the highest mean *VWC* of all observed sites with a maximum of 68 % *VWC*, while at SGD_H1 the lowest topsoil moisture contents are observed (12 %). Hence, a difference of up to 56 % in mean *VWC* is observed within a spatial distance of less than 1 km (mean fall *VWC* at SGD_G1 compared to SGD_H1).

Apart from the analysis of the seasonal trends, in Figure 4.6 a shortcoming of the comparison of laboratory analyses and field measurements is apparent. For the sites SGD_G1 and SGD_G2 the values of *VWC* in spring, and for the latter in fall as well, are higher than the determined saturated water contents θ_s derived from laboratory analyses. For these two sites, the field measurements show values above the given θ_s for long periods throughout the data series, about 2 % mean deviation, but up to 12 % for the 90^{th} percentile. This mismatch of field and laboratory values was found in several studies as well: For silt loam Wessolek et al. (1994) observed a deviation of about -4 % of the estimated θ_s from the maximum of *VWC* measured in-situ. Pachepsky et al. (2001) specify the average difference between field and laboratory water contents as -0.6 % but found deviations of up to -10 % for samples with a sand content of less than 50 %. The analyses of Cornelis et al. (2001) revealed a difference between field observations and predicted saturated water content from soil samples of -5 % to +5 %. The explanations hypothesized are the combination of entrapped air in the field soil, alterations in bulk density in the laboratory samples (Morgan et al., 2001), spatial variability, hysteresis (Pachepsky et al., 2001), or the number of samples (Cornelis et al., 2001). For the present studies deviation, the high organic content of the two soil profiles presumably leads to hysteresis effects and alterations in the bulk density of the undisturbed soil core samples, resulting in this disagreement.

4.3 Comparison of soil water dynamics in 2011 to data in 2012

The vegetation period of 2011 and 2012 differ from each other in their meteorological characteristics. Table 4.4 shows the mean seasonal values as they were observed at WD_F for the seasons of the vegetation period 2011 and 2012 as well as the annual and 30 year averages.

2011 appeared to have been an unusual year in terms of precipitation and hours of sunshine averaged over the whole vegetation period and even more so for the individual seasons. Spring and fall were exceptionally dry and sunny, while summer months had higher rainfall compared to the 30 year mean. In contrast, 2012 tended towards the average in seasonal values of precipitation and temperature. The precipitation over the vegetation period though is slightly increased compared to the 30 year average (6 % more). Comparing the two years with each other, 2011 featured a far more pronounced seasonal variation in precipitation than 2012 while the air temperature amplitude was slightly less distinctive. 2011 was 1 K warmer and featured about 20 % less precipitation during the vegetation period, and, even weightier, less than half the amount of rain in spring and fall respectively. Also the distribution of the precipitation throughout the year differs: While the 30-year-average of days with precipitation comes to 191 days, in 2011 only 172 days with rain were recorded (10 % less than the 30-year average), and on the contrary 2012 featured 215 rainy days (13 % more).

Thus, it can be assumed that these meteorological differences have a considerable impact on soil hydrology. Therefore distinct temporal progresses in the soil water dynamics at the SoilStations themselves could be expected and presumably also the effects on the spatial variability would be pronounced differently. A comparison of the temporal evolution of *VWC* (Figure 4.1 to Figure 4.4) at the SoilStations, and of *SWT*, respectively (Figure 4.2 to Figure 4.5), however, does not confirm the intuitive conclusion that soil water dynamics of 2012 are less distinct with smaller amplitudes and higher water contents and lower water tensions, respectively, in general. Again, it is rather depending on the single soil profiles' characteristics and groundwater table depths how much the soil water dynamics of 2012 differ from the ones in the prior year.

Table 4.4 Meteorological parameters during vegetation periods 2011 and 2012 and 30-year-average (1981-2010), averaged for seasons. Spring (AM), summer (JJA) and fall (SON) and mean value for the whole vegetation period (01 April - 31 October). Observations at WD_F. T_a = air temperature, *RR* = precipitation sum, so = hours of sunshine.

season	time	T_a [°C]	*RR* [mm]	so [h]
spring	2011	10.0	40	646
	2012	9.5	108	473
	30 year	10.8	100	391
summer	2011	16.9	287	513
	2012	16.6	249	558
	30 year	17.1	235	620
fall	2011	10.4	88	329
	2012	9.8	171	288
	30 year	9.7	204	307
vegetation period	2011	14.5	408	1280
	2012	13.5	485	1149
	30 year	13.8	469	1264

The typical sinusoidal cycle of *VWC* change, as it was identified for 2011 at all stations, although with distinct intensities, is apparent in 2012 as well: During the summer months a defined drying of the upper soil layers, in particular the layers within the rooting depth, is visible, followed by a rewetting from soil surface towards lower depths in fall. Due to a lack of longer periods without precipitation, the dry phase effects of April/May 2011 are not replicated at any time in the vegetation period of 2012. In general, the same range of *VWC* values is found at all sites compared to 2011, with a slight tendency to higher water contents in average. The differences of mean *VWC* and maximum *VWC* in 2012 compared to 2011 are given in Table 4.5. Within the layers down to 40 cm depth the mean *VWC* in 2012 is higher or comparable for the most soil profiles, except DGD_G3, which is discussed below. Only in inferior layers of the profiles within the housing areas mean *VWC* is slightly diminished. The maximum *VWC* are more variable at the green space sites, yet showing increased values to the most part.

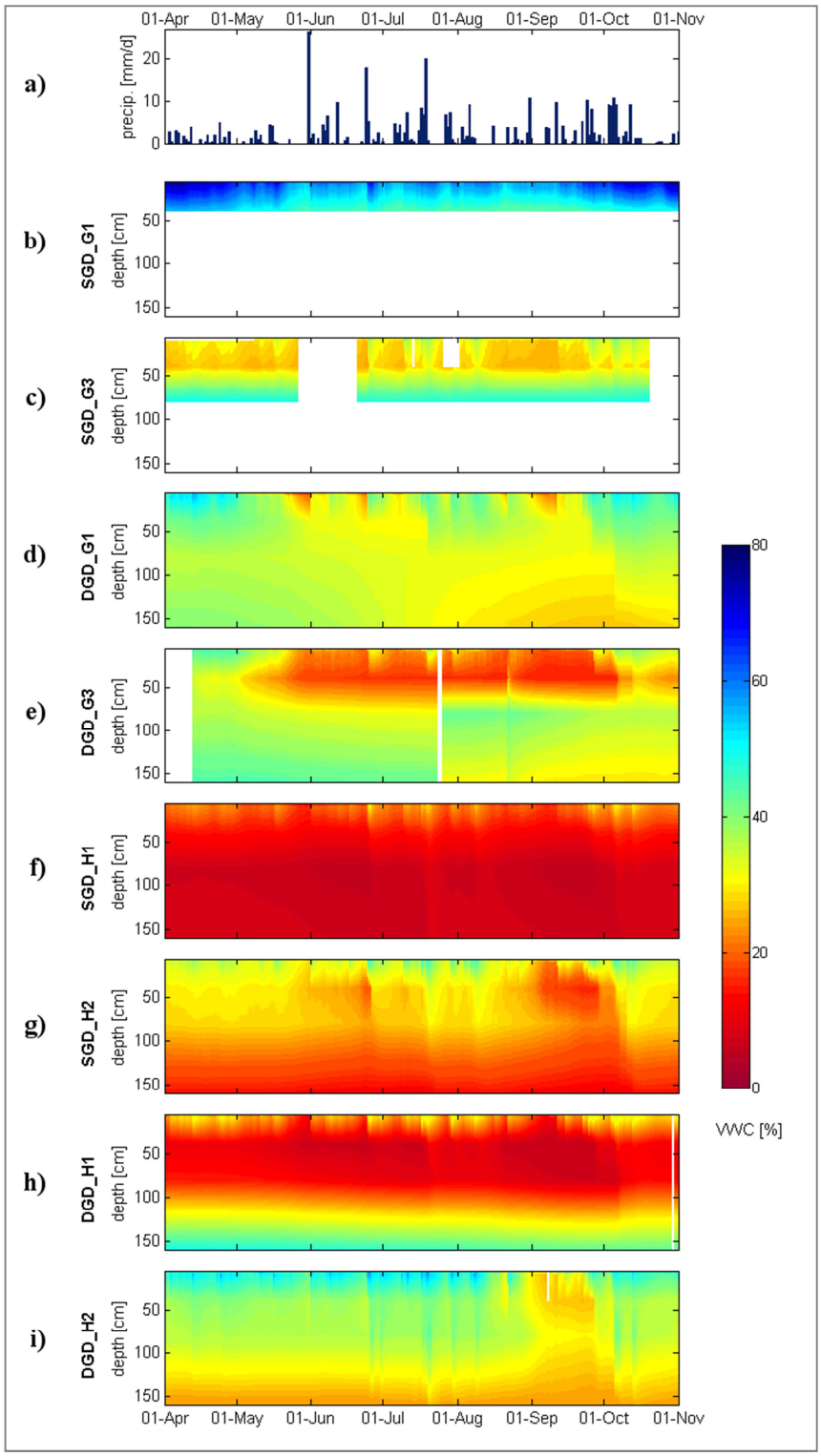

Figure 4.4 Precipitation at reference station WM (a, upper row) and 2D time-depth evolution of volumetric water content (*VWC*) at eight exemplary soil profiles in 2012 (linear interpolation between measurement depths).

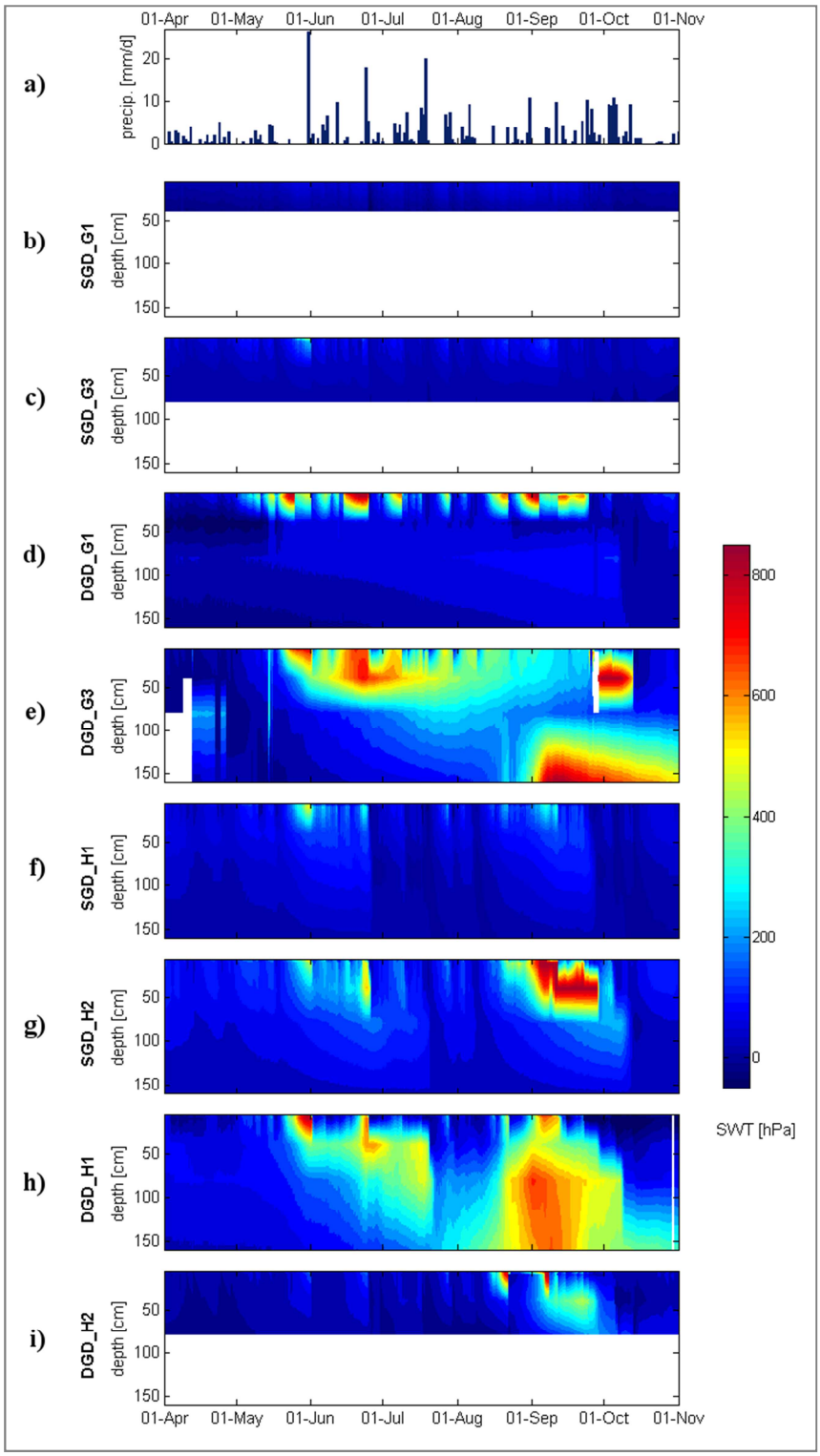

Figure 4.5 Precipitation at reference station WM (a, upper row) and 2D time-depth evolution of soil water tension (*SWT*) at eight exemplary soil profiles in 2012 (linear interpolation between measurement depths). Values of *SWT* estimated to be > 850 hPa are depicted in the dark red color, white spaces indicate non-gap-filled missing data.

Table 4.5 Deviation of maximum and mean *VWC* in 2012 compared to 2011 for all SoilStations and depths ($\Delta VWC_{year} = VWC_{2012} - VWC_{2011}$) in percent [%].

	ΔVWC_{year}	5 cm	10 cm	40 cm	80 cm	160 cm
SGD_G1	max	0.4	1.7	-1.8		
	mean	-0.5	3.3	0.0		
SGD_G3	max	10.2	-1.5	9.0	0.5	
	mean	8.9	2.6	1.8	2.9	
DGD_G1	max	8.8	6.4	0.7	-0.3	-3.1
	mean	6.5	6.4	2.4	1.1	0.1
DGD_G3	max	-1.2	2.1	1.4	5.3	0.2
	mean	-1.7	-3.3	-1.6	1.8	-6.2
SGD_H1	max	4.0	1.6	-0.3	0.0	-0.1
	mean	2.7	2.6	0.4	0.3	0.4
SGD_H2	max	11.4	-2.4	-2.3	0.5	-3.8
	mean	3.9	0.9	-1.1	3.0	0.1
DGD_H1	max	3.5	3.7	1.3	-0.8	-0.9
	mean	4.7	4.4	0.3	-0.7	-1.1
DGD_H2	max	5.7	-0.3	-0.5	-1.5	2.0
	mean	3.3	-0.4	1.5	-1.0	1.9

a) Green spaces with shallow groundwater table

At SGD_G1, with an estimated groundwater depth of 0.4 m the constant high *VWC* values and low *SWT* values, respectively, are found again. The lower groundwater table at SGD_G3 (1.2 m, Figure 4.4c and Figure 4.5c) also effects a constant *VWC* in the subsoil (depths below 40 cm) throughout the period (40-45 %). The more constant precipitation during the year increased the *VWC* in the upper soil here (up to 8.9 % absolute higher mean *VWC* in 5 cm depth, Table 4.5). Water percolated into deeper regions (≥ 40 cm) after precipitation events more often, compared to 2011. Due to the missing dry-phase in late spring, no considerable drying occurs at this site (nor at SGD_G1) at any time. *SWT* thus remains at constant low values of less than 250 hPa (Figure 4.5c)

b) Green spaces with deep groundwater table

At the low groundwater table district's green spaces (DGD) again the annual course of soil hydrological parameters is more pronounced compared to the shallow groundwater district, as it was found to be in 2011. Yet the two observed profiles tend

to some deviations from the progress in 2011: At the grass-covered profile DGD_G1 (Figure 4.4d) the spring rain percolation reduces the drying of the upper soil in spring and summer, leading to a less intensive decrease of *VWC* within lower depths of the profile in summer and fall, as it was found to proceed into depth in 2011. Instead, the short phases of little precipitation are visible within the upper 40 cm, interrupted by a deeper percolation of water after rain events. Thus, the mean as well as the maximum *VWC* in layers down to 40 cm is higher in 2012 compared to 2011 (in 5 and 10 cm depth more than 6 %, in 40 cm depth 2.4 % at average, Table 4.5). Measurements of *SWT* (Figure 4.5d) also indicate a less intensive drying in depths of 40 cm and 80 cm as the tensiometers' measurement range of 850 hPa is not exceeded here in early summer as it occurred in 2011. In fall again a loss of *VWC* is visible in depths below 1 m. This repeated occurrence supports the assumption made for 2011 that intensive percolation together with root water uptake leads to this effect.

The SoilStation DGD_G3, located within a stock of trees, in contrast shows a more intensive variability of soil water dynamics with higher amplitudes during the course of the vegetation period 2012 (Figure 4.4e) compared to the prior year. Again, the reduction of *VWC* starts in spring in 40 cm depth but increases faster and to a greater vertical extend this time, presumably due to the intensive root water uptake down to this depth (the rooting depth is about 45 cm, Table 3.2). This is also visible in the deviation of mean *VWC* (Table 4.5), which is lower for these depths. The *VWC* of the upper soil layers (5 and 10 cm) is even more diminished and precipitation events do not lead to a rewetting for the longer term, as they do not percolate as deep as they were found to do in 2011. This near-surface drying this time is also visible in *SWT* data (Figure 4.5e) in June, whereas later in the summer *SWT* is lower, affected by regular summer precipitation. The water flow is clearly visible in terms of gradients between the *SWT* of the measurement depths: after precipitation the topsoil shows low values which continue into depth over time, and analogous a drying during low-precipitation periods succeeds from upper layers to the lower. In comparison, a drying starting from the rooting depth, i.e. 40 cm, due to root water uptake is pictured as a decrease of *SWT* starting in the deeper layer progressing towards upper layers. This effect is clearly

visible in June 2012 as it was also found for August 2011. In 2012 again this soil profile shows the effect of slow percolation most clearly starting September, in terms of a *VWC* decrease (down to about 30 % compared to 39 % in 2011) as well as in a *SWT* increase up to 850 hPa in 160 cm depth. In depths above the rooting depth (about 50 cm) an increase of *SWT* to values above 850 hPa appears in the early fall. This finding supports the hypothesis stated for the observations of 2011 that in this depth an intensive root water uptake occurs, as a water supply by layers in 80 cm and below is not possible due to the low saturated hydraulic conductivity there (only 16 cm d^{-1} in 160 cm depth, Table 4.3). A possible explanation for the lower *VWC* throughout 2012 could be that the continuous precipitation in this year is, to the most part, evapotranspirated from the upper soil layers or transpirated by the deeper rooting plants and trees, as more solar radiation in 2012 (9 % more hours of sunshine) potentially increased the photosynthesis rate. Single precipitation events of higher intensity and more water amount would have lead to more infiltration and percolation, and thus to more refilling of water in greater depths, as it was observed in 2011.

The observations of the green space water dynamics in 2012 (sections 4.3a and b) again show that a high groundwater table influences the water contents and tensions within the whole soil column. Even though the range of *VWC* and *SWT* differs from 2011 at the soil profiles compared to themselves, comparing the sites with each other shows similar trends and reactions to precipitation and seasons.

c) Housing areas

At the housing areas SoilStations at both districts the differences of *VWC* between 2011 and 2012 are not particularly remarkable. Again the absolute values are lower in general throughout the vegetation period. The frequent rain events lead to percolation down to the same depths. At the shallow groundwater districts' housing area *VWC* of the more sandy profile SGD_H1 progresses almost identically as in 2011 (Figure 4.4f). The percolation seems to be constantly high, again interrupted by short time peaks after rain events. Only *SWT* in early summer differs owing to the dry period in 2011 which is abundant in 2012 (Figure 4.5f), so that almost no increase of *SWT* within the upper soil

layers occurs. At soil profile SGD_H2 with a more loamy texture in the upper soil (down to 10 cm) this difference in spring and summer *SWT* also appears, with only slight signs of short time drying in 2012 (Figure 4.5g), complemented by a higher *VWC* in 5 cm depth (Figure 4.4g and Table 4.5). Notably in 40 cm depth the *VWC* is higher in early spring (33 % compared to 27 % in 2011). Water contents in greater depths (below 80 cm) remain again at constant low levels due to the sandy substrate. However, in fall 2012 this soil profile differs distinctly from the prior year, as it was also found for DGD_G3. In depths down to 80 cm the *VWC* considerably decreases, staring in September (most definite in 40 cm depth from 30 % down to 13 %) and lasting until mid-October. As presumed before, vegetation root uptake of water as well as a more constant evapotranspiration of the less intensive yet more frequent precipitation from the upper soil layers in combination with less infiltration and percolation and capillary rise from lower areas (layers with reduced saturated hydraulic conductivities of only 85 cm d^{-1}) might cause this effect for the more loamy soil texture. This effect is visible also in fall 2012 *SWT* reaching values above 850 hPa.

Within the deep groundwater districts' housing areas (DGD_H1 and DGD_H2) *VWC* progress in 2012 is similar to 2011 at both sites (Figure 4.4h and i). The percolation depth of precipitation does not differ significantly, nor do absolute values deviate much. Yet *SWT* at DGD_H1 (Figure 4.5h) exhibits differences in soil water dynamics within the soil column which are not that apparent in the constantly low *VWC* values. Apart from a less intensive drying in spring and summer due to more frequent rain events, this profile also features the very pronounced increase of *SWT* in fall within deeper areas (below 40 cm). Because no roots were found in these depths, most likely slow percolation in combination with a lack of refill from water infiltrating into topsoil layers in late May causes this effect. At the profile DGD_H2 this remarkable effect in fall 2012 is also visible. Here, the fairly constant *VWC* values feature a definite decrease in fall, most intensive at the sandy textured layers, e.g. from 35 % down to 28 % in 40 cm depth, but even in the more loamy layer down to 80 cm (Figure 4.4i). In the sandy upper layer this is also apparent in a *SWT* increase, even though this effect is less intensive (Figure 4.5i).

Some conclusions can be drawn from the analysis of *VWC* and *SWT* progression within the soil profiles during the vegetation period 2012, supplementing the knowledge gained from 2011 analyses. The meteorological conditions during late summer and fall (August to October 2012) lead to more distinct drying within different areas of the soil columns, depending on soil texture (presumably soils with loamy texture and low saturated hydraulic conductivities in the upper layers are more prone to this impact) as well as vegetation (root water uptake). As a percolation of water from precipitation is diminished at these soils, increases in *SWT* in layers below are observed. While the presence of layers with low saturated hydraulic conductivities certainly has an influence at the deep groundwater district sites (DGD_G), at profiles with a high groundwater table depth (SGD_G) no exceptional effects can be made out for fall 2012 due to the capillary refill of water from lower soil layers into the upper areas. With the exception of profile DGD_G3, the constant rain events throughout the vegetation period lead to less variable water dynamics in the upper soil layers. A consideration of the seasonal trends of the topsoil water content in 2012 provides additional information, given in the following section.

d) Comparison of the variability of topsoil moisture

The mean seasonal topsoil water content in 5 cm depth for 2012 is shown in Figure 4.6. The precipitation observed at WD_F for these seasons summed up to 108 mm in spring (AM), 249 mm in summer (JJA) and 171 mm in fall (SON).

Most clearly the effect of the more equally distributed precipitation sums stands out in the form of a general increase of the 5 cm *VWC* at almost all profiles, as well as the shift of type 1 seasonal trends towards type 2a at all four DGD_G stations. This type features a decrease of *VWC* in summer followed by a recovery in fall. This tendency is plausible, caused by higher spring precipitation, decreased summer precipitation in 2012 compared to 2011, but more than twice the fall rain amounts. Thus, spring *VWC* is not diminished to the same extend as observed in 2011. Furthermore, during summer months at the deep groundwater district green spaces (DGD_G) evapotranspiration reduces the topsoil water content more noticeably, while a refilling through capillary

rise from lower areas appears not to occur, while it presumably does take place at shallow groundwater district sites SGD_G3 and SGD_G4.

The constant increase of topsoil *VWC*, i.e. type 1 seasonal trends, is found at SGD green spaces with less shallow groundwater tables (0.9 m and 1.2 m respectively), as well as at the sandy and loamy sand housing area's upper layers SGD_H1 and DGD_H1, at the latter two stations at a very low absolute *VWC* level. At SGD_G1 and SGD_G2, the soil profiles with a constant high groundwater table, type 2a seasonal trend can be identified again with comparable intensity. At SGD_H2, the more loamy soil texture in 5 cm depth follows a slight type 2b seasonal trend in 2012. Its distinctness is comparable to the more dampened amplitude of this trend observed at DGD_H2 in 2012, as it was more pronounced in 2011.

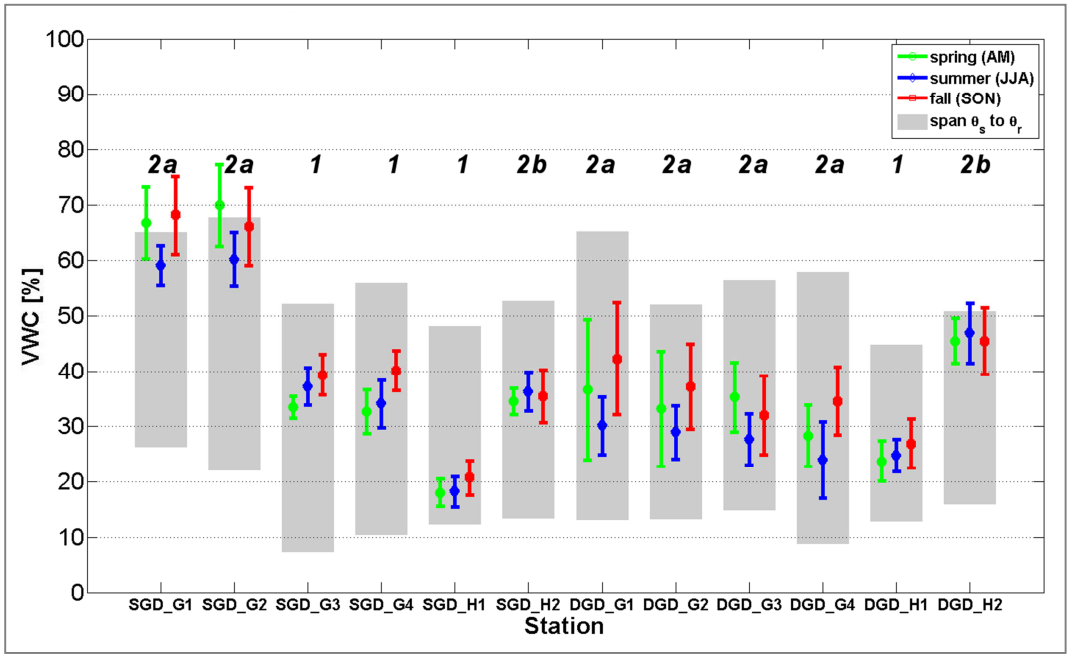

Figure 4.6 Seasonal variability of mean topsoil volumetric water content (*VWC*) (5 cm depth) at soil profiles in 2012. The standard deviation is illustrated as thin bars, grey boxes indicate the span between θ_r (residual volumetric water content) and θ_s (saturated volumetric water content) provided by laboratory analyses. Numbers above the bars name the type of seasonal trend.

Type 3 seasonal trend, i.e. a decrease of topsoil moisture from spring to fall, does not occur at the observed sites in 2012. This is most probably due to the higher precipitation rates in fall. As in 2011 it was only effective at DGD_G3, the loamy textured soil beneath a stock of trees at the deep groundwater districts green space, in 2012 this soil profile reveals an increase of *VWC* in 5 cm depth towards fall. Most likely evapotranspiration from near-surface layers does not occur to the same extend as it did the year prior. In addition, the interception loss that is assumed to contribute to the decrease of *VWC* in 2011 at this site might be less intensive.

The standard deviations of topsoil seasonal mean *VWC* own comparable characteristics as in 2011, with a great spread in spring, but at type 2a sites also in fall. The drying within the upper layers in September, mentioned above, most likely contributes to this statistical peculiarity, because during this phase *VWC* in 5 cm decreases and afterwards increases to typical high values in late fall again. The by far widest range during spring and fall show soil profiles DGD_G1 and DGD_G2. This is most likely resulting from the combination of the high pasture grass vegetation, deciduous trees and ground cover plants respectively, leading to increased transpiration, the more loamy soil texture, allowing higher *VWC* after precipitation, and the low groundwater table depth without visible signs of capillary rise and refilling.

4.4 Discussion of the soil water variability at urban sites and its possible impact on local climate

The datasets on the variability of soil water dynamics of urban soils presented in this study offer a unique pool of information on urban soil water dynamics. They demonstrate well that soil water dynamics at urban sites behave in very distinct manners. Very shallow groundwater (as observed here within 0.4 m below surface) leads to constant high *VWC* and low *SWT*, induced by capillary rise, whereas soils with a deep groundwater table depth show a distinct variation of *VWC* and *SWT* during wet and dry phases of the two seven-month investigation periods. At green space sites with a groundwater depth of 0.9 and 1.2 m, relatively high topsoil moistures, increasing in the course of the vegetation period with exceptional high summer precipitation especially in 2011, and less enduring increase of *SWT* of the upper soil layers during dry

phases, indicate a slight effect of the shallow groundwater table on the upper layers' soil hydrology through capillary rise as well. In contrast, at green spaces with a deep groundwater table (> 1.6 m) no signs of capillary rise and topsoil refilling from groundwater can be made out, and drying occurs in greater depths and more prolonged. Even though the observed vegetation periods of 2011 and 2012 were distinct in the distribution of rain events and seasonal precipitation amounts, in both years the soil profiles show comparable trends in the dynamics of water content and tension, yet to a varying degree. Thus, soil properties, groundwater table depth and vegetation have a far more substantial impact on soil hydrology than meteorological conditions do in soils with this wide variability of pedological and hydrological characteristics.

A distinct effect from low precipitation periods, associated with a lack of water refill from the surface, can be made out according to the districts' mean groundwater table depth and nearly independent from the urban land use: The observations made in the three-week dry phase in April 2011 show, that in soil with shallow groundwater a decrease of only about 10 % of *AWC* occurs, whereas at in soil with deep groundwater table about 35 % of *AWC* are lost. Thus, the effect of groundwater table depth on drying processes and surface soil moisture can clearly be confirmed to occur at the observed green space sites: groundwater most prominently leads to increased water contents and less water tension in the upper layers of soils with a shallow groundwater table (0.4 m), less distinct in soils with a water-table of about 1 m, and unverifiable in soils with a groundwater table depth below 1.6 m. As a consequence, soil drying in areas with a deep groundwater table depth and the reduction of available water in the upper soil layers during times of little precipitation will result in reduced recharge and evapotranspiration, and thus reduced latent heat fluxes and minor cooling effectiveness of these soils. This relationship was demonstrated by the modeling approach of Maxwell and Kollet (2008) who identified largest latent heat fluxes occurring in areas with shallow groundwater (< 2 m below surface) and a decrease of latent heat fluxes below 2 m water-table depth. In the present study this relationship between groundwater table depth and water content of the upper soil layers is, in all conscience, analyzed in soils of urban areas for the first time.

In case of natural or anthropogenic reduced groundwater levels (> 1.6 m below surface), the dominating effect of soil texture and organic matter content is clearly identified within the *VWC* and *SWT* annual progression for both vegetation periods 2011 and 2012. This impact of soil properties on temporal soil moisture variability and patterns is described in many studies for different scales (e.g. Robock and Vinnikov, 2000; Western et al., 2002) and has been monitored for non-urban land use soils in case studies, as described in Chapter 2.2 (e.g. Famiglietti et al., 1999; Pan et al., 2012; Robinson et al., 2008). However, apart from the immediate effects of a sealed surface which are not subject to the investigations, in this study the impact of urban land use is not found to be distinct in this study.

As mentioned, surface water content and availability can be a determining factor for local climate variability by inducing higher actual evapotranspiration rates. Brubaker and Entekhabi (1996) as well as Daly and Porporato (2005) stated that soil surface moisture availability is one determining factor for evapotranspiration and thus influences latent heat fluxes and air temperature. While varying climate impacts on soil moisture have been observed (e.g. Illston et al., 2004), the inverted correlation is known and often stated, but research on soil moisture feedback on climate most often focuses on local recycling of evapotranspiration for rainfall (D'Odorico and Porporato, 2004; Findell and Eltahir, 1997). Especially on a local and microclimatic scale, the impacts of soil surface evaporation and of evapotranspiration by vegetation covering on air temperature and human comfort due to reduced felt air temperature is little researched in field measurements (Krakauer et al., 2010). Until now, these observations were made for natural environments. Surveys regarding these effects especially in an urban environment have, to best knowledge, not been carried out so far.

Due to the heterogeneous structure of urban areas, soils within cities are highly variable within small spatial scales, as the observations of the SoilStations in the present study reveal. Thus, soil water dynamics rather vary at these scales as well, as shown. Hence, their impact on the local climate will also differ at small-scale. It can be expected from this finding that the cooling effectiveness of soils through latent heat fluxes varies, depending on soil properties and groundwater table depth. Presumably, a

shallow groundwater table, as observed in SGD, contributes to higher latent and diminishes sensible heat fluxes, in comparison to deep groundwater table district sites DGD. As the recent survey by Damm et al. (2012) within the urban environment of Bottrop, Germany, indicated, an improvement of the use of soil as water storage can lead to a reduction of “urban hotspots”, i.e. sources of increased sensible heat fluxes, by increasing the cooling capacity of urban soils. In the following Chapter 5 this relation is further examined by evaluating and interpreting the measurements of the MeteoStations.

5 Variability of urban meteorological parameters

The heterogeneous urban surface exerts an impact on the local meteorological parameters. Depending on greater weather conditions, season and daytime, this impact varies in its intensity (e.g. Houet and Pigeon, 2011; Voogt, 2003). In Chapter 5.1, first the observed variability of the meteorological parameters at urban sites in Hamburg is described. Afterwards focus lies on the consideration of the urban air temperature. In Chapter 5.2 the nighttime UHI effect as it is found within the measurement network is analyzed, regarding spatial peculiarities and factors influencing its intensity. The daytime air temperature variability between the MeteoStations is considered in Chapter 5.3. And as this parameter is the one that is mainly influenced by evapotranspiration, a closer look at soil moisture as a possible impacting factor on air temperature is taken.

5.1 Annual and seasonal variability at urban sites

The measurements of the meteorological parameters at the six observed MeteoStations show clear differences in the mean diurnal cycles (01 September 2011 to 31 August 2012)[14] as depicted in Figure 5.1 and Figure 5.2. Air temperature (T_a) measurements reveal most apparently a distinction between the inner city sites C and the suburban sites SGD and DGD. While the inner city sites feature the highest mean T_a at all times, pronounced during the daytime and more definite at night, MeteoStations at the suburbs are significantly cooler during the night. At a second level a distinction between the suburban sites is evident as well: the two sites within the deep groundwater district (DGD) are slightly warmer during the night compared to both shallow groundwater districts' sites (SGD). Starting late morning and reaching up to late afternoon both districts have a comparable mean diurnal T_a evolution. In third order, even a more detailed distinction can be made at the inner-district-level. The city centre sites perform alike in their mean annual diurnal cycle with a slightly faster warming during the morning hours at C_2. Within DGD the green space site is cooler than the

[14] This timeframe was chosen for analysis because MeteoStation C_2 was setup not until late August 2012. Thus, a complete data set of all MeteoStations is only available from that time on.

housing area during the night, about 0.3 K, and shows similar T_a during daytime, while at SGD both sites resemble. Here, the housing area site SGD_H exhibits a remarkable feature: in the morning a faster increase of T_a *is* observed throughout the year, and is thus clearly visible in the mean diurnal cycles. This phenomenon has been under research in detail by temporarily running additional measurement stations at different sites within the same housing area (Beuchel, 2012). This effect appears within the whole suburb area of this district. However, an explanation is not obvious, yet.

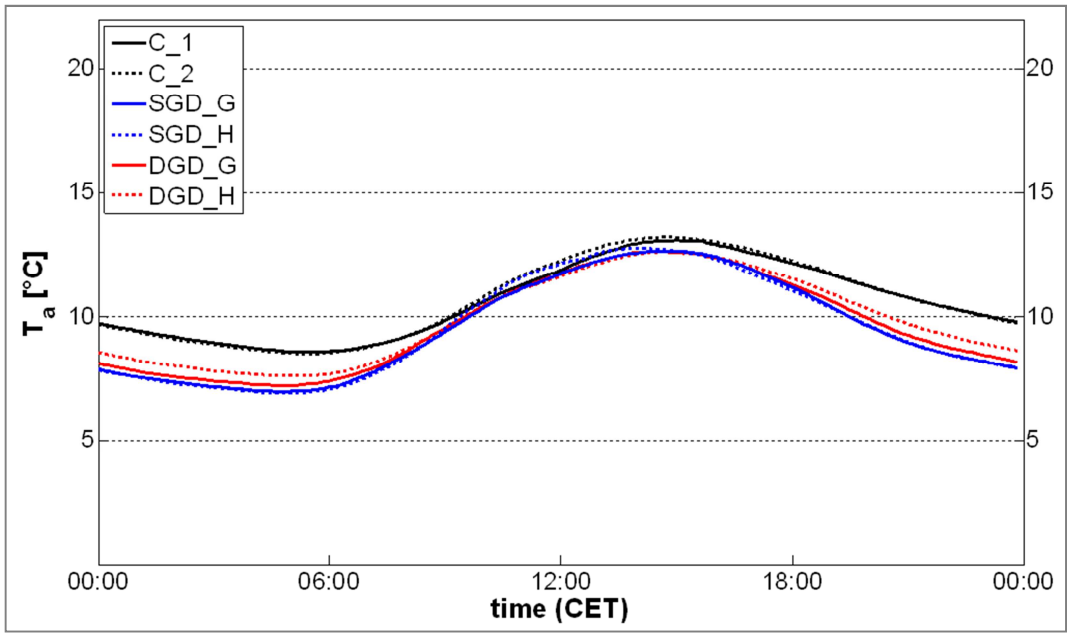

Figure 5.1 Mean diurnal cycle of air temperature (T_a, 10min-mean) for 01 September 2011 to 31 August 2012.

Apart from a different diurnal cycle in the annual mean T_a, also variations of specific humidities (q) are found. The specific humidity, the ratio of water vapor to dry air, is considered instead of looking at the relative humidity, as q is independent from air temperature. Thus, it is a better parameter to compare mean values of humidity at several sites. Again, the most pronounced differences occur first between the districts, but then also at the inner-district level between the land use types at both suburbs. While at the inner city sites C_1 and C_2 the amount of water in the air is at a nearly constant level throughout the whole course of the day (Figure 5.2), the suburb sites have

a somewhat more defined diurnal cycle. During daytime *q* increases, with higher values at SGD compared to DGD. The green space site SGD_G also features the highest absolute air water contents, with a prolonged higher *q* until after midnight. At the inner city sites an additional distinction can be drawn: The “modern core” site C_2 within the new built-up district HafenCity, which is very close to the river Elbe, is more humid than the “old core” site C_1, more distant to open water. These observations for the sites in district C, as well as for the inner-district land use differences between the suburban categories green space (G) and housing area (H), indicate a dependency of air humidity from water availability, as it is to be expected. Open water, as present at C_2, as well as a higher rate of vegetated areas and uncovered soil, i.e. green spaces, provides the water for an actual ET amount closer to the climatic possible ET, which is depending on saturated vapor pressure and air temperature, respectively. However, vegetation appears to be more effective to air humidity than open water, as at both suburban districts higher *q* values are found for daytime compared to C_2.

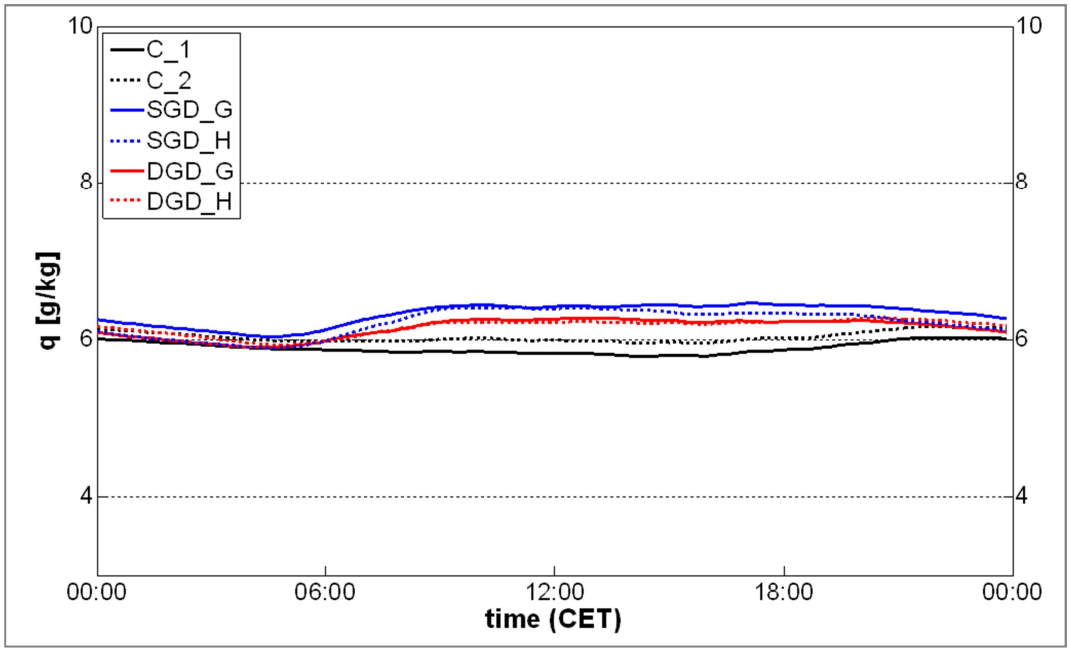

Figure 5.2 Mean diurnal cycle of specific humidity (*q*, 10min-mean), 01 September 2011 to 31 August 2012.

As shown, differences at the inter- as well as at the inner-district scale are visible already in the mean diurnal cycle of a whole year. It can be presumed, that these characteristics are found to be even more distinct during certain conditions that promote the development of differences in air temperature and air humidity, respectively. A simple division into seasonal mean diurnal cycles shows that the greater climatic conditions, e.g. higher air temperatures in general as given during summer months, promote the formation of a site-characteristic behavior of the meteorological parameters.

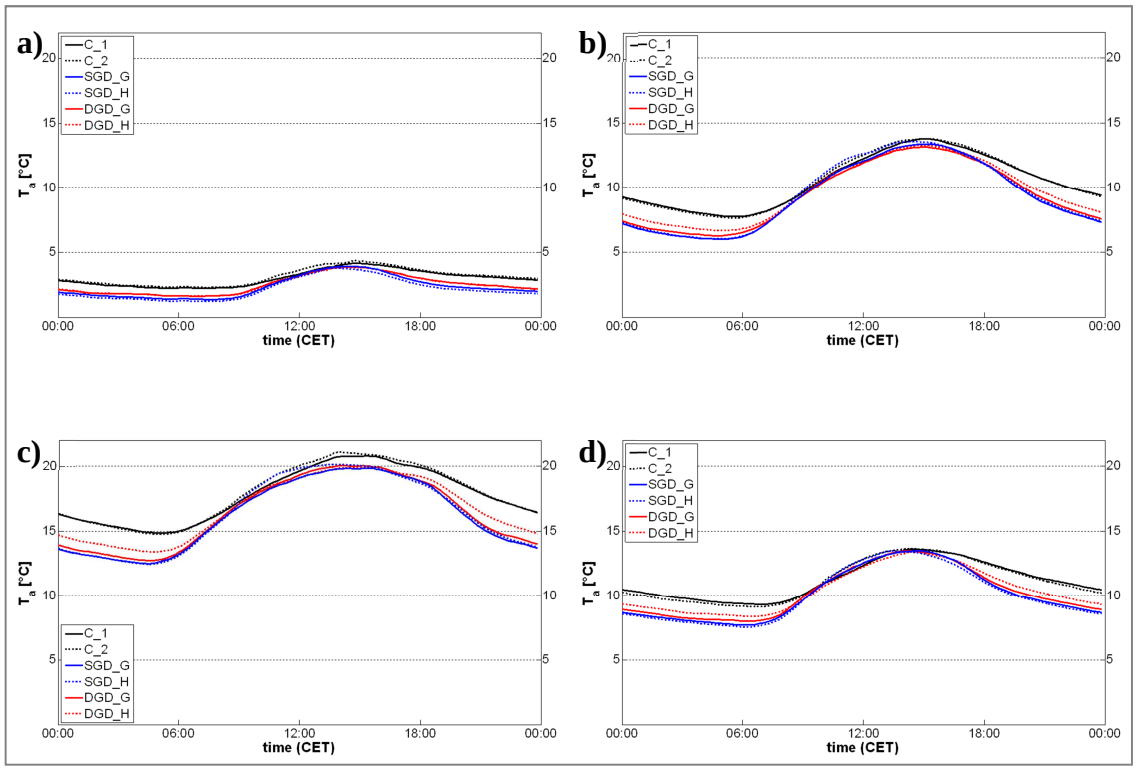

Figure 5.3 Seasonal mean diurnal cycle of air temperature (T_a, 10min-mean). **a)** winter (DJF) **b)** spring (MAM) **c)** summer (JJA) **d)** fall (SON), for 01 September 2011 to 31 August 2012.

During winter (Figure 5.3a) the measurements at the MeteoStations deviate the least from each other. From late morning (about 11:00) to the afternoon (about 15:00) no clear distinction can be made, while for evening and nighttime the T_a at the inner city stations is slightly increased compared to the suburban sites. The amplitude of the diurnal cycle during winter season is generally low (about 3 K). In mean diurnal cycle

of spring the nighttime differences between sites at district C and the suburban MeteoStations become more evident (Figure 5.3b), as also the housing area station DGD_H is relatively warmer from sunset to sunrise than the rest of the stations. From late morning to late afternoon the inner city stations C_1 and C_2 are now slightly warmer at average. This tendency continues for summer months' mean diurnal cycle (Figure 5.3c), where the sites in district C are significantly warmer at all times, deviating up to 3 K at average from the coolest station SGD_G after midnight and still about 1 K in the afternoon. During fall season (Figure 5.3d) the diurnal cycles again converge, with almost no differences during the day and, similar to spring, a nighttime increased T_a at the inner city stations (up to 3 K) and less pronounced at DGD_H.

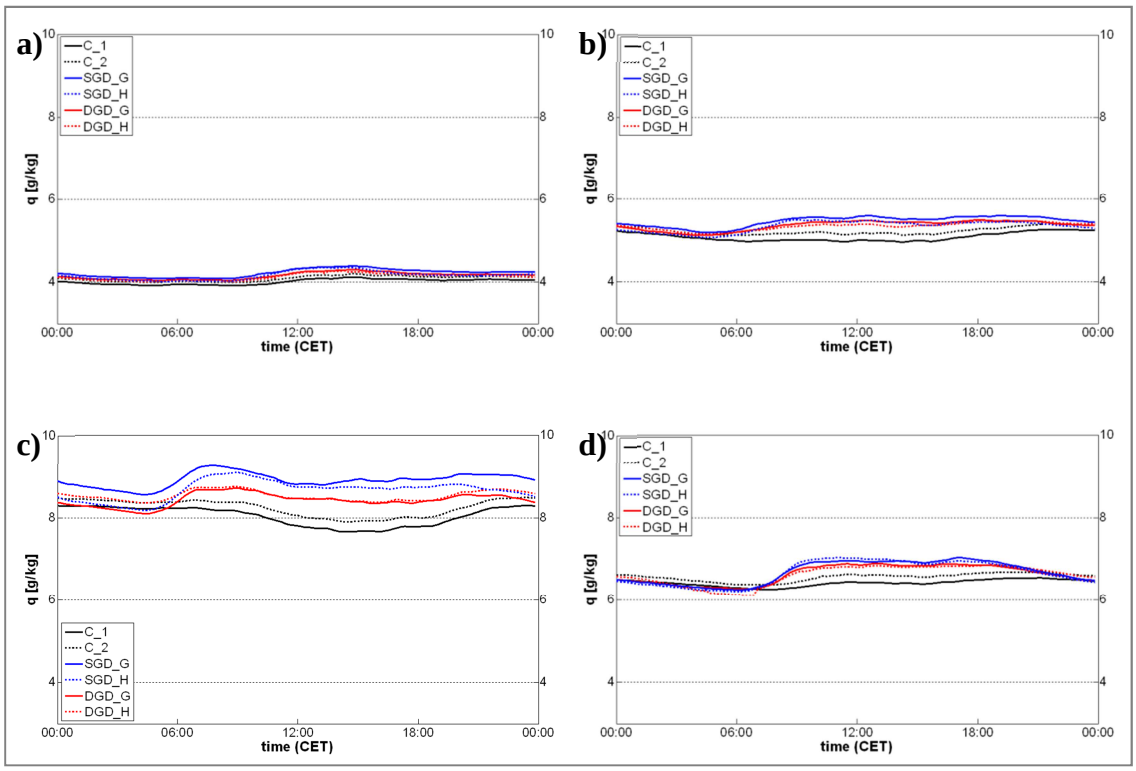

Figure 5.4 Seasonal mean diurnal cycle of specific humidity (q, 10min-mean). **a)** winter (DJF) **b)** spring (MAM) **c)** summer (JJA) **d)** fall (SON), for 01 September 2011 to 31 August 2012.

Air humidity also features distinct mean diurnal cycles for the seasons, as shown in Figure 5.4. While during winter season the specific humidity at the six MeteoStations is almost conform (Figure 5.4a), during spring higher humidities are found at the suburban

sites compared to the inner city sites (Figure 5.4b). Here, station C_2 tends to have a slightly increased specific humidity in general compared to C_1. Yet both stations are less humid than the suburban MeteoStations, with q values up to 0.6 g kg^{-1} lower. This trend continues to manifest for summer months (Figure 5.4c), where differences between suburban and inner city sites from sunrise (06:00) to early night (21:00) are most pronounced, with a maximum deviation of 1.5 g kg^{-1} during noon. In this season the two districts DGD and SGD exhibit specific diurnal cycles of humidities: the shallow groundwater districts sites SGD_H and even more the green space site SGD_G feature increased q values throughout the whole time, and especially during daytime with up to 0.5 g kg^{-1} higher values compared to DGD. In the latter district the sites of both land use categories, green space and housing, reveal a diurnal cycle of q with a very similar course.

A remarkable feature during summer months' diurnal cycles of humidity is the rapid increase around 06:00 at the suburban stations. Presumably the solar radiation initiates evapotranspiration relatively immediate after sunrise and water is transpirated and evaporated from plants and soil surface, respectively. At the inner city sites, however, this effect does not occur due to a lack of available water and vegetation cover. For fall season (Figure 5.4d) the diurnal cycles of q tend to be less distinct again, yet with again lower and more constant values at the city sites.

As these diurnal cycles of T_a and q show, the six urban sites own individual characteristics, according to district on the one hand, and land use classes on the other hand. To make these specific features better comparable, a consideration of the deviations from a reference site outside the network is useful. This is realized in the following Chapter 5.2.

5.2 Observation of the urban heat island

a) *Air temperature deviations from a rural site*

In this section the mean deviations of air temperature T_a of the six MeteoStations from the rural reference station WD_G, about 40 km outside of Hamburg, is analyzed for the observed one-year-period (01 September 2011 to 30 August 2012). This time

period is characterized by an average air temperature of 9.9 °C, a maximum air temperature of 34.5 °C, a minimum air temperature of -17.5°C and a total amount of precipitation of 577 mm (observations at the city station WD_F). The inner city stations C_1 and C_2 show the highest positive deviation from the rural site with an annual mean of about +1.0 K (Figure 5.5). Concurrently, values of the 90th percentile reach up to +4.5 K, while the values of 10th percentile are still positive values around +0.5 K. The stations at the deep groundwater district reveal only little urban heating effects, i.e. positive differences from the rural reference. At the housing area's MeteoStation (DGD_H) a small positive mean deviation of +0.25 K is observed, but with a considerable variability including a change of sign (-0.8 K and +2.2 K for the 10th and 90th percentile, respectively). Furthermore, the mean deviation is negligible at the green space DGD_G. The percentiles are distributed uniformly to negative and positive values. The district with a shallow mean groundwater table exhibits a minor negative deviation from the reference station of about -0.2 K at both sites (SGD_G and SGD_H). The distribution is also nearly uniform here with ±1.0 K 10th and 90th percentiles.

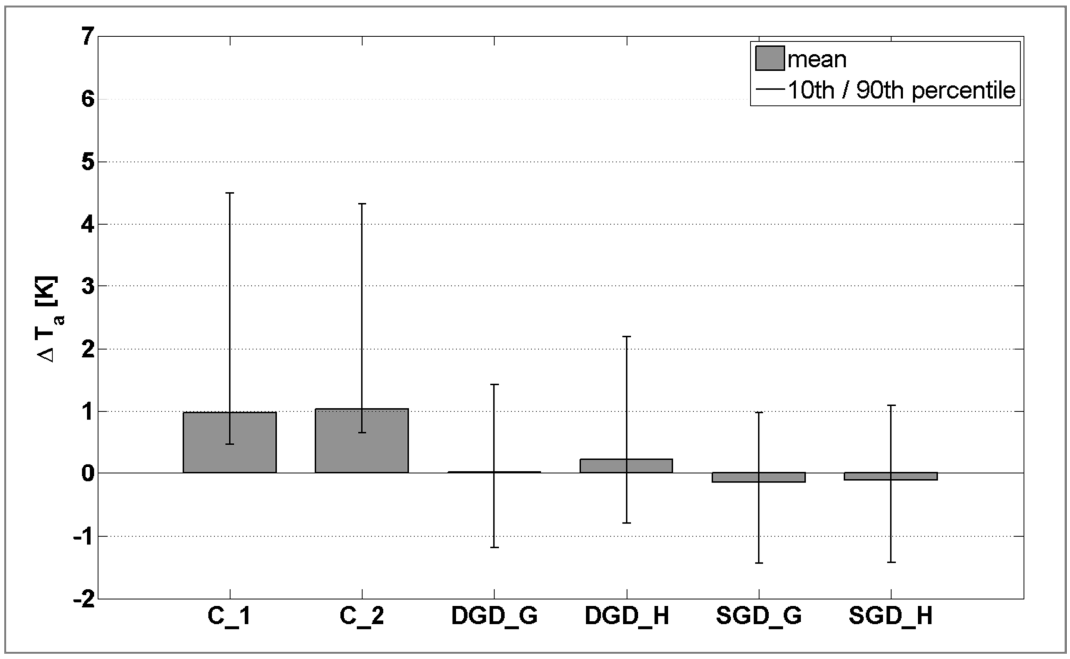

Figure 5.5 Mean deviation of air temperature (ΔT_a) of MeteoStations from reference station WD_G for the period 01 September 2011 to 31 August 2012. Thin bars indicate 10th and 90th percentiles.

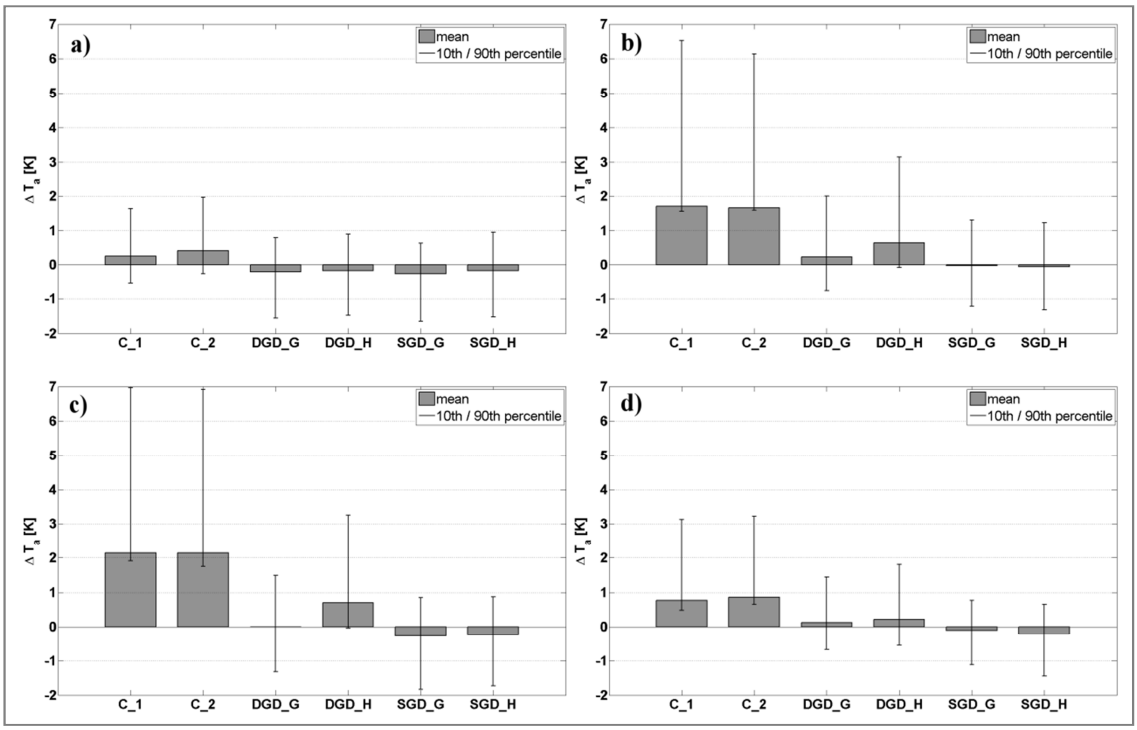

Figure 5.6 Mean deviation of air temperature (ΔT_a, 1hr-mean) of MeteoStations from reference WD_G for **a)** daytime (08:00 -20:00 CET) in the period 01 September 2011 to 31 August 2012, **b)** nighttime (20:00 to 08:00 CET), same period, **c)** nighttime in summer (01 June to 31 August 2012), **d)** nighttime in winter (01 December 2011 to 28 February 2012). Thin bars indicate the 10th and 90th percentile.

The urban heat island effect, which is already apparent from the overview of T_a deviations in Figure 5.5, is confined to nighttime: Looking at the daytime values (Figure 5.6a) it becomes evident that mean T_a deviations during the day are almost zero with evenly distributed variances in positive and negative values. At the suburb sites, the slightly negative mean differences might indicate a "daytime cooling island", as it was observed also by e.g. Myrup et al. (1993) and Svensson and Eliasson (2002). In contrast during nighttime (Figure 5.6b), the urban heat island is very pronounced. High nocturnal T_a differences and a wide spread to positive deviations from the rural reference station WD_G are found at the MeteoStations in the city area for both stations C_1 and C_2 with +1.7 K, and less pronounced at deep groundwater district's housing area DGD_H. These three sites also show a skewed distribution towards high positive deviations (90th percentile 2.5 to 4.8 K above the mean but the 10th percentile only 0.1 K below). At the deep groundwater green space site DGD_G only a slightly higher mean

of about +0.3 K can be observed. At the shallow groundwater district (SGD) no considerable nighttime warming is visible, and deviations are distributed almost uniformly around the mean. Considering seasonal trends within nighttime differences of T_a, during summer months (Figure 5.6c), the UHI effect is by far more pronounced compared to winter (Figure 5.6d). The diurnal temperature cycle is much smaller during winter than during summer and consequently the UHI are damped in winter time.

It is worthwhile to note that the rank order of the MeteoStations' average T_a deviation remains constant independent from the considered time frames. Inner city stations (C_1 and C_2) differ the most from WD_G, followed by the deep groundwater district's housing area station DGD_H and the nearby green space site DGD_G. SGD_H and SGD_G deviate always slightly negatively from the reference. This ranking is reasonable because inner city structures in general feature the highest UHI formation (Voogt, 2003). The DGD district's location, closer to the city core than SGD, its slightly higher sealing ratio in general, and its dryer conditions due to a deeper mean groundwater table, might be the reasons for ranking second as a district and DGD_H housing area ranking third overall as a site with nearby buildings, effective through higher heat capacity.

b) *Impacting factors on UHI manifestation*

The UHI effect occurs throughout the year, but depends on prevailing conditions. Higher deviations can be observed during summer and at night when daily temperatures amplitudes are typically high (summer) and wind speed is low (nighttime). Therefore it is worthwhile to have a closer look at factors impacting on differences in T_a.

High wind speed leads to intensive turbulence and mixing within the boundary layer. Thus, existing temperature differences will be reduced. High cloud coverage prevents nighttime cooling by enhanced down welling long wave radiation. Conversely, a clear sky leads to higher radiative cooling of the surface. Thus, UHI effects have been observed to occur mainly during phases with low wind speeds (Schlünzen et al., 2009) and little or no cloud coverage (Morris et al., 2001). The measurements of the present study confirm these findings (Figure 5.7).

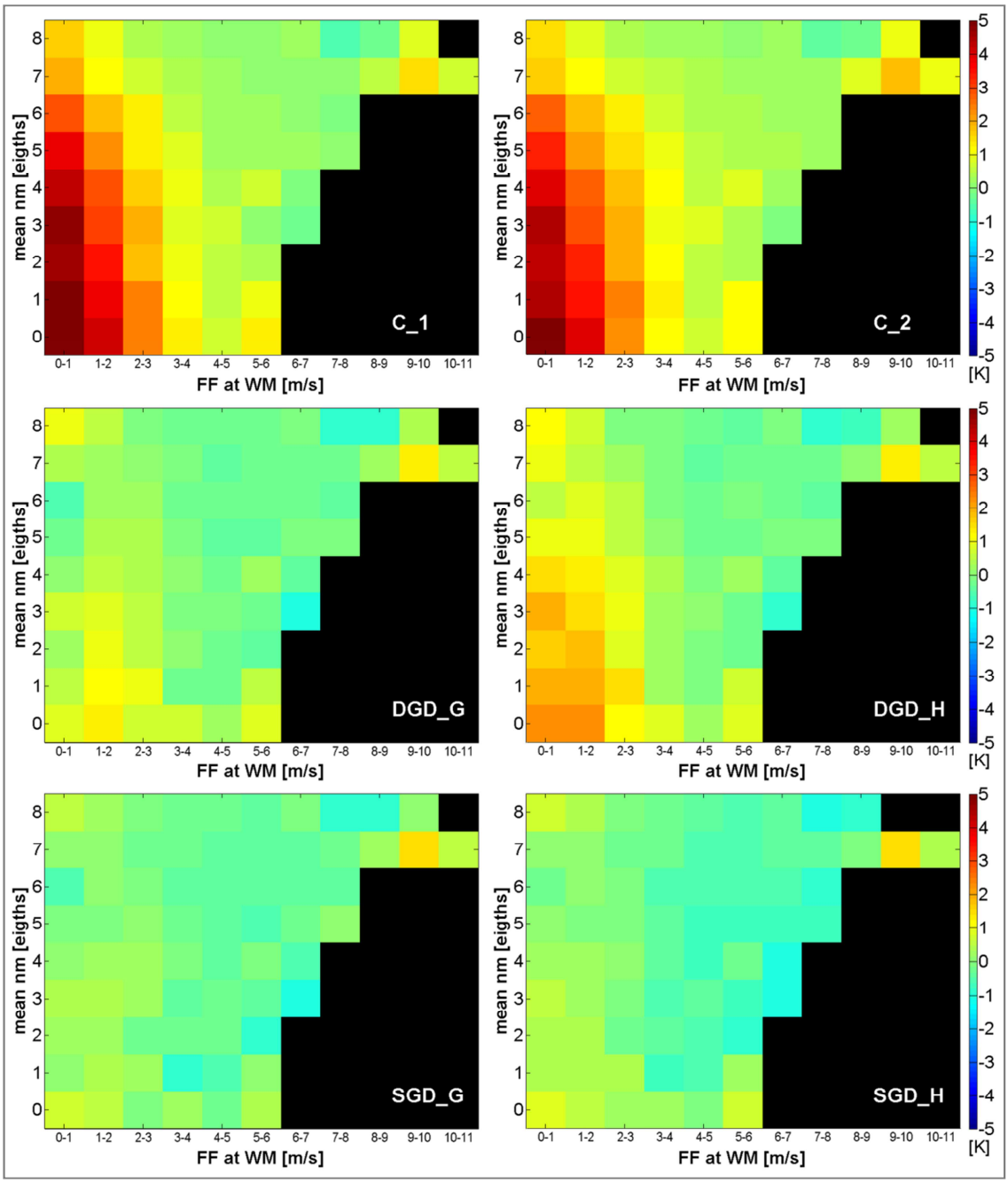

Figure 5.7 Mean deviation of air temperature (1hr-mean) of MeteoStations from reference WD_G during nighttime (20:00. to 08:00 CET) for one year (01 September 2011 to 31 August 2012). Color indicates the T_a deviation in K. x-axis: classes of wind speed (*ff*) at reference station WM, y-axis: classes of mean cloud coverage (*nm*) during the previous six hours.

Predominantly the inner city sites C_1 and C_2 and secondly the suburb housing area site DGD_H feature considerably increased T_a during nighttime if mean wind speed is below 2 m $s^{-1}$and average cloud coverage of the previous six hours is less than $7/8^{th}$. At the DGD_G green space station slightly increased T_a deviations are visible for wind speeds below 2 m s^{-1} and less than $3/8^{th}$ cloud coverage. At the SGD district stations this effect is hardly detectable because the UHI effect is low there in any case.

This analysis implies that a further analysis of the measurement data should be restricted to cases where the impact of surface and location is high and little influenced or changed by superior factors like high wind speed or cloud coverage. This filter on data ensures that the effects of surface and structure of the site's characteristic environment, like heat capacity and vegetation, is the dominant impacting factors on local climate. Thus, in the following evaluation, data is selected from situations with low wind speed ($\leq$ 2 m s^{-1}) and only partly cloudy or cloudless sky ($\leq 6/8^{th}$).

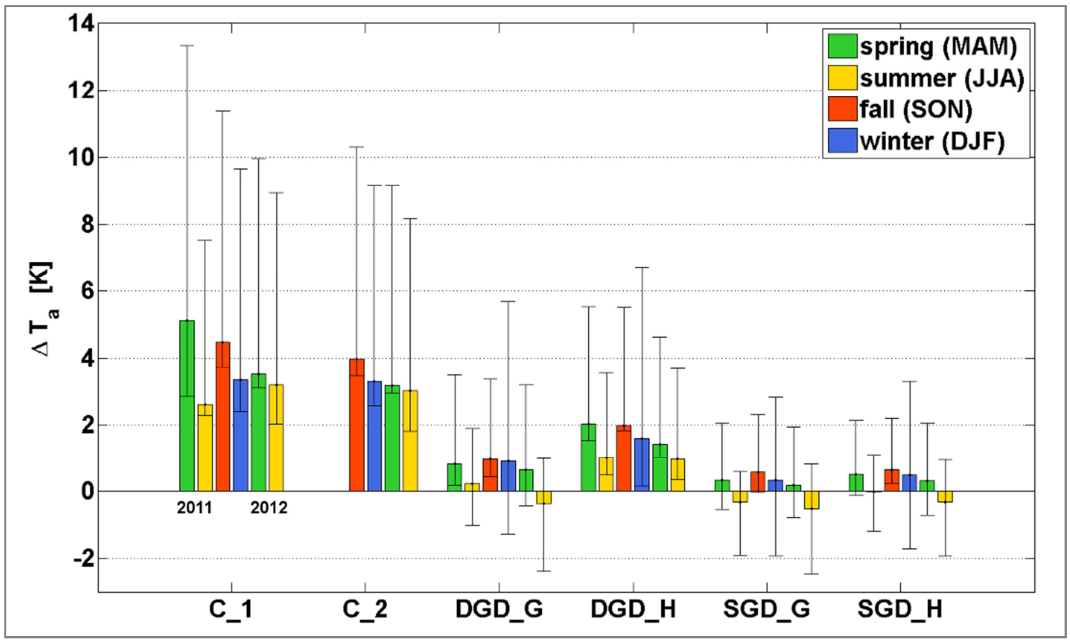

Figure 5.8 Mean deviation of air temperature (ΔT_a, 1hr-mean) from reference WD_G during nighttime (20:00 to 08:00 CET) grouped by season from 01 March 2011 to 31 August 2012. Data filtered by time steps with average wind speed at WM $\leq$ 2 m s^{-1} and mean cloud coverage of the previous 6 hours $\leq 6/8^{th}$, thin bars indicate 10^{th} and 90^{th} percentiles.

Figure 5.8 depicts the filtered mean T_a deviation of the MeteoStations from reference WD_G, grouped by season, with an extended observation period starting in March 2011. The already mentioned dominant positive divergence of the inner city stations C_1 and C_2 throughout all seasons, including 10^{th} percentiles higher than 1 K, get even more visible with a mean value of up to 5.2 K during spring 2011. The deep groundwater table district's housing area DGD_H also feature constant higher mean T_a and positive 10^{th} percentiles compared to the reference. Air temperature of the green space in this district (DGD_G) only deviates less than 1 K on average. Within the district with a shallow groundwater level (SGD) negative differences from the rural reference station WD_G occur more often, mainly in summer 2011 and in 2012. These two stations diverge the least throughout the year; also the 10^{th} and 90^{th} percentiles are relatively narrow and more equally distributed around the mean. Thus, SGD_G, SGD_H and WD_G feature comparable T_a diurnal cycles. In fall 2011 exceptionally high positive deviations at all stations are found, in combination with also high 10^{th} percentiles. This season was extraordinary dry and warm, as the observations at WD_F show (see also Table 4.4): 87.5 mm precipitation in comparison to the 30 year mean of 204 mm, 10.4 °C mean air temperature (30 year mean: 9.7 °C) and 329 h of sunshine (30 year mean: 307 h). This might be the reason for the high values of air temperature deviation.

5.3 Observation of the impact of topsoil moisture on air temperature

The nighttime the UHI is controlled by the heat capacity of buildings and surfaces, and the local circumstances as stated above. Soil moisture is rarely considered as an influencing factor for urban climate. Yet it can potentially also affect the nighttime urban heat island since water in soil considerably alters the heat capacity of the soil. As another effect, the availability of soil moisture limits evapotranspiration. This effect will occur mainly during daytime since evapotranspiration increases in general with increasing net radiation. Reduced evapotranspiration due to limited soil moisture is usually compensated by an enhanced sensible heat flux, which can be detected by the HUSCO network in terms of an increased daily warming of air temperature T_a.

In the following both effects will be analyzed: At first, the impact of soil moisture on the night time UHI will be quantified. Second, the relevance of soil moisture for the daytime warming in an urban environment is assessed. This analysis focuses on topsoil moisture, defined as the mean soil moisture of the upper five centimeter of the soil, because it has the largest impact on evapotranspiration processes.

a) Effect on nighttime air temperature

The strength of the linear relation between nighttime UHI and topsoil moisture can be estimated by a linear regression approach. Therefore, mean nighttime ΔT_a deviation with respect to the rural reference station WD_G is defined as a dependent variable:

$$\Delta T_a = T_{nightmean}(\text{station}) - T_{nightmean}(\text{WD\_G}) \qquad \text{(Equation 6)}$$

with $T_{nightmean}$ equal to the average T_a from 20:00 to 08:00 CET.

Soil moisture represents the explanatory variable for the regression. As a measure of soil moisture, the dimensionless topsoil water content of the 5 cm measurement depth was calculated considering van Genuchten (1980). It is defined as the measured volumetric water content (*VWC*) normalized with the residual and saturated values of *VWC*, Θ, as given in equation 3. The normalization allows for a better comparison of soil moisture at different stations and takes distinct water availabilities within the different soils into account. Essentially, the residual water content, i.e. soil moisture at the permanent wilting point, and the saturated water content are regarded as limits of the range of the available water. When the field measurements of *VWC* exceeded the saturated water content observed in laboratory analyses, a normalized water content larger than 1 is calculated. This mismatch is discussed in Chapter 4.2.

The results of the linear regression calculation are depicted in Figure 5.9 for the four suburban MeteoStations with data matching the given criteria. To focus on prevailing conditions promoting a nocturnal UHI, days have been selected according to same criteria is in the previous section 5.2b). The inner city stations are not considered since they are almost entirely sealed and thus do not provide soil moisture measurements. Further information in Figure 5.9 is given by the standard error of estimate and the 95 %

confidence bands, i.e. the area in which 95 % of all data points are located, as well as the 95 % prediction bands, i.e. the area in which the linear regression line lies with a probability of 95 %. In addition, the coefficient of correlation (r) and the slope of the linear fit are listed. Account must be taken that these statements are only valid under the assumption that a linear relation exists between the ΔT_a and the normalized soil water content Θ.

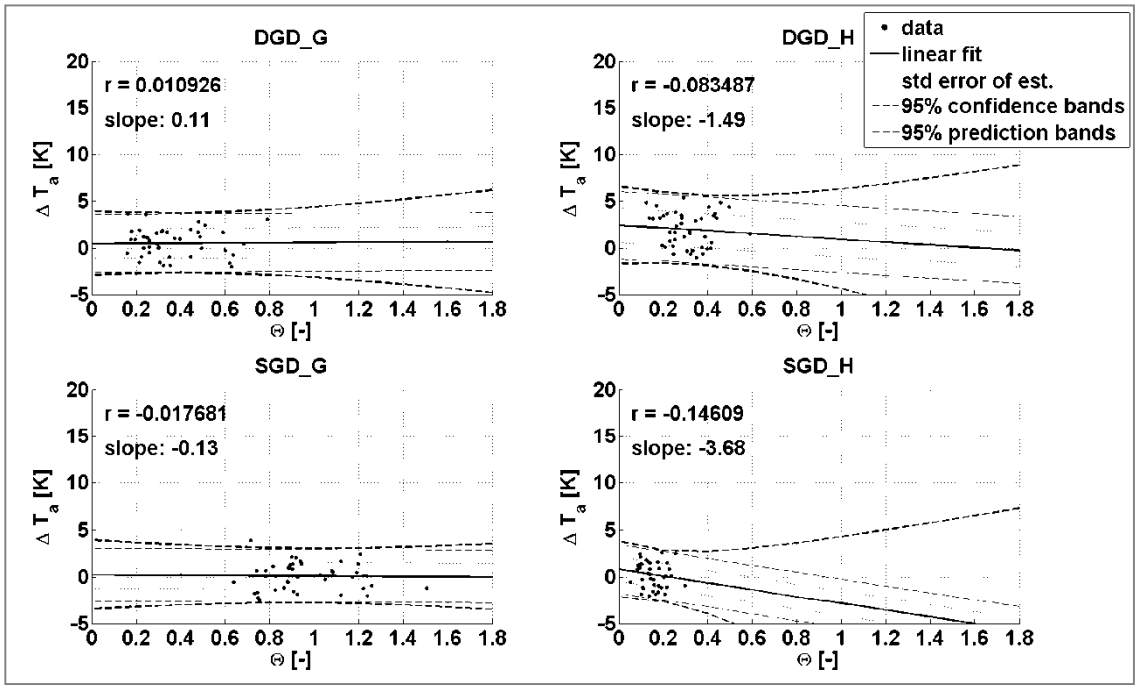

Figure 5.9 Relation between normalized topsoil water content Θ (5 cm depth) and the mean deviation of nighttime air temperature ΔT_a (WD_G - station). Days of the period 01 September 2011 to 31 August 2012 meeting the following requirements: mean wind speed ≤ 2 m s^{-1}, mean cloud coverage $\leq 6/8^{th}$. Signatures indicating linear fit, standard error of estimate, as well as 95 % confidence and prediction bands. r = correlation coefficient, slope = slope of linear regression line.

This regression analysis reveals no clear correlation between topsoil water content and mean nighttime deviation of air temperature from the rural reference. Coefficients of correlation come to -0.14 to 0.01 which signifies an explained variance of ΔT_a by topsoil moisture Θ of only 0.01 % to 1.96 %. Thus, there is not a significant relationship between these two variables, and the UHI effect intensity is likely not to be coupled with topsoil moisture contents.

b) Effect on daytime air temperature

Compared to the findings of non-filtered mean annual data (Figure 5.5), the seasonal mean nighttime air temperature deviations (Figure 5.8) are high. It can be concluded from this, that the excluded data, e.g. daytime air temperature deviations with wind speed > 2 m s^{-1}, most likely show minor differences. However, daytime air temperature is - apart from nocturnal cooling rates - relevant for human thermal comfort as well (Mayer and Hoppe, 1987) and thus should be considered in detail.

The evolution of air temperature during daytime is locally influenced by the partitioning of the incoming radiation into latent and sensible heat flux. This partitioning is partly controlled by soil moisture and in particular topsoil moisture. This relation has been confirmed e.g. by Kuttler et al. (2012), comparing model results of vegetated areas with high and low soil moisture in an urban environment. To quantify the magnitude of the impact of the factor soil moisture on the local T_a, a closer look on daytime temperature deviations is reasonable. As a reference for the calculations of T_a deviations, a site without natural soil, i.e. an entirely sealed surface, is most suitable, because evapotranspiration is almost negligible there (except shortly after precipitation events). In addition, the filter rule needs to be adapted to prevailing conditions that promote a coupling of topsoil moisture and air temperature: First, the mean wind speed should exceed more than 2 m s^{-1} leading to a mixing of near-surface air. This enables evapotranspiration from the soil surface. Second, less that $6/8^{th}$ of mean cloud coverage ensures sufficient solar radiation. These conditions characterize situations which are most suitable for evapotranspiration.

Figure 5.10 depicts the mean deviation during daytime (08:00 to 20:00 CET) T_a at the suburb MeteoStations from the reference station C_1 (inner city sealed courtyard) for all days applying the same filter rules as before. In this analysis the suburb MeteoStations show a mean T_a deviation from the inner city station of -0.35 K to -0.5 K with only marginal differences among each other with variations in the order of the sensor accuracy (see Table 3.4). However, the observed deviation is larger than the accuracy of the air temperature sensors, and thus it is significant. Moreover, 90^{th} percentiles indicate a large spread of down to -1.9 K at SGD_G, and mean deviations

are negative for all stations. Only station SGD_H shows a positive 10th percentile (+0.5 K) which is due to the faster increase of T_a at this station in the morning (as it is described in Chapter 5.1).

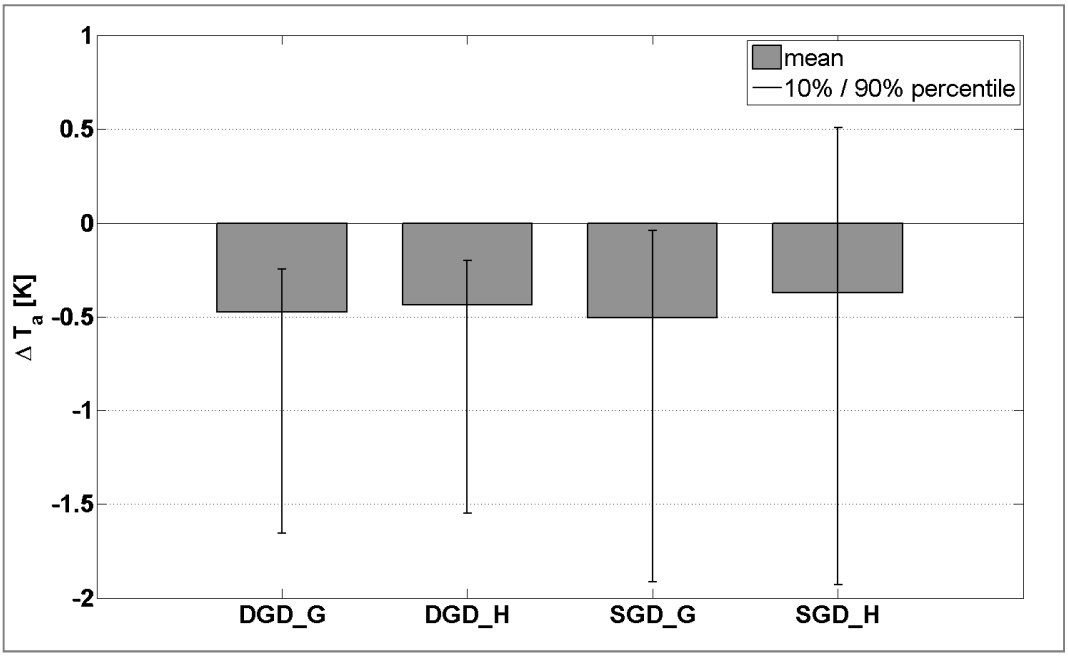

Figure 5.10 Mean deviation of air temperature (ΔT_a, 1hr-mean) of suburban MeteoStations from reference station C_1 for the period 01 September 2011 to 30 August 2012 during daytime (08:00 to 20:00 CET). Data filtered by time steps with average wind speed at WM > 2 m s^{-1} and mean cloud coverage of the previous 6 hours ≤ 6/8th. Thin bars indicate the 10th and 90th percentile.

Hence, sites with unsealed soils are slightly cooler compared to sites with sealed surfaces, even during the day and with turbulence induced by wind speed > 2 m s^{-1} and substantial solar radiation (cloud coverage ≤ 6/8th). Evapotranspiration of water from topsoil[15] is a possible factor causing this negative deviation of T_a. To test this hypothesis, again the linear regression method applied before is used to test whether a linear relation between the increase of T_a during the course of the day as a dependent

[15] Water for transpiration is provided from soil areas within the entire rooting depth, which is in the majority of cases deeper than the topsoil (5 cm). Hence the transpiration-component of the ET is depending on soil moisture of the rooting depth, while the evaporation-component results from available water within the topsoil. As a differentiation between these two components within the performed measurements is not feasible yet, this generalized hypothesis is proposed with the consciousness of this limitation.

variable, and soil moisture as an explanatory variable existed. Measurement data considered for this analysis are selected to match the same conditions, supplemented by the requirements of more than 1500 W h m^{-2} solar irradiance at that day and 0 mm of precipitation at all stations to exclude situations with most likely unlimited water supply.

As a measure for the possible impact of topsoil water evapotranspiration on T_a, the absolute warming, i.e. the span of T_a, during the course of the matching days is calculated as the difference between maximum and minimum T_a. The results of the linear regression analysis are given in Figure 5.11, including coefficient of correlation and slope of the linear regression line. Again these statements are only valid assuming that a linear relation exists between the span of T_a and normalized soil water content Θ.

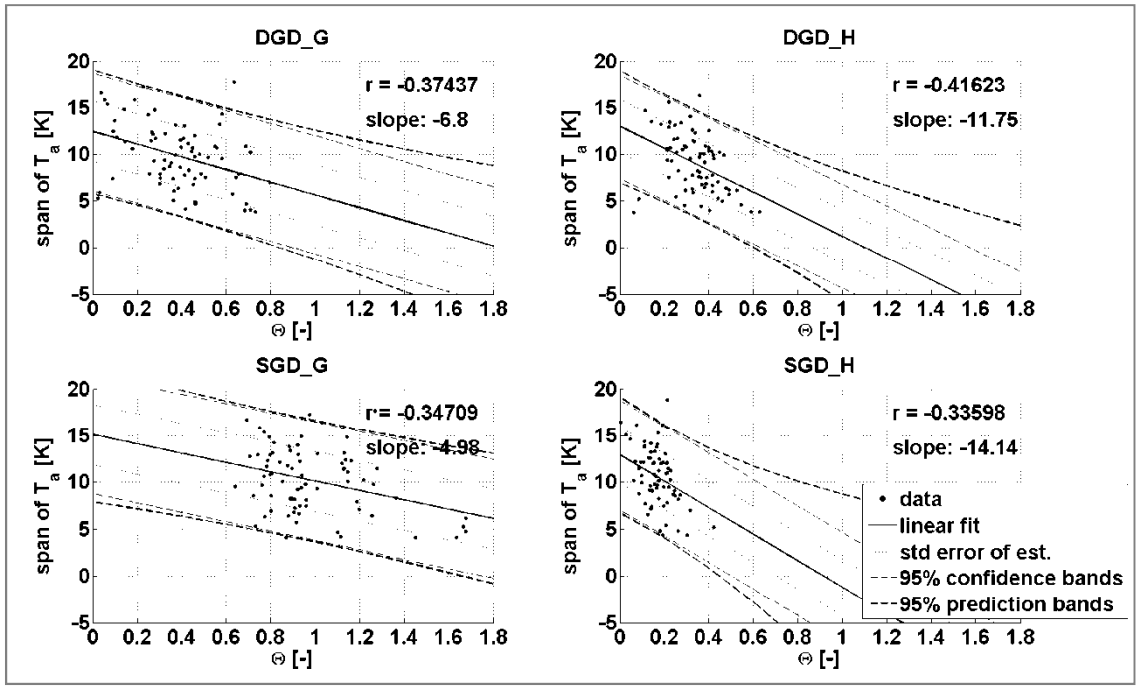

Figure 5.11 Relation between normalized topsoil water content Θ (5 cm depth) and the span of air temperature T_a (T_{max} - T_{min}). Days of the period 01 September 2011 to 31 August 2012 meeting the following requirements: precipitation sum of day = 0, mean wind speed $\geq$ 2 m s^{-1}, mean cloud coverage $\leq 6/8^{th}$, sum of global radiation $\geq$ 1.5 kW h m^{-2}. Signatures indicating linear fit, standard error of estimate, as well as 95 % confidence and prediction bands. r = correlation coefficient, slope = slope of linear regression line.

At all four MeteoStations a negative linear relationship is observed. The higher the soil water content Θ is, the narrower is the span of T_a. The correlation coefficient for this relation lies between -0.34 and -0.42, resulting in a coefficient of determination R^2 of 0.11 to 0.17. This signifies that 11 to 17 % of the variation in the span of T_a can be explained by soil moisture for the selected days. The remaining 83 to 89 % are due to unknown variables, e.g. meteorological occurrences or inherent variability. To test whether this linear relationship is significant, a t-test for the slope was carried out. The null hypothesis could be rejected under the assumption of a decorrelation time of 5 days (resulting from autocorrelation analysis). Thus, it can be concluded on a 95 % significance level that there is a linear relationship between topsoil moisture and T_a.

The negative slope of the linear relation can be interpreted as an indicator for the rate of decrease in the span of T_a with increasing topsoil water content Θ, and thereby indicates the sensitivity of this relationship. The larger the absolute value of the slope is, the faster the span of T_a during the day increases with reduced topsoil moisture Θ. Vice versa, small absolute values of slope indicate a slower increase of the span of T_a with dryer soils. The site SGD_H, characterized by a sandy soil substrate within the housing area, features by far the largest absolute slope. This can be interpreted as an indicator for a significantly higher air temperature increase during days when topsoil moisture decreases only slightly (e.g. a few days after a precipitation event), compared to the other three sites, where the linear regression has a very similar trend. It is to be further examined whether this exceptional tendency of SGD_H might be a cause for the anomalous T_a increase in the morning compared to the other MeteoStations within the measurement network (as mentioned in Chapter 5.1).

5.4 Discussion of the observed air temperature variability at urban sites

In this chapter urban air temperature anomalies were confirmed for the city of Hamburg. The observed mean annual air temperature deviations from the rural reference of +1.0 K at the city core and 0.25 K at a suburb housing site correspond well with the observations from long-term climate records by Schlünzen et al. (2009) who found a higher average air temperature of +1.1 K for another city centre station and

+0.5 K at a suburban area. The approach of Bechtel and Schmidt (2011) to map the urban temperature differences using floristic mapping data of Hamburg provides very comparable values as well: For the grid cells around stations C_1 and C_2 the deviations from the rural reference were predicted to be +0.9 K to +1.0 K and > +1.1 K respectively, for DGD district +0.6 K to +0.9 K and for SGD +0.5 K to +0.6 K. These values are very similar to the measured temperature deviations as they reveal the same ranking of the observed districts within Hamburg for the intensity of their T_a differences.

The nocturnal UHI effect is also detectable in Hamburg, with sizeable prominence in the city centre (+1.7 K) and a suburban housing area (+0.7 K). The finding of a prominent UHI like this is remarkable because the city of Hamburg in its structure and location is thought to be untypical in developing such a pronounced phenomenon due to maritime climate and prevailing high wind speeds (Schlünzen et al., 2009). However, these observations fit well to the results of the simulations of Hoffmann (2012): The maximum UHI is stated as +1.2 K for Hamburg, located within the downtown and harbor area - the area where the measurement stations C_1 and C_2 are located. As in these simulations the UHI effect is calculated for a shorter period of time (8 p.m. to 12 a.m.) it is plausible that its maximum UHI value is smaller compared to the measured value in the present study. Furthermore, the measured deviations for the city centre stations from the rural reference are also in good conformity with findings of other studies for UHI effects in the moderate latitudes. For example for Gothenburg, Sweden, up to 8 K have been measured (Svensson and Eliasson, 2002), at the present study's site C_1 and C_2 up to +7 K during summer nights occur. And Voogt (2003) states that the typical UHI effect ranges from +1 K to +3 K even for large cities. For European cities with more than 1 million inhabitants he indicates a maximum UHI of +10 K.

The analysis of measurement data from a one year period allows the identification of the typical impacting factors for nocturnal UHI: Low wind speeds and cloud coverage are dominant factors, influencing the intensity of the nighttime increased temperatures of inner city sites compared to rural sites. These confirmations of the UHI

generalizations from Oke (1982), have also been confirmed e.g. for Szeged, Hungary by Unger (1996), for Melbourne, Australia, by Morris et al. (2001) and for Buenos Aires, Argentina, by Figuerola and Mazzeo (1998). Within the present study, in addition the possible influence of soil water content on the nighttime UHI is observed, which constitutes a new approach within UHI research. Yet it is found that topsoil moisture is likely not to have an impact on nighttime temperature deviations of suburban sites from a rural reference.

During daytime, positive air temperature deviations from the rural reference are found to be small for the city centre (+0.3 K, +0.4 K respectively). Only at the suburb sites mean daytime air temperatures are slightly lower (down to -0.25 K) compared to the rural reference. These observations are in accordance to the findings of Myrup et al. (1993) who found suburban sites in Davis, CA, USA, as often to be cooler compared to rural sites than warmer, depending on meteorological conditions like wind speed and solar radiation. Differences between urban parks and green spaces and the surrounding built-up areas were found to typically be +1 K to +2 K for Vancouver, Canada, during summer days (Spronken-Smith and Oke, 1998). Within the present study's suburban sites, only lower values occur during daytime (within sensor accuracy, < 0.2 K), yet during the night at DGD the housing area is about +1 K warmer at average than the green space. This disagreement is presumably due to the location of the Vancouver measurement sites within more densely built-up structures. As for Gothenburg Upmanis et al. (1998) found nighttime deviations of green spaces from built-up areas in the range of -1.7 K to -5.9 K, depending on park sizes and greater meteorological conditions, these findings match better to the observations in Hamburg. The relevance of the type of vegetation in combination with soil properties for the local T_a differences could not be observed in detail, as the suburban sites in the present study feature comparable vegetation cover, i.e. short grass and high pasture grass, respectively, yet different soils. However, as stated e.g. in the study of Damm et al. (2012), the plant-available water (*AWC*) is a crucial value determining this relevance of soils. Consequently, a dense vegetation cover ensures the actual ET rate to reach nearly the potential ET, as far as soil properties provide a high water capacity. The observation of slightly lower mean

daytime air temperatures at the green space sites compared to the housing area sites allows concluding that this effect applies for higher grass vegetation and nearby deep rooting trees compared to short grass cover.

Averaged over a one year period the suburb stations are 0.35 to 0.5 K cooler than the city centre station C_1 during daytime for selected conditions featuring wind speeds above 2 m s^{-1} and cloud coverage of $6/8^{th}$ or less. The higher ratio of unsealed surfaces in the suburbs is a possible cause for this temperature deviation. These findings correspond to the observations of e.g. Houet and Pigeon (2011) for Toulouse, who found a daily maximum difference between high density urban core sites and areas with detached houses and gardens of 0.1 ±0.5 K for summer months with clear sky conditions and low wind speed.

A new approach concerning the impact of soil water availability at the surface is attempted: Although no impact of soil moisture on nighttime air temperature is found, a linear regression analysis implies that soil moisture is correlated to the span of T_a, i.e. warming during the course of the day, with an explained variance of 11 to 17 %. It needs to be further investigated whether this effect is partly biased due to seasonal variations in absolute T_a values and soil moisture, as in the summer time a higher span can be caused by higher temperatures and lower soil moistures in general.

6 Surface-atmosphere exchange fluxes in two urban districts

The state of the lower atmosphere, i.e. the boundary layer, is modified by two main processes: fluxes of momentum, namely wind, resulting from differences in atmospheric pressure, and heat and moisture fluxes from the surface. The latter is a result of the energy conversion of solar radiation at the surface (Stull, 1988). These processes are valid for natural as well as for urban environments. Therefore the energy budget of urban areas can, in analogy to the general energy balance equation, be expressed as:

$$R_n = H + LE + G \qquad \text{(Equation 7)}$$

with R_n = net all-wave radiation (> 0), H = sensible heat flux (< 0), LE = latent heat flux (< 0), G = storage heat flux (< 0, soil heat flux and storage) (e.g. Pearlmutter et al., 2009)[16]. The share of each flux depends, inter alia, on the water availability at the surface, which determines the actual evaporation and, including transpiration, LE, respectively. Furthermore, the associated sensible heat flux H contributes to an increase of air temperature (e.g. Stull, 1988). Hence it is important to measure the fluxes that represent the link between the pedosphere and the atmosphere. These measurements can certainly be helpful to determine soil moisture impacts on urban local air temperature more precisely. Thus, eddy covariance data has been collected at the two suburban districts. This data may give additional clues on whether latent heat fluxes, depending on topsoil water contents as the controlling factor for actual evapotranspiration, have a considerable impact on air temperature at the urban site.

As described in Chapter 3.1, the eddy covariance systems were mounted at different heights and within distinct land use categories: At the shallow groundwater district SGD the system collects data in 30 m height above the housing area (SGD_EC). During westerly air flow situations the source area of the fluxes is located within the housing area. During east direction winds fluxes originate from a mixed land use of detached houses and green space areas. The second eddy covariance system, monitoring fluxes at

[16] This equation 7 is valid under the assumption that the net heat advection is negligible and no significant anthropogenic heat flux is present.

the deep groundwater district DGD, measures 2.5 m above the vegetated ground of the green space (DGD_EC). Here, wind directions from 180° to 360° provide information of fluxes from the pasture grass land (see Chapter 3.3). These very distinct measurement heights and source areas determine the fact that these measurements are not comparable with each other and need to be considered separately. Yet each system provides valuable information on specific issues concerning the exchange between surface and atmosphere within the observed areas.

6.1 Flux measurements at the annual scale

To get an overview on the flux partitioning at the sites for different source areas, Figure 6.1 depicts the relationship between daily mean *LE* and *H* for the time 01 September 2011 to 31 December 2012. At the shallow groundwater district SGD the two possible source areas are regarded separately. The source area SGD_EC1, lying in eastern direction from the measurement station with a mixed land use of detached houses and green space, shows a rather constant trend of *H* and *LE* fluxes considering the whole measurement period. While in fall and winter fluxes are lower in general, during spring a tendency towards increased sensible heat, and during summer towards increased latent heat fluxes up to 250 W m^{-2} are visible. With increasing values of the fluxes, the deviation of the single data points from the regression line increases. Thus, when the amount of available energy is high, flux partitioning takes place either tending towards *H* or towards *LE*, but not with equal share for both heat fluxes.

With western wind direction the source area SGD_EC2 is mainly determined by one or two-storey buildings within a housing district. Here the latent heat flux *LE* is smaller than the corresponding sensible heat flux *H*, as indicated by the slope of the regression line and the distribution of the data. During spring a broad range of *H* occurs with up to 290 W m^{-2} at daily average, with corresponding 100 W m^{-2} energy flux partition to *LE*. In summer months the energy conversion into *LE* is increased, resulting in an almost equal share of *H* and *LE* on the total fluxes, in the range of 100 to 200 W m^{-2} daily mean. This higher share of *H* on the total energy conversion, compared to SGD_EC1,

could be attributed to the higher sealing ratio and built-up surface within the source area of the fluxes here.

The eddy covariance system at the deep groundwater district's green space site DGD_EC reveals a somewhat different picture. Here, energy partition tends mainly towards latent heat fluxes, reaching nearly 300 W m^{-2} in summer, while sensible heat flux values lie below 100 W m^{-2} throughout all measurements. The linear regression line is comparably steep and thereby indicates the tendency towards a higher energy partition share of *LE*. This trend is reasonable because the measured fluxes originate from the green space surface, i.e. high pasture grass covered soil. A considerably increased evapotranspiration rate from densely vegetated unsealed land is to be expected during the vegetation period, and especially in summer.

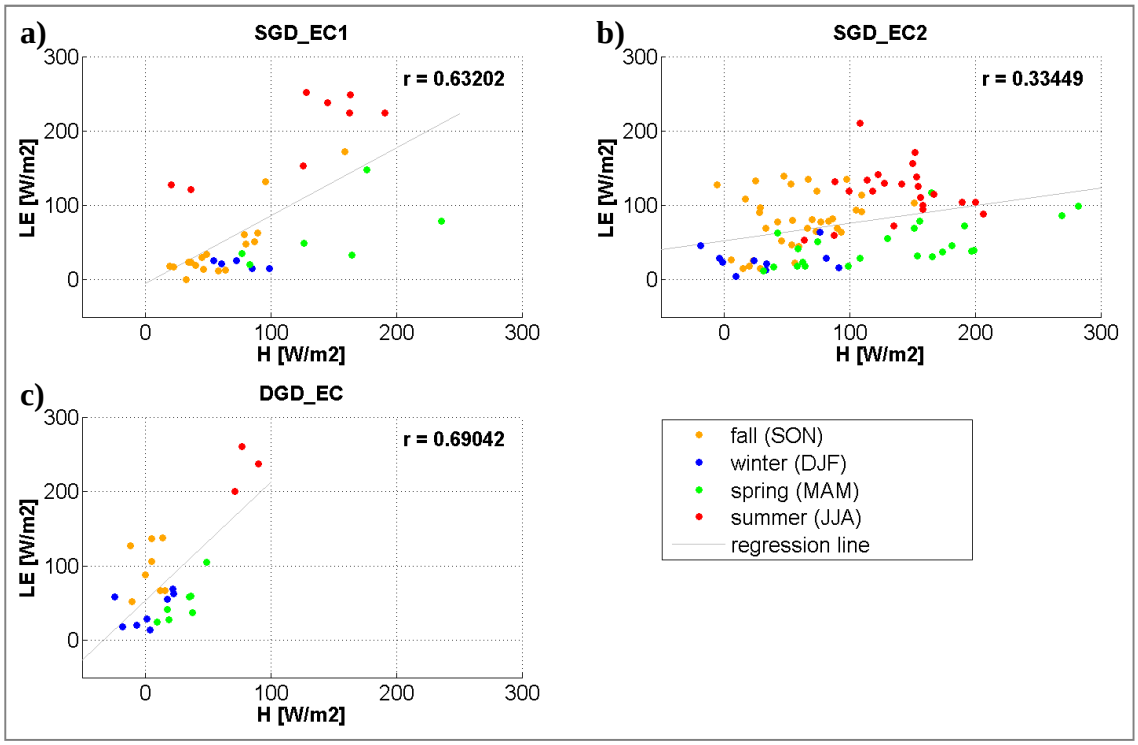

Figure 6.1 Distribution of sensible heat fluxes (*H*) and latent heat fluxes (*LE*) at the eddy covariance system stations, average daily flux (10:00 to 15:00 CET). Source areas: **a)** SGD_EC1, **b)** SGD_EC2, **c)** DGD_EC. Data from 01 September 2011 to 31 December 2012, seasons indicated by color, grey line shows linear regression line, r = coefficient of correlation.

The share of *H* and *LE* on the energy fluxes at the two districts and three source areas, respectively, gives a first impression of the differences in the conversion of available energy. Following this, a closer look at the annual cycle can be helpful to interpret the temporal evolution and the impacting factors determining these fluxes. As a measure for the contributions of turbulent latent heat fluxes to the available energy conversion at the land surface, the evaporative fraction *EF* (see Chapter 3.3) is considered in Figure 6.2 and Figure 6.3 for the two observed districts at the vegetation period scale of 2012 (01 March to 01 November). Complementary, precipitation and solar irradiance are regarded, as they are two main parameters that control the share of turbulent sensible and latent heat fluxes on the total energy conversion: Solar irradiance is the main energy source, determining the available energy at the surface. Precipitation on the other hand can be crucial for the topsoil water availability, as shown in Chapter 4. The water availability, in turn, influences the share of *LE* on the energy conversion by limiting the actual evapotranspiration. Furthermore, additional information on the local conditions is given concerning the temporal evolution of the topsoil moisture (5 cm depth) at the SoilStations within the districts. These values can be regarded as a measure for the evaporation from the soil surface and the transpiration through the vegetation. At SGD no distinction between the two different air flow directions and source areas of the fluxes, respectively, is made as rather fluxes at the entire district should be analyzed at the annual scale and a separation would lead to larger data gaps due to improper wind directions. Therefore the topsoil moisture is given for all SoilStations within SGD.

For the course of the evaporative fraction *EF* measured at the eddy covariance station within the shallow groundwater district SGD in 2012 (Figure 6.2), a general trend towards an increase from the beginning of the vegetation period (*EF* of 0.2 to 0.4) to late summer is visible (*EF* of up to 0.8). A 3rd order polynomial fit was calculated to depict the seasonality of the *EF* more markedly, as the mere data points show an intensive scattering. This fit has its maximum in mid-September. As data points show a rapid decrease in late October down to an *EF* of 0.3, the polynomial fit tends to decrease here. This seasonality in *EF* can be explained as follows. During spring and early

summer the vegetation grows and progressively transpires. As solar radiation increases, plant growth and photosynthesis rates increase. Concurrently, soil moisture decreases due to two factors, the processes of ET: Plant roots take up water from soil for photosynthesis and transpiration, respectively. In addition, evaporation from the soil surface occurs to the extent of which a deficit of vapor pressure in the near-surface atmosphere exists. The highest daily *EF* occur during late summer and fall months with several values reaching the maximum of about 0.85 from late August to early September. At this time, the transpiration of the vegetation reaches its climax (e.g. Wang et al., 2008). In particular, pasture grass and trees essentially contribute to latent heat fluxes in suburban areas (Peters et al., 2011). These high *LE* rates are presumably supported by the constant summer precipitation (see Chapter 4.3 and Table 4.4) which provides sufficient water for plant root uptake, and thus no limitation of evapotranspiration rates by water availability exists. This water uptake from plants gets also evident in the topsoil moisture data, as its local minimum at all SoilStations within SGD is reached in late August and early September. It can be assumed that topsoil water decreases due to the combined loss by high transpiration from plants and evaporation from the surface. Additionally, reduced water infiltration is given due to interception loss from the maximum leaf area of the vegetation. Thus, evapotranspiration and hence *EF* seems not to be significantly limited by soil moisture in late summer. The water supply for plants is presumably not limited in this area at any time. As solar radiation decreases and the vegetation period comes to an end, precipitation amounts are high in early and low in late October. Concurrently topsoil water content rises again. The abrupt low *EF* from mid-October on are likely to be caused by the coactions of missing precipitation and the time of leaf fall with reduced transpiration from trees.

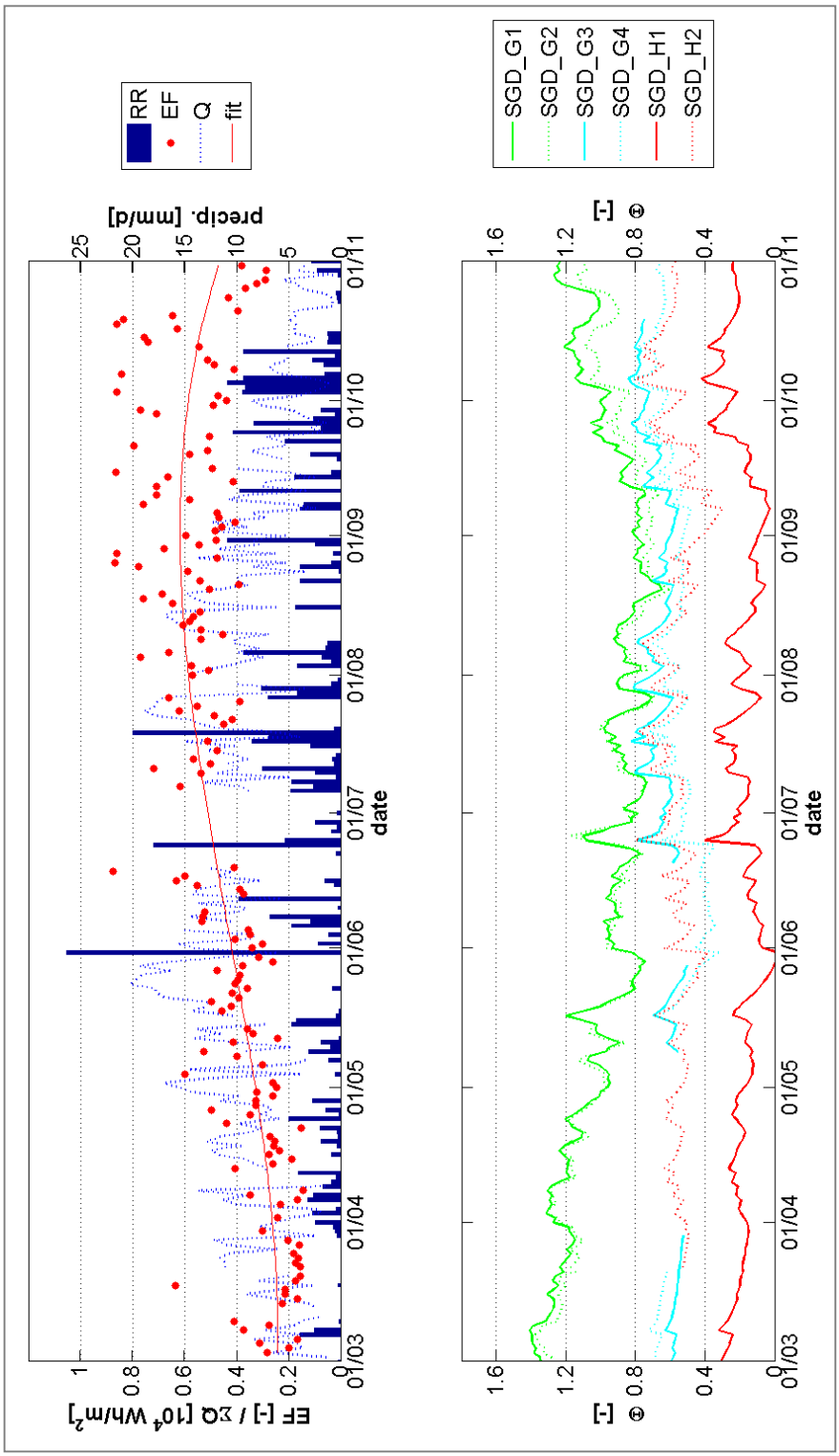

Figure 6.2 Annual cycle of parameters at SGD. 01 March to 01 November 2012. Top: Measurements of eddy covariance system SGD_EC. Daily averaged evaporative fraction (*EF*) from 10:00 to 15:00, 3rd degree polynomial fit of *EF*, daily sum of solar radiation (*Q*) and precipitation at WM (*RR*). Bottom: Normalized soil moisture (Θ) at six SoilStations within SGD.

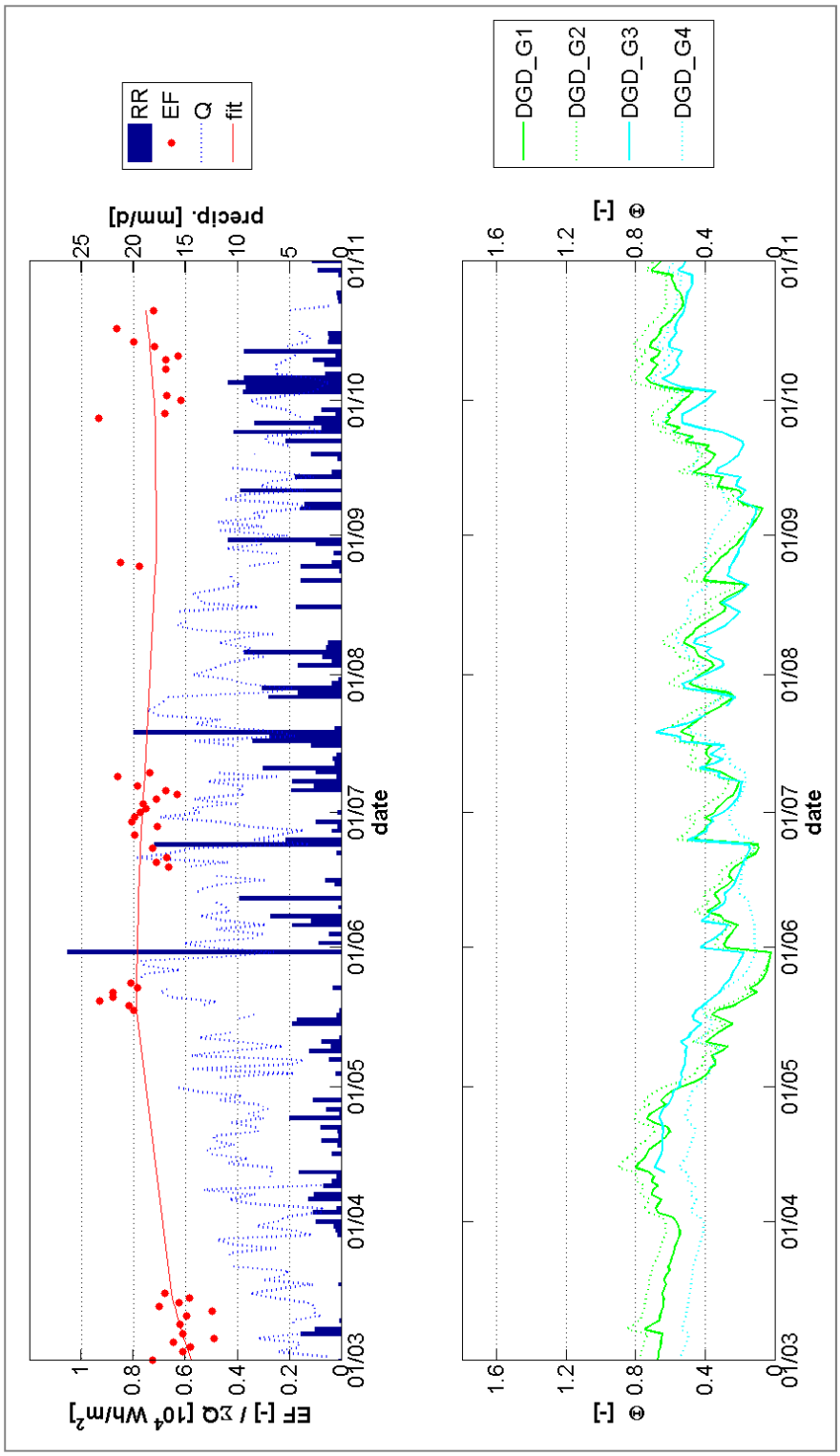

Figure 6.3 Annual cycle of parameters at DGD. 01 March to 01 November 2012. Top: Measurements of eddy covariance system DGD_EC. Daily averaged evaporative fraction (*EF*) from 10:00 to 15:00, 3rd degree polynomial fit of *EF*, daily sum of solar radiation (*Q*) and precipitation at WM (*RR*). Bottom: Normalized soil moisture (Θ) at four SoilStations within SGD.

However, it is observable that the *EF* values vary highly from day to day. Hence a wide scatter is visible throughout the whole vegetation period, with even a broader spectrum in late summer and early fall. The reasons for this scatter can be contributed to several factors: On the one hand, diurnal variations in *EF* influence the daily average value. These diurnal variations could presumably be influenced by cloudiness, yet, there is no consensus in literature on this effect (discussed e.g. in Farah et al., 2004). Also the air temperature determines the vapor pressure and thereby limits the latent heat fluxes. On the other hand the footprint of the measured energy fluxes is large with a heterogeneous compound of urban structures, surfaces and vegetation. For different wind directions the source area changes, and thus differences in fluxes are to be expected. Thus, this scatter can be assumed to be an urban-specific characteristic of the *EF*.

At the eddy covariance system mounted 2.5 m above the vegetated surface of a high pasture grass land within the deep groundwater district (DGD_EC), unfortunately only little data is available for the vegetation period 2012. In addition to several technical issues limiting the amount of collected data, only about 57 % of the data originate from the valuable wind directions 180° to 360° (compare Table 3.11). Nevertheless, some trends in the ratio of latent and sensible heat fluxes can be analyzed (Figure 6.3). The *EF* appears to be at a higher and more constant level throughout the vegetation period, compared to SGD_EC, with already high values in early spring (0.6) and less reduced in late fall (0.6 to 0.8). This comparably little seasonality demonstrates well the different source area and measurement height at this station DGD_EC compared to the station SGD_EC. The proximity to the vegetated surface effects higher latent heat fluxes in general and thus high values of *EF*. In addition the maximum values for *EF* reach nearly 1, signifying that the energy flux partitioning proceeds almost entirely into latent heat fluxes. The topsoil moisture within the DGD green space shows a decrease in summer at all four SoilStations as well, also most likely due to vegetation root uptake, interception loss and evaporation. Yet at this district it appears to be a limiting factor for ET just as little as at SGD.

One striking characteristic of the distribution of *EF* at the DGD site is the fewer scatter of the daily values. The share of *LE* on the total fluxes appears to vary less from day to day. The proximity to the more homogenous grassland can be an explanation for this effect.

6.2 Flux measurements at the diurnal scale

For the observations of the impact of distinct surfaces, and in particular soils on energy partitioning, phases of several days without precipitation can be helpful, as they were already analyzed in Chapter 4, for example. The lack of precipitation ensures that not water that is temporarily accumulated at the surface contributes to the measured ET, but only the actual soil moisture. Additionally, days with high solar radiation are most suitable, as a high net radiation enlarges the partitioned fluxes and thus the effects of interest get more visible. Therefore continuous dry phases can be very valuable for a more detailed look on heat fluxes and their dependence on source area characteristics. An analysis of the fluxes measured at SGD_EC1 and SGD_EC2 during two 4-day-periods without precipitation. As the fluxes of these two source areas are measured at the same station but for different wind directions, a comparison of the same days is not possible. Thus, two phases comparable in air temperature, solar radiation and prior precipitation are selected (Figure 6.4a and b). During these days the mean air temperature was 16.0 °C, the average cloud coverage was 4.6/8th and the average wind speed at 10 m height (DWD_F) was 2.8 m s^{-1}. Figure 6.4b shows a phase in mid-August 2012 with the fluxes' source area lying within the heterogeneous structure of houses and green space (SGD_EC1). During these days an average air temperature of 17.3 °C, a mean cloud coverage of 1.9/8th and an average wind speed of 3.8 m s^{-1} were measured. Yet these two periods are the best comparable dry phases in 2012, as they both featured high solar radiation and no rain, and they occurred within four weeks.

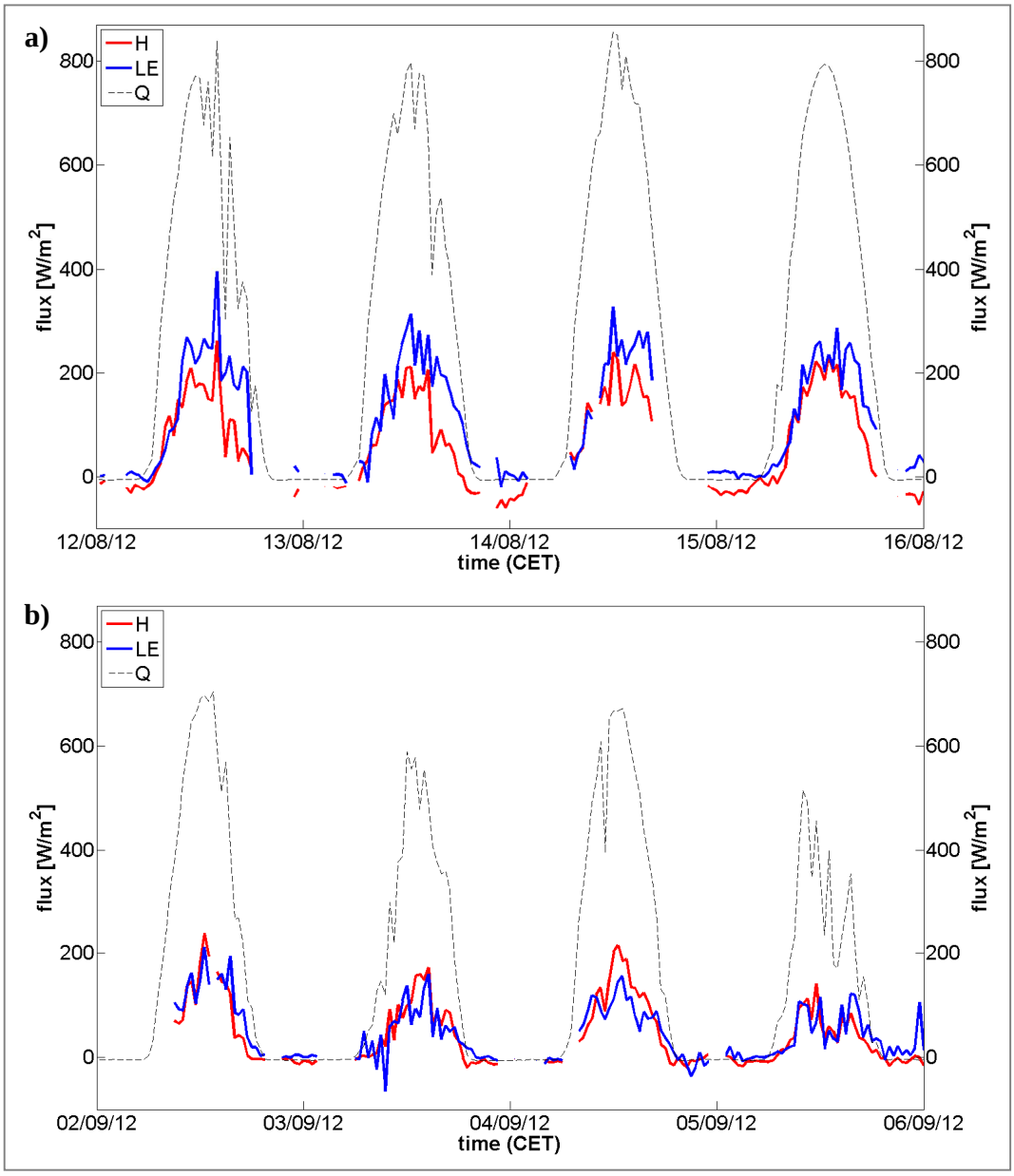

Figure 6.4 Eddy covariance measurements during 4-day-dryphase. Measurements of solar radiation (*Q*), sensible heat flux (*H*) and latent heat flux (*LE*) **a)** at SGD_EC2 from 02 to 06 September 2012, wind direction at measurement station 230° to 330°. **b)** at SGD_EC1 from 12 to 16 August 2012, wind direction at measurement station 80° to 180°.

Sensible and latent heat fluxes with their source within the housing area (Figure 6.4a) share an almost equal amount. Both *H* and *LE* reach a maximum value of about 200 W m^{-2} and their diurnal course appears alike during the day. While on 04 September *H* is increased during the early afternoon, for the other days *LE* and *H* do not show large deviations from each other at any time. Fluxes originating from the mixed land use area with buildings and green spaces (Figure 6.4b) show a somewhat different distribution. Here, *LE* appears to be higher than *H* throughout the dry phase at all days, with up to 100 W m^{-2} difference for 30 minutes calculated fluxes. Also apparent is a faster decrease of sensible heat flux *H* in the afternoon hours, while *LE* remains at a higher value until sunset. The higher absolute values of fluxes during these days are due to a higher solar radiation in general. However, as Spronken-Smith (2002) showed for fluxes over suburban terrain, diminished solar radiation has an impact on the absolute values of *H* and *LE*, but not on the role of *H* as the dominant heat sink compared to *LE*.

These different diurnal progressions suggest that within the housing area the energy partitioning proceeds to sensible heat and evapotranspiration in equal measure, as the water supply for *LE* is limited. Otherwise higher values of *LE* would be expected. A different contribution of latent heat flux to the available energy at the surface is given for fluxes originating from the mixed land use area with buildings and green spaces.

6.3 Discussion of the measured fluxes over suburban terrain

With the data on the annual course of the evaporative fraction *EF* a first approach on explaining the coherences between evapotranspiration and *LE*, respectively, and urban surfaces is made. However, the vegetation period of 2012 is not an ideal timeframe for the analysis of latent and sensible heat fluxes in their dependence on dry and wet surfaces. The year 2012 featured increased precipitation sums for summer (6 % more precipitation compared to 30-year-average, see Table 4.4) and a relatively constant precipitation throughout the whole year (215 days with rain, see Chapter 4.3). These circumstances provide little opportunity for the interpretation of dry phases, i.e. several days in succession without precipitation but high solar radiance. But these dry periods

would supply useful information on the role of distinct topsoil moisture on the local fluxes of *LE*.

The two 4-day-periods give an impression of the differences between the turbulent heat fluxes over the distinct urban land use structures. The partitioning of the turbulent fluxes is controlled by surface characteristics, i.e. the amount of evapotranspiration and the surface thermal properties. It gets obvious that a higher ratio of vegetation within the source area of turbulent fluxes probably causes a shift of energy partitioning towards *LE* during daytime. These initial findings for two distinct source areas are in good conformity with the results of other studies: Offerle et al. (2006a) found comparable values for *H* and *LE* over a suburban residential area in Łódz, Poland, during a dry period, while over a more rural area with a high percentage of vegetated surface *LE* is 50 W m^{-2} higher at average throughout the course of the day. On a dry and sunny day in April 2011 a comparison of a suburban and an urban site in Oberhausen, Germany, by Goldbach and Kuttler (2013) revealed a similar tendency. While *H* is significantly higher than *LE* at the urban site with up to 200 W m^{-2} shortly after noon, latent heat fluxes from the suburban site are higher than sensible heat fluxes throughout the day, with a maximum deviation of about 150 W m^{-2}.

With the evaluated data no direct impact of topsoil moisture can be shown yet, presumably due to the meteorological conditions in 2012 without permanent phases with no precipitation. However, an influence of water availability on *LE* is evident. At the annual scale effects of high and continuous precipitation can be found, as well as an impact of the phenological progression or dense vegetation in general, as given at DGD_EC in terms of a high pasture grass land. At the diurnal scale the higher percentage of vegetated surfaces at DGD_EC1 compared to DGD_EC2 presumably leads to a relatively increased *LE* compared to *H* within the energy flux partitioning during dry days.

In conclusion it can be said that the observations of the turbulent fluxes are worthwhile. They can provide useful additional information on the influence of surface characteristics, as e.g. surface sealing, topsoil moisture and vegetation coverage, on turbulent fluxes and partitioning of the available energy into sensible heat flux (i.e. air

temperature) and latent heat flux (i.e. evapotranspiration). Eddy covariance measurements can link the analysis results of the MeteoStation and SoilStation data. Yet a more detailed look at the eddy covariance data needs to be performed.

7 Synthesis and Conclusion

Soils in an urban environment feature very distinct characteristics due to their pedogenesis, substrates and anthropogenic alterations. Typical for anthropogenic land use modification are for example high bulk densities due to soil compaction, varying contents of organic matter or coarse material, or the occurrence of construction waste. Furthermore the most obvious anthropogenic impact is the destruction of soil surface due to sealing. These modified soil characteristics also cause the formation of distinctive soil water dynamics.

The prior aim of this study was an estimation of the relevance of this specific urban soil hydrology on local urban climate. A deeper knowledge on the processes and influencing factors of the interactions between pedosphere and atmosphere in the urban environment at the micro scale was to be gained. To deal with this research topic, a measurement network was planned and set up within the interdisciplinary project HUSCO. This network of twelve pedological measurement stations (SoilStations), six meteorological stations (MeteoStations) and two eddy covariance systems monitored pedological and atmospheric parameters at three different urban districts. At the inner city district two MeteoStations were operated at sealed areas. The two suburban areas, which featured distinct mean groundwater table depths, each provided data from two MeteoStations and six SoilStations, allocated among a green space and a housing area, and an additional eddy covariance system. These sites have been selected with regard to certain criteria, e.g. types of urban development, spatial structure, prevailing soil texture and vegetation.

The analysis of the measurement data collected with this network during the years 2011 and 2012 allowed a detailed view on the variations in soil hydrological processes as well as on local surface-near atmospheric conditions. In particular, it gives the following answers to the questions stated in the Introduction (Chapter 1).

How variable are soil moisture contents and water tension at the studied urban sites?

The results of this study indicate significant differences in annual urban soil water dynamics of the observed soil profiles. Soil profiles with constant high volumetric water contents (*VWC*), low soil water tensions (*SWT*)[17] and only a slight annual cycle in all measurement depths are found at green spaces with a very shallow groundwater table (as observed here within 0.4 m below surface). Hence, these soils are almost saturated throughout the vegetation period. On the contrary, generally low water contents within the majority of the observed depths throughout the year occur at the three mainly sandy housing areas' soil profiles. Precipitation events lead to short-time increases of water content and decreases of tension for only a few days or weeks. Particularly during longer phases with little precipitation these soils show a decrease in *SWT* starting at the surface and progressing into depth within the subsequent weeks. This effect is most pronounced at the deep groundwater districts' housing area profile with a loamy sand soil texture, where discernibly the drying reaches the 160 cm measurement depth and also shorter periods of little precipitation lead to a notable decrease of water tension within the upper meter of the profile. A very pronounced progression of topsoil water, i.e. 5 cm depth *VWC*, decrease into depth is also found for soils at the deep groundwater table district green spaces. These profiles show a distinct variation of *VWC* and *SWT* during wet and dry phases of the two investigated vegetation periods. Concurrently, in these profiles the drying of layers in 40 cm depth and below is sustained. A less pronounced decrease of relatively high water content during dry phases in depths below 40 cm, but fluctuations in *VWC* and *SWT* in the upper layers (40 cm depth and above) is observed at green spaces with an intermediate groundwater table depth of about 1 m within the district with a shallow groundwater table per definition.

In general, major fluctuations in *VWC* are found within the upper half meter of the soil column. Absolute values at the individual soil profiles on the annual scale lie

[17] The sole consideration of soil water content is not sufficient to understand and describe the water dynamics within a soil profile, nor to compare different soils or make statements on their relevance for local near-surface atmospheric conditions. In addition the soil water tension must be regarded to get evidence on the direction of the water movement. Furthermore, relating the water content to the plant-available water provides valuable information on the water availability for evapotranspiration.

between 10 % and 30 % *VWC* at the sandy profiles in the observed housing areas and between 55 % and 70 % at profiles rich in organic matter content of green space areas with a high groundwater table. Soil water tension is constantly low throughout the season here, while at the more loamy soils at the deep groundwater table green spaces it shows an absolute span of 850 hPa *SWT* or more. In lower depths, *VWC* as well as *SWT* remain at more constant values for the majority of soils, most often within the range of 5 % absolute *VWC* around the mean, and *SWT* below 200 hPa.

A comparison of the two vegetation periods, 2011 and 2012 shows similar temporal progressions of the water dynamics at the soil profiles, with moderate differences in the absolute values. For example, the mean annual water content values in 5 cm depth vary by up to 9 volume %, whereas in lower depth water contents only vary from about -4 % to +2 volume %. These variations are most likely caused by meteorological differences, e.g. more constant precipitation or less solar radiation.

Observations of the seasonal mean *VWC* of the topsoil, i.e. the 5 cm measurement depth, show for the majority of soil profiles a trend to increasing *VWC* from spring to fall in 2011. In 2012, however, most of the topsoils are dryer in summer and rewet in fall. This analysis reveals the potential range of near-surface water contents within urban areas at the spatial scale. The highest mean water content measured is 68 % *VWC* in spring at a green space station with shallow groundwater. The lowest average water content found is 12 % at a housing area backyard less than 1 km distant in the same season. This signifies that a difference in water content of more than half of the entire soil volume can occur within the same urban district.

What role do soil properties and urban land use play in controlling soil water dynamics?

The soil water dynamics in urban areas first and foremost depend on the water supply in terms of a sufficient delivery from surface or lower depths. Yet the spatial and temporal distribution of water is dominated by the specific urban soil properties. Soil substrate, texture and organic matter content determine physical properties like pore volume, bulk density and hydraulic conductivity. Thus, the impact of soil properties on

urban soil water dynamics is intrinsically large, as it is the case for soils in natural environments. These facts are confirmed in the present study by complementary field mapping and laboratory analyses, and by setting them into relation with the observational data.

Just as for soils of natural environments, distinct percolation rates are found to be depending on soil hydraulic parameters. Therefore, sandy soil profiles often show a fast percolation from soil surface to lower measurement depths but no enduring water storage. At more loamy textured layers precipitation water can be stored for a prolonged period. Similarly, a lack of rain leads to long-term drying at soil profiles with fine soil textures, causing lower *VWC* and higher *SWT* in lower depths up to several months after the dry phase. Water movement in these soils in general proceeds slowly according to the potential gradients. Thereby the progression of water is retarded, identifiable from the low saturated hydraulic conductivities (< 50 cm d^{-1}). Moreover, very the loamy layers with a high bulk density, as found at sites with high anthropogenic impact, like the application of substrate, can cause the stagnation of water and serve as a barrier to deeper layers, obstructing percolation. On the contrary, soils with layers of low bulk densities and high hydraulic conductivities are able to provide water for deeper areas shortly after precipitation events. Layers rich in organic matter are able to store water from precipitation or capillary rise due to their high available water capacity (*AWC*). Concluding, layers that feature high organic matter contents or high contents of construction waste and loam have a major impact on the water movement within the soil column. The observation of the seasonal topsoil water trends shows exactly this: Soils with these layers are found to deviate in their topsoil moisture progression from the prevailing trend of the particular vegetation period. As a consequence, as topsoil water content and availability are controlling factors for evaporation from the soil surface, the evapotranspiration (ET) rate of soils is likely to be to some extend determined by the characteristics of the layers below.

The monitoring of water content and tension also reveals a considerable influence of vegetation on the water dynamics within the rooting depth. Root soil water uptake can be clearly identified, most prominent at sites with deep rooting trees or dense pasture

grass vegetation. In these soil profiles *SWT* increases considerably and prolonged within the rooting depth in the course of the vegetation period. Meanwhile *VWC* is diminished due to increasing transpiration rates with the progression of the phenological cycle. Water for transpiration is taken from all layers within the rooting depths. At the observed profiles with grass vegetation this equals about the upper 40 cm. For soils vegetated with trees the rooting depth usually reaches deeper, provided that soil properties do not hinder the growth as it is found at one green space profile with construction waste in the upper half meter. The water uptake by deciduous trees is also higher compared to the uptake by grass, depicted in steeper temporal gradients of *VWC* and *SWT* during the course of the vegetation period. In addition, probably interception by crowns of trees might reduce the input of precipitation at these sites.

The impact of urban land use on soil water dynamics is not found to be distinct at the observed sites. However, differences in specific soil layering and substrate, as the observed housing areas' sites mostly feature coarser textures, determine differences in soil water dynamics.

To which extent does the groundwater table depth have an impact on soil moisture of the upper layers?

The observed soil profiles with permanently shallow groundwater table of about 40 cm depth show only minor low frequency fluctuations of the constant high *VWC* and low *SWT* at all depths. At soils with a local deep groundwater table below 1.6 m, distinct variations of *SWT* and *VWC*, depending on the amount and temporal distribution of precipitation, indicate no signs of capillary rise. Here variations in soil water dynamics depend predominantly on the soil texture. A drying in low-precipitation periods proceeds to greater depths and has a prolonged effect, which is not found this substantial for shallow groundwater (about 0.4 m depth). An intermediate local groundwater table of about 1 m depth indicates an insufficient refilling to the upper layers during phases with little precipitation, while water tension remains at low to moderate high values. Therefore, presumably a slight effect of intermediate groundwater on the upper layers' soil hydrology through capillary rise exists.

Within a three-week dry phase in April 2011, distinct changes in the water content are measured. Relative to the available water capacity of the upper 40 cm, the observed decreases in *VWC* range from 8 % to 38 % of the *AWC*. While the observations at the suburban shallow groundwater district show a decrease of about a tenth of *AWC* within the upper 40 cm, at the other district nearly a third of *AWC* are lost through evapotranspiration and percolation. These findings signify an impact of groundwater table depth on the water content of the upper soil layers during low precipitation periods. With appropriate soil physical properties that support capillary rise into and within the unsaturated zone, the groundwater table depth is most likely to be the major determining factor for the occurrence of upwards directed water movement within the soil column.

Groundwater management, as given at some housing area sites, obviously reduces the water supply for capillary rise. Therefore at these sites a deep water table depth is present, regardless of the mean groundwater table depth in the district per definition. As no groundwater provides water for a refilling, soil physical properties are the main determining factor for the hydrological quality and quantity of these soil profiles.

As these answers to the questions on urban soils indicate, the heterogeneity of urban soils appears to increase the already pronounced complexity of soil hydraulic processes. In urban areas the main controlling factors on water dynamics vary within small spatial scales. As a consequence the processes and feedbacks within the urban pedosphere become even more complex. These hydraulic factors and processes also affect the water availability at the surface, which in turn affects the actual evapotranspiration rates of these urban soils. Thereby, their effectiveness as a local cooling factor is influenced as well. The described variability of urban soil and the coupled topsoil water availability is thus most likely to influence the near-surface atmospheric conditions. Whether this conclusion is valid is discussed by answering the questions in the following:

How variable are the meteorological parameters in Hamburg in spatial terms, as observed with the measurement network?

The urban sites in this study, monitored with six MeteoStations, show individual characteristics in the local formation of meteorological parameters, i.e. air temperature (T_a) and specific humidity (q). First and foremost the temporal evolution, in terms of mean diurnal cycles at annual and seasonal scales, is distinct for the urban categories. Inner city areas show a different performance compared to the suburban areas. T_a is generally increased at the city centre stations at all day times and during all seasons. Compared to the lowest measured annual mean diurnal cycle, the inner city stations are up to 1.5 K warmer, while during summer nights even larger temperature deviations occur. Concurrently the humidity q remains constantly at lowest values at the inner city sites throughout the day, almost independent from season.

In second order, subordinate to the distinction of the urban categories, the two observed suburbs deviate from each other. While during the daytime only slight differences in T_a are visible, during the night the sites within the deep groundwater district are warmer compared to the stations at the shallow groundwater district. Yet these deviations are in the order of less than 0.5 K. Differences in the diurnal course of q are pronounced during the day, when sites at the deep groundwater district exhibit reduced humidity values compared to the second suburban district. Relative to the inner city as well as to each other q deviations are most pronounced during spring and summer daytime. Up to 1.5 g kg^{-1} less mean water vapor is measured at the city centre. The maximum difference in q between the two suburban stations is only a third of this value, as this ratio is already given for T_a deviations.

In third order, within each of the three districts, the measurements at the two MeteoStations reveal local variations on a less pronounced scale. Within the city centre a slightly larger amplitude of T_a is found for the station at the parking lot close to the river Elbe, yet only in the order of less than 0.2 K at average. The specific humidity at this site is increased during daytime, due to the nearby water supply contribution to higher actual ET. Within the deep groundwater districts' suburb the housing area shows a definite increased nighttime T_a compared to the nearby green space, while during

daytime no significant differences are observed. This distinction cannot be made for the shallow groundwater district, yet a faster increase of T_a in the morning is observed for the housing area here. Apparently, the heat capacity of the buildings does not lead to an increased nighttime T_a here, possibly due to the dominance of the second-order effect.

Compared to a rural reference site, spatial differences in the annual mean local T_a are given in the order of 1 K for the inner city. Only a quarter of this deviation is found for the deep groundwater housing area site, while the corresponding green space shows no differences in mean T_a from the rural site. Actually, the suburban sites with a shallow groundwater table are even 0.2 K cooler than the reference station outside of Hamburg at the annual average. However, it becomes obvious that differences in meteorological parameters at the spatial scale are not constant over time, as they are more pronounced during certain seasons and times of the day.

How pronounced is the nocturnal urban heat island effect observed within the network? Which conditions have an impact on its intensity? Which spatial peculiarities can be made out?

The nighttime deviation of T_a at urban sites compared to a rural reference is found to be significant for Hamburg. At the annual mean it lies in the order of +1.7 K for the city core, and +0.7 K for the deep groundwater suburban housing area, while at green space stations and the housing area of the shallow groundwater suburban district the urban heat island (UHI) effect does not occur. For summer months the UHI is even more pronounced at the sites where it is detected. At the shallow groundwater district, however, during summer a negative deviation of -0.3 K is found. These values are in good conformity with the observations of studies in other temperate latitude cities.

Furthermore, a ranking for the spatial formation can be defined, according to the urban district: The inner city stations show the highest T_a differences from the rural reference, followed by the deep groundwater district's housing area station and the nearby green space site. The shallow groundwater district sites deviate slightly negatively, but not from each other. This ranking is reasonable because inner city structures are known to feature the highest UHI formation. For the deep groundwater

district, its location closer to the city core than the shallow groundwater district, its slightly higher sealing ratio in general, and its dryer conditions due to a deeper mean groundwater table, are presumably the reasons for ranking second. A ranking according to the urban land use within this deep groundwater table district is visible, according to the surface sealing ratio and vegetation coverage, respectively. A possible explanation for the negative deviation of the shallow groundwater district's T_a from the rural reference can be the presumably higher evapotranspiration rates from high topsoil moistures, which are not necessarily given at the rural site.

The main impacting factors to intensify the UHI are low wind speeds of less than 2 m s^{-1} and little or no clouds (less than $6/8^{th}$ of cloud coverage). If these conditions are present, the UHI manifestation comes up to three times the mean annual value at the inner city sites (+5.2 K) and deep groundwater district sites (housing area: +2 K, green space +1 K) in spring 2011.

Do significant daytime temperature differences occur? If yes, which circumstances lead to their occurrence and which impacting factors on their intensity can be identified?

Annual mean air temperature deviations from the rural reference are only small. And yet different signs of this deviation are found for the observed districts. For the inner city sites small positive differences in mean T_a arise but in the order of less than a fifth of the observed nighttime UHI effect. In the suburban sites very little pronounced negative daytime T_a deviations are found. To observe the impact of evapotranspiration on daytime air temperature a comparison of T_a deviations of the suburban sites from the city centre was performed. Only days matching adequate conditions for ET, i.e. wind speeds of more than 2 m s^{-1} inducing turbulence and a sufficient solar forcing given by a maximum cloud coverage of $6/8^{th}$, are considered. This analysis reveals that the deviations of the suburban sites from the inner city sites are at a comparable level for all four MeteoStations for the selected conditions, as the annual mean daytime T_a deviations lie between -0.35 K and -0.5 K. While suburban sites are distinctly cooler during the night compared to the city centre, this daytime relation is less pronounced,

yet significant as well. Hence, sites with unsealed soils are slightly cooler compared to sites with sealed surfaces, even during the day and with turbulence induced by wind speed > 2 m s^{-1} and substantial solar radiation. Presumably evapotranspiration of water from topsoil is a factor causing this negative deviation of air temperature.

Is soil moisture a significant impacting factor for local air temperature?

For the nighttime T_a deviations of suburban sites from the rural reference (UHI) no evidence for an influence of topsoil water content could be found. Instead of these absolute T_a differences between the sites, the analysis of relative local values of air temperature provides additional information on a possible relation between soil surface water content and T_a. It is found that the normalized soil water content Θ is correlated to the daytime span of T_a, defined as difference between the diurnal maximum and minimum T_a, with an explained variance of 11 % to 17 % for situation meeting appropriate conditions for ET. Thus, an influence of topsoil water availability on the local air temperature is likely to exist. Local topsoil moisture can therefore be regarded as one significant impacting factor for the daytime increase of air temperature.

With regard to the finding that topsoil water availability depends on water supply, soil texture and vegetation cover, these factors are presumably also relevant for this effectiveness of soil on local T_a. A first indication that supports this assumption can be found in the observed difference of mean daily air temperature deviations of the suburban sites from the inner city reference with a sealed surface: The site that features a constantly high water availability in the topsoil, i.e. the shallow groundwater districts' green space with high organic matter content, shows the largest negative deviation and is thus the coolest site during daytime. Concurrently, the site with the lowest topsoil water content deviates from the inner city site the least at the annual average, i.e. the sandy profile at the housing area within the same district with very high hydraulic conductivities in the upper soil. Moreover, this site also exhibits an unusual fast air temperature increase in the morning compared to the slower warming green space site nearby. Hypothesizing that this increase occurs due to a lack of evapotranspiration, the comparison of these two sites, located within the same district yet different in topsoil

water content and soil water dynamics, also indicates that topsoil water is a significant impacting factor for local air temperature.

A conclusion that can be drawn is that the factors that mainly promote high topsoil moisture contents are likely to be also most relevant for the local effectiveness of soils on near-surface air temperature. In particular, soils with a high available water capacity in the upper layers, like loamy sands with moderately high bulk densities and a moderate saturated hydraulic conductivity, or soils with high organic matter content, appear to be most suitable to have that impact. In addition, a high groundwater table enhances the capillary rise of water to the topsoil and therefore it supports the local climatic effectiveness. Furthermore, vegetation influences the ET as well through the transpiration of water taken up by roots from lower soil depths.

The link between topsoil moisture and local air temperature are turbulent heat fluxes. They are controlled by the availability of soil water and their divergence affects the change in air temperature. Thus, measurements of turbulent heat fluxes provide additional information on the contribution of soil moisture to the local near-surface air temperature variability. The preliminary analysis of these fluxes, as measured by two eddy covariance systems calculating turbulent fluxes of sensible heat (i.e. change of air temperature) and latent heat (i.e. evapotranspiration), reveals major differences in the magnitude of evapotranspiration during the vegetation period:

Which trends of latent and sensible heat fluxes can be observed at the annual and the diurnal scale and by which parameters are they presumably induced?

Above the suburban district with a shallow groundwater table the analyzed fluxes include two distinct assumed source areas, a housing district and a heterogeneous area of houses and green space. At the annual scale the vegetation phenological cycle is mirrored in the form of a slow increase of evaporative fraction (*EF*) rates, i.e. the ratio of latent heat fluxes *LE* to the total heat fluxes, from spring to late summer, and a fast decrease of the trend in late fall. Complementary, an impact of the high and continuous precipitation in summer 2012 can be assumed to contribute to an increased *EF*. A broad

scatter of *EF* can be made out, with increasing intensity towards the end of summer. These differences in the relative share of *LE* are presumably, inter alia, induced by the surface characteristics of different source areas. The measurements at low height above the pasture grass covered green space at the deep groundwater district show higher values of *EF* in general throughout the vegetation period with a less defined amplitude and less scatter. The more homogeneous surface cover and the higher transpiration rates from plants can be assumed to be a cause for that.

The presumable inducing parameters of these differences in energy partitioning between the sites - spatially as well as over time - are the ratio of unsealed surfaces within the flux source area and the seasonal progression of vegetation coverage. These two main factors very likely lead to higher *LE* fluxes compared to *H* fluxes. However, with the conducted measurements during the vegetation period in 2012 the available water at the surface in terms of topsoil moisture could not be shown to be a significant impact factor, yet. The impact of water availability on the ET rates is evident through the influence of precipitation though. Probably the analysis of another vegetation period with less constant precipitation and prolonged dry phases would provide additional information on the relevance of topsoil moisture on evapotranspiration rates and flux partitioning.

At the diurnal scale, data is interpreted for different flux areas within the shallow groundwater district. During daytime of 4-day phases without precipitation different distributions of the absolute heat fluxes on *LE* and *H* are found. Fluxes originating from the area with a higher rate of vegetated surface show higher values for *LE* compared to *H*. A conclusion can be that again the source areas' characteristics determine the ratio of flux partitioning. Thus, distinct urban land use structures can be expected to induce different trends in the energy conversion from solar radiation to latent and sensible heat fluxes. Eventually, data from more extensive dry phases will certify this hypothesis, as a longer lasting deficiency of precipitation will cause even lower topsoil moistures in different scales at all sites. In these cases the impact of vegetation root water uptake and transpiration gets even more relevant, as a comparison of days at the beginning of the

period and at a state of advanced drought probably provide information on the scale of the contribution of topsoil moisture to the *EF*.

As a synthesis of the gained knowledge on the individual processes within the observed local urban pedosphere and atmosphere, the following answer to the question stated in the Introduction can be given.

To which extend do soil parameters and groundwater table depth have an impact on urban local climate?

Urban local climate is the result of the interaction of numerous factors modifying the large scale climate at a micro scale. As the urban landscape is inherently heterogeneous, all spheres are likely to also show inhomogeneities. A great variability of soil water dynamics was found for the observed urban soils in spatial terms and at the temporal scale. In particular the supportive effects of fine soil textures, high organic matter content and near-surface groundwater tables on increased and constant topsoil moisture were demonstrated. Air temperatures showed distinct daytime spans correlated with topsoil water contents, as smaller increases occurred at higher soil moistures. Higher specific humidities were found in areas with a higher mean groundwater table, while areas with a high ratio of sealed surfaces exhibited most pronounced nocturnal UHI effects, increased daytime temperatures and lowest water vapor contents. Higher rates of turbulent latent heat fluxes occurred above areas with less sealed and more vegetated surfaces.

A precise value of the share of soil properties and groundwater level on urban local climate modifications cannot be given, yet. Because of the findings above, however, it can certainly be stated that soils and groundwater do contribute to the formation of a specific local urban climate.

8 Outlook

Observing the impact of soils on local urban climate is a worthwhile effort. The investigations performed in this study and the underlying HUSCO approach deliver primary and basic information and specific values on the relationship between the urban pedosphere and atmosphere and their interaction at the micro scale. A dependence of the magnitude of the soil impact on local urban climate from soil properties and groundwater table depth was demonstrated. This detection constitutes a novelty in the urban climate and soil research and contributes to a deeper understanding on the formation of local climate in an urban environment.

Concerning the methodology of the present study, a future improvement of the coupling of the measurement data from the two spheres and a more detailed look at the individual processes should be aimed at:

- The use of modeling approaches in addition to the HUSCO network itself can be beneficial. A calculation of temporal soil water movements within the profiles might provide information on the incidence of groundwater capillary rise at the sites with an intermediate groundwater level (about 1 m). At these profiles the increased topsoil moisture was found, but no definite explanation could be given. A more precise determination of the cases of groundwater capillary rise and refilling of upper soil layers will be helpful to make out the circumstances and influencing factors that promote these processes.
- A more detailed evaluation of the collected eddy covariance method is necessary to deepen and consolidate the knowledge gained on turbulent heat fluxes over the urban district. Vegetation periods with a more pronounced sequence of dry phases and intensive precipitation events are very likely to be valuable for this analysis. Further data analysis techniques, e.g. using Penman-Monteith to predict the net evapotranspiration and compare it to the measured fluxes (e.g. Debruin and Holtslag, 1982) or state-of the art land surface-modeling, might help to get a more detailed view on the processes between atmosphere and urban land

surfaces. Furthermore, longer time series will provide more evaluable data of turbulent fluxes matching the criteria. They are essential to make meaningful statements on the dependence of the energy partitioning on greater climatic conditions and on urban source areas.

- Regarding the data evaluation an extension of the measurement series will be helpful. One aim should be to broaden the data base at the temporal scale, including several comparable and contrary periods and seasons, e.g. long dry phases in spring and summer or summer with little precipitation versus summer with high precipitation. This data can provide information on the significance of the measurement results as a selection of adequate cases, by using filters as performed in this study, with a sufficient number of measurements is necessary. In particular concerning the observations on the impact of topsoil moisture on the span of air temperature, an analysis of seasonally segregated data would be helpful to reduce the probable inherent seasonal effect.

Eventually, additional measurement stations can supply further information:

- Setting up more measurement stations in other districts throughout Hamburg is a useful addition for the project. A focus could lie on intermediate groundwater tables of 0.5 to 1.5 m or on shallow groundwater tables in areas with only little organic matter content, as given in the typical marshland areas in Hamburg. Also, suburban areas with a higher building density should be considered as an intermediate district type between inner city and detached housing areas. These measurements could provide information on the gradient of the urban heat island within Hamburg. Additive stations in suburban housing areas and green spaces eventually can be informative about the role of the suburban areas location within the city. At present, the limited number of measurements sites cannot cover the entire range of land use classes or common soils within the area of Hamburg.
- At this stage of the investigations made in this study, a clear distinction between mere evaporation from soil surface and transpiration of water by plant through

root water uptake cannot be performed. Apparently the water availability within the rooting depth is the crucial factor. A closer inspection of the role of different vegetation types should be part of further investigations. Therefore estimation of the water uptake of plants in combination with sap flow measurement would provide more detailed information on the quantity of transpiration of trees. The transpiration output of grasses and bushes could be estimated by leaf area index calculations carried out in botanical field mapping. As transpiration is a main component of the latent heat fluxes measured with the eddy covariance technique, a consideration of the phenology of the prevailing trees within the corresponding source areas would be helpful to give evidence on the share of mere evaporation on the evaporative fraction.

In the context of the predicted global climate change, the understanding of processes at local scale enables to develop appropriate and specific adaptation strategies. As in the course of global warming an increase in the intensity and frequency of heat waves and a decrease in summer precipitation for Northern and Central Europe is predicted (Alcamo et al., 2007), possibilities to locally counteract these tendencies are certainly useful for decision makers and urban planners:

- In terms of urban soils, their presumable capacity to attenuate the daytime air temperature increase when featuring higher topsoil moisture contents can contribute to a local cooling during heat waves. This would lead to an increase in human comfort and probably less heat stress in the corresponding urban districts. One possible measure to achieve this effect is the irrigation of vegetated open areas and green spaces. A more unusual method could be a temporary increase of local groundwater, or to be more precise a reduced groundwater lowering, during summer months. Herewith the topsoil water content is likely to be less decreased, as a refilling of the upper layers can proceed, provided that the soil texture promotes a capillary rise of water. However, a conflict of interests may be created in respect to the maintenance of dryness in basements of buildings in these areas.

- Furthermore, the cooling function of urban soils can qualify soils to be worthy of protection in the context of soil protection by law. This applies especially to areas with a shallow groundwater table and when soil substrate promotes capillary rise, e.g. loamy substrate or high organic matter content. Thus, also consequences for urban planning are given, as unsealed soils - and green spaces in particular - are beneficial for local climate not only due to their vegetation but also due to their soil moisture contents in the upper layer. Surface sealing therefore is to be considered as a critical intrusion in local climatic processes apart from the increased heat capacity and surface runoff. Groundwater measures are likewise to be seen rather critically from a climatic point of view with regard to urban development.
- The monitoring of the exchange processes and interspherial relationships provides a basis for the improvement and validation of parameterizations used in numerical models. The data collected within the HUSCO network is very likely to be beneficial for the use as a reference in e.g. micro scale climate models regarding urban climate or the projected climate change. The knowledge gained can contribute to a more detailed parameterization as it underlines the relevance of different soil properties and soil textures for processes within the local urban boundary layer.

Publications

The contents of Chapter 4 and Chapter 5 served as a basis for two manuscripts, which have been submitted for publication in 2013:

Wiesner, S., A. Eschenbach, and F. Ament, 2013a: Urban air temperature anomalies and their relation to soil moisture observed in the city of Hamburg. (submitted to *J. Appl. Meteor. Climatol.*)

Wiesner, S., F. Ament, A. Gröngröft, L. Kutzbach, and A. Eschenbach, 2013b: Analyzing spatial variability of urban soil water dynamics based on a soil monitoring network in Hamburg. (submitted to *Geoderma*)

References

Ad-hoc-Arbeitsgruppe Boden, 2005: *Bodenkundliche Kartieranleitung*. 5 ed. Schweizerbart'sche Verlagsbuchhandlung.

Alcamo, J., J. M. Moreno, B. Nováky, M. Bindi, R. Corobov, R. J. N. Devoy, C. Giannakopoulos, E. Martin, J. E. Olesen, and A. Shvidenko, 2007: Europe. Climate Change 2007: Impacts, Adaptation and Vulnerability. *Contribution of Working Group II to the Fourth Assessment Report of the Intergovernmental Panel on Climate Change*, M. L. Parry, O. F. Canziani, J. P. Palutikof, P. J. van der Linden, and C. E. Hanson, Eds., Cambridge University Press, 541-580.

Anders, I. and B. Rockel, 2009: The influence of prescribed soil type distribution on the representation of present climate in a regional climate model. *Clim. Dyn.*, 33**,** 177-186.

Arnfield, A. J., 2003: Two decades of urban climate research: A review of turbulence, exchanges of energy and water, and the urban heat island. *International Journal of Climatology*, 23**,** 1-26.

Balogun, A. A., J. O. Adegoke, S. Vezhapparambu, M. Mauder, J. P. McFadden, and K. Gallo, 2009: Surface Energy Balance Measurements Above an Exurban Residential Neighbourhood of Kansas City, Missouri. *Boundary-Layer Meteorology*, 133**,** 299-321.

Basara, J. B., B. G. Illston, C. A. Fiebrich, P. D. Browder, C. R. Morgan, A. McCombs, J. P. Bostic, R. A. McPherson, A. J. Schroeder, and K. C. Crawford, 2011: The Oklahoma City Micronet. *Meteorol. Appl.*, 18**,** 252-261.

Bechtel, B. and K. J. Schmidt, 2011: Floristic mapping data as a proxy for the mean urban heat island. *Climate Research*, 49**,** 45-58.

Bechtel, B. and C. Daneke, 2012: Classification of Local Climate Zones Based on Multiple Earth Observation Data. *IEEE J. Sel. Top. Appl. Earth Observ. Remote Sens.*, 5**,** 1191-1202.

Beuchel, S., 2012: Kleinräumige Temperaturvariabilität in einem hamburgischen randstädtischen Gebiet, University of Hamburg.

Bogena, H. R., M. Herbst, J. A. Huisman, U. Rosenbaum, A. Weuthen, and H. Vereecken, 2009: Potential of Wireless Sensor Networks for Measuring Soil Water Content Variability. *Vadose Zone J.*, 9**,** 1002-1013.

Brubaker, K. L. and D. Entekhabi, 1996: Analysis of feedback mechanisms in land-atmosphere interaction. *Water resources research*, 32**,** 1343-1357.

Burba, G. and D. J. Anderson, 2007: Introduction to the Eddy Covariance Method: General Guidelines and Conventional Workflow. LI-COR Biosciences, Ed., 141.

Burghardt, W., 1994: Soils in urban and industrial environments. *Zeitschrift für Pflanzenernährung und Bodenkunde*, 157**,** 205-214.

Campbell, C. S., 2001: Response of ECH2O soil moisture sensor to temperature variation. *Decagon Devices Inc. Application Note AN70TP-10*, Decagon Devices Inc.

Campbell, C. S., G. S. Campbell, D. Cobos, and L. Bissey, 2009: Calibration and evaluation of an improved low-cost soil moisture sensor, Application Note.

Campbell Scientific Inc., 2006a: CS616 and CS625 Water Content Reflectometers Instruction Manual. Revision 8/06. Campbell Scientific, Inc.

Campbell Scientific Inc., 2006b: Open Path Eddy Covariance System. Operator's Manual CSAT3, LI-7500, and KH20. Campbell Scientific, Inc.

Campbell Scientific Inc., 2009a: Instruction Manual: Gill WindSonic Ultrasonic Wind Sensor. Campbell Scientific, Inc.

Campbell Scientific Inc., 2009b: Instruction Manual: Model HMP45C Temperature and Relative Humidity Probe. Campbell Scientific, Inc.

Campbell Scientific Inc., 2009c: CR1000 Measurement and Control System Operator's Manual. Campbell Scientific, Ltd.

Campbell Scientific Inc., 2010a: Instruction Manual: CSAT3 Three dimensional Sonic Anemometer. Campbell Scientific Inc.

Campbell Scientific Inc., 2010b: Model 107 Temperature Probe Instruction Manual. Revision 6/10. Campbell Scientific, Inc.

Campbell Scientific Inc., 2010c: Instruction Manual: Gill Instruments WindSonic Two Dimensional Sonic Anemometer. Campbell Scientific, Inc.

Campbell Scientific Ltd., 2010: 52202/52203 Tipping Bucket Raingauge User Manual. Campbell Scientific, Ltd.

Campbell Scientific Ltd., 2011: IR100/IR120 Infra-red Remote Temperature Sensor User Manual. Campbell Scientific, Ltd.

Chen, X. and Q. Hu, 2004: Groundwater influences on soil moisture and surface evaporation. *Journal of Hydrology*, 297**,** 285-300.

Cobos, D. and C. Campbell, 2007: Correcting temperature sensitivity of ECH2O soil moisture sensors. *Application Notes*, Decagon Devices.

Cornelis, W. M., J. Ronsyn, M. Van Meirvenne, and R. Hartmann, 2001: Evaluation of pedotransfer functions for predicting the soil moisture retention curve. *Soil Sci. Soc. Am. J.*, 65**,** 638-648.

Coutts, A. M., J. Beringer, and N. J. Tapper, 2007: Impact of increasing urban density on local climate: Spatial and temporal variations in the surface energy balance in Melbourne, Australia. *J. Appl. Meteor. Climatol.*, 46**,** 477-493.

Czarnomski, N., G. W. Moore, T. G. Pypker, J. Licata, and B. J. Bond, 2005: Precision and accuracy of three alternative instruments for measuring soil water content in two forest soils of the Pacific Northwest. *Can. J. For. Res.-Rev. Can. Rech. For.*, 35**,** 1867-1876.

D'Odorico, P. and A. Porporato, 2004: Preferential states in soil moisture and climate dynamics. *Proc. Natl. Acad. Sci. U. S. A.*, 101**,** 8848-8851.

Daly, E. and A. Porporato, 2005: A review of soil moisture dynamics: From rainfall infiltration to ecosystem response. *Environ. Eng. Sci.*, 22**,** 9-24.

Damm, E., S. Höke, and P. Doetsch, 2012: Erfassung und Optimierungspotential der Kühlleistung von Böden dargestellt an ausgewählten Flächen der Stadt Bottrop. *Bodenschutz*, 12**,** 94-98.

Debruin, H. A. R. and A. A. M. Holtslag, 1982: A simple parameterization of the surface fluxes of sensible and latent heat during daytime compared with the Penman-Monteith concept. *Journal of Applied Meteorology*, 21**,** 1610-1621.

Decagon Devices Inc., 2010: 5TM Water Content and Temperature Sensors: Operator's Manual. Version 0. Decagon Devices, Inc.

Delleur, J. W., 2003: The evolution of urban hydrology: Past, present, and future. *J. Hydraul. Eng.-ASCE*, 129**,** 563-573.

DIN-ISO10390, 2005: Bodenbeschaffenheit - Bestimmung des pH-Wertes.

DIN-ISO10694, 1996: Bodenbeschaffenheit - Bestimmung von organischem Kohlenstoff und Gesamtkohlenstoff nach trockener Verbrennung (Elementaranalyse).

DIN-ISO11265, 1994: Bodenbeschaffenheit - Bestimmung der elektrischen Leitfähigkeit.

DIN-ISO11277, 2002: Bestimmung der Partikelgrößenverteilung in Mineralböden – Verfahren mittels Siebung und Sedimentation.

Dorigo, W. A., W. Wagner, R. Hohensinn, S. Hahn, C. Paulik, A. Xaver, A. Gruber, M. Drusch, S. Mecklenburg, P. van Oevelen, A. Robock, and T. Jackson, 2011: The International Soil Moisture Network: a data hosting facility for global in situ soil moisture measurements. *Hydrol. Earth Syst. Sci.*, 15**,** 1675-1698.

Dutton, J. A., 1986: *Dynamics of Atmospheric Motion*. Dover Publications.

Eliasson, I. and M. K. Svensson, 2003: Spatial air temperature variations and urban land use - a statistical approach. *Meteorol. Appl.*, 10**,** 135-149.

Famiglietti, J. S., J. A. Devereaux, C. A. Laymon, T. Tsegaye, P. R. Houser, T. J. Jackson, S. T. Graham, M. Rodell, and P. J. van Oevelen, 1999: Ground-based investigation of soil moisture variability within remote sensing footprints during the Southern Great Plains 1997 (SGP97) Hydrology Experiment. *Water resources research*, 35**,** 1839-1851.

Farah, H. O., W. G. M. Bastiaanssen, and R. A. Feddes, 2004: Evaluation of the temporal variability of the evaporative fraction in a tropical watershed. *International Journal of Applied Earth Observation and Geoinformation*, 5**,** 129-140.

Figuerola, P. I. and N. A. Mazzeo, 1998: Urban-rural temperature differences in Buenos Aires. *International Journal of Climatology*, 18**,** 1709-1723.

Findell, K. L. and E. A. B. Eltahir, 1997: An analysis of the soil moisture-rainfall feedback, based on direct observations from Illinois. *Water resources research*, 33**,** 725-735.

Freie und Hansestadt Hamburg, 2008: Digitale Bodenkarte Hamburg Versiegelung 2008. Behörde für Stadtentwicklung und Umwelt - Amt für Umweltschutz (U21).

Freie und Hansestadt Hamburg, 2010a: Daten des höchsten/niedrigsten Grundwasserflurabstands für Hydrojahre 1995/1996. Behörde für Stadtentwicklung und Umwelt - Amt für Gewässerschutz (U1).

Freie und Hansestadt Hamburg, 2010b: Digitale Bodenkarte Hamburg Bodenart. Behörde für Stadtentwicklung und Umwelt - Amt für Umweltschutz (U21).

Freie und Hansestadt Hamburg, 2010c: Biotopkartierung. Behörde für Stadtentwicklung und Umwelt - Amt für Umweltschutz (U21).

Gentine, P., D. Entekhabi, and J. Polcher, 2011: The Diurnal Behavior of Evaporative Fraction in the Soil-Vegetation-Atmospheric Boundary Layer Continuum. *J. Hydrometeor.*, 12**,** 1530-1546.

Givoni, B., 1991: Impact of planted areas on urban environmental quality: A review. *Atmospheric Environment. Part B. Urban Atmosphere*, 25**,** 289-299.

Goldbach, A. and W. Kuttler, 2013: Quantification of turbulent heat fluxes for adaptation strategies within urban planning. *International Journal of Climatology*, 33**,** 143-159.

Grimmond, C. S. B., 2006: Progress in measuring and observing the urban atmosphere. *Theoretical and Applied Climatology*, 84**,** 3-22.

Grimmond, C. S. B. and T. R. Oke, 1986: Urban Water Balance 2. Results from a suburb of Vancouver, British Columbia. *Water resources research*, 22**,** 1404-1412.

Grimmond, C. S. B. and T. R. Oke, 1999: Evapotranspiration rates in urban areas. *lUGG 99 Symposium*, Birmingham, UK, IAHS, 9.

Grimmond, C. S. B., J. A. Salmond, T. R. Oke, B. Offerle, and A. Lemonsu, 2004: Flux and turbulence measurements at a densely built-up site in Marseille: Heat, mass (water and carbon dioxide), and momentum. *Journal of Geophysical Research-Atmospheres*, 109.

Hartge, K. H. and R. Horn, 2009: *Die physikalische Untersuchung von Böden*. 4 ed. E. Schweizerbart'sche Vertragsbuchhandlung.

Henry, J. A. and S. E. Dicks, 1987: Association of urban temperatures with land use and surface materials. *Landsc. Urban Plan.*, 14**,** 21-29.

Herbst, M., P. T. W. Rosier, D. D. McNeil, R. J. Harding, and D. J. Gowing, 2008: Seasonal variability of interception evaporation from the canopy of a mixed deciduous forest. *Agricultural and Forest Meteorology*, 148**,** 1655-1667.

Hoffmann, P., 2012: Quantifying the influence of climate change on the urban heat island of Hamburg using different downscaling methods, University of Hamburg.

Houet, T. and G. Pigeon, 2011: Mapping urban climate zones and quantifying climate behaviors - An application on Toulouse urban area (France). *Environ. Pollut.*, 159**,** 2180-2192.

Idso, S. B., R. J. Reginato, R. D. Jackson, B. A. Kimball, and F. S. Nakayama, 1974: 3 stages of drying of a field soil. *Soil Sci. Soc. Am. J.*, 38**,** 831-837.

Illston, B. G., J. B. Basara, and K. C. Crawford, 2004: Seasonal to interannual variations of soil moisture measured in Oklahoma. *International Journal of Climatology*, 24**,** 1883-1896.

Jaeger, E. B. and S. I. Seneviratne, 2011: Impact of soil moisture-atmosphere coupling on European climate extremes and trends in a regional climate model. *Clim. Dyn.*, 36**,** 1919-1939.

Jansson, C., P. E. Jansson, and D. Gustafsson, 2007: Near surface climate in an urban vegetated park and its surroundings. *Theoretical and Applied Climatology*, 89**,** 185-193.

Kipp & Zonen, 2010: CMP/CMA series manual. Kipp & Zonen.

Kljun, N., P. Calanca, M. W. Rotachhi, and H. P. Schmid, 2004: A simple parameterisation for flux footprint predictions. *Boundary-Layer Meteorology*, 112**,** 503-523.

Klute, A. and C. Dirksen, 1986: Hydraulic conductivity and diffusivity. Laboratory methods. *Methods of soil analysis - part 1. Physical and mineralogical methods: Soil Science Society of America Book Series No. 5*, A. Klute, Ed., Soil Science Society of America, 687-734.

Kondo, J., N. Saigusa, and T. Sato, 1990: A parameterization of evaporation from bare soil surfaces. *J. Appl. Meteor. Climatol.*, 29**,** 385-389.

Krakauer, N. Y., B. I. Cook, and M. J. Puma, 2010: Contribution of soil moisture feedback to hydroclimatic variability. *Hydrol. Earth Syst. Sci.*, 14**,** 505-520.

Krauss, L., C. Hauck, and C. Kottmeier, 2010: Spatio-temporal soil moisture variability in Southwest Germany observed with a new monitoring network within the COPS domain. *Meteor. Z.*, 19**,** 523-537.

Kuttler, W., 2011: Climate change in urban areas, Part 1, Effects. *Environmental Sciences Europe*, 23**,** 11.

Kuttler, W., N. Müller, D. Dütemeyer, and A.-B. Barlag, 2012: Prognose- und Diagnoseanalysen zur Verbesserung des Stadtklimas - Stadtklimatische Untersuchungen in Oberhausen und Simulationen verschiedener Minderungsstrategien zur Reduktion der thermischen Belastung im Hinblick auf den Klimawandel, 41 pp.

Lafrenz, J., Ed., 2001: *Hamburg und seine Partnerstädte*. Selbstverlag Institut für Geographie der Universität Hamburg.

Lee, S.-H., K.-S. Lee, W.-C. Jin, and H.-K. Song, 2009: Effect of an urban park on air temperature differences in a central business district area. *Landscape and Ecological Engineering*, 5**,** 183-191.

Lemon, E. R., 1956: The Potentialities for Decreasing Soil Moisture Evaporation Loss. *Soil Sci. Soc. Am. J.*, 20**,** 120-125.

LI-COR Inc., 2004: LI-7500 Open path CO2/H2O Analyzer - Instruction Manual. LI-COR Inc.

LI-COR Inc., 2012: Eddy Pro Eddy Covariance Software. Version 3.0 User's Guide and Reference. LI-COR Inc.,.

Logsdon, S. D., G. Hernandez-Ramirez, J. L. Hatfield, T. J. Sauer, J. H. Prueger, and K. E. Schilling, 2009: Soil Water and Shallow Groundwater Relations in an Agricultural Hillslope. *Soil Sci. Soc. Am. J.*, 73**,** 1461-1468.

Martinez-Fernandez, J. and A. Ceballos, 2003: Temporal stability of soil moisture in a large-field experiment in Spain. *Soil Sci. Soc. Am. J.*, 67**,** 1647-1656.

Matzarakis, A., H. Mayer, and M. G. Iziomon, 1999: Applications of a universal thermal index: physiological equivalent temperature. *International Journal of Biometeorology*, 43**,** 76-84.

Mauder, M., C. Liebethal, M. Gockede, J. P. Leps, F. Beyrich, and T. Foken, 2006: Processing and quality control of flux data during LITFASS-2003. *Boundary-Layer Meteorology*, 121**,** 67-88.

Maxwell, R. M. and S. J. Kollet, 2008: Interdependence of groundwater dynamics and land-energy feedbacks under climate change. *Nat. Geosci.*, 1**,** 665-669.

Mayer, H. and P. Hoppe, 1987: Thermal comfort of man in different urban environments. *Theoretical and Applied Climatology*, 38**,** 43-49.

Mittelbach, H., I. Lehner, and S. I. Seneviratne, 2012: Comparison of four soil moisture sensor types under field conditions in Switzerland. *Journal of Hydrology*, 430**,** 39-49.

Morgan, K. T., L. R. Parsons, and T. Adair Wheaton, 2001: Comparison of laboratory- and field-derived soil water retention curves for a fine sand soil using tensiometric, resistance and capacitance methods. *Plant and Soil*, 234**,** 153-157.

Moriwaki, R. and M. Kanda, 2004: Seasonal and diurnal fluxes of radiation, heat, water vapor, and carbon dioxide over a suburban area. *J. Appl. Meteor. Climatol.*, 43**,** 1700-1710.

Morris, C. J. G., I. Simmonds, and N. Plummer, 2001: Quantification of the influences of wind and cloud on the nocturnal urban heat island of a large city. *J. Appl. Meteor. Climatol.*, 40**,** 169-182.

Myrup, L. O., C. E. McGinn, and R. G. Flocchini, 1993: An analysis of microclimatic variation in a suburban environment. *Atmospheric Environment Part B-Urban Atmosphere*, 27**,** 129-156.

Nachabe, M., N. Shah, M. Ross, and J. Vomacka, 2005: Evapotranspiration of two vegetation covers in a shallow water table environment. *Soil Sci. Soc. Am. J.*, 69**,** 492-499.

Nichols, W. E. and R. H. Cuenca, 1993: Evaluation of the evaporative fraction for parameterization of the surface energy balance. *Water resources research*, 29**,** 3681-3690.

Oechtering, L. and T. Däumling, 2012: Hamburger Projekte und Maßnahmen des vorsorgenden Bodenschutzes *Bodenschutz*, 12**,** 50-58.

Offerle, B., C. S. B. Grimmond, K. Fortuniak, and W. Pawlak, 2006a: Intraurban differences of surface energy fluxes in a central European city. *J. Appl. Meteor. Climatol.*, 45**,** 125-136.

Offerle, B., C. S. B. Grimmond, K. Fortuniak, K. Klysik, and T. R. Oke, 2006b: Temporal variations in heat fluxes over a central European city centre. *Theoretical and Applied Climatology*, 84**,** 103-115.

Oke, T. R., 1973: City size and the urban heat island. *Atmos. Environ.*, 7**,** 769-779.

Oke, T. R., 1982: The energetic basis of the urban heat-island. *Q. J. R. Meteorol. Soc.*, 108**,** 1-24.

Oke, T. R., 1984: Towards a prescription for the greater use of climatic principles in settlement planning. *Energy and Buildings*, 7**,** 1-10.

Oke, T. R., 2004: *Initial guidance to obtain representative meteorological observations at urban sites*. World Meteorological Organization.

Pachepsky, Y., W. J. Rawls, and D. Gimenez, 2001: Comparison of soil water retention at field and laboratory scales. *Soil Sci. Soc. Am. J.*, 65**,** 460-462.

Pan, W., R. P. Boyles, J. G. White, and J. L. Heitman, 2012: Characterizing Soil Physical Properties for Soil Moisture Monitoring with the North Carolina Environment and Climate Observing Network. *Journal of Atmospheric & Oceanic Technology*, 29**,** 933-943.

Pearlmutter, D., E. L. Kruger, and P. Berliner, 2009: The role of evaporation in the energy balance of an open-air scaled urban surface. *International Journal of Climatology*, 29**,** 911-920.

Peters, E. B., R. V. Hiller, and J. P. McFadden, 2011: Seasonal contributions of vegetation types to suburban evapotranspiration. *J. Geophys. Res.-Biogeosci.*, 116**,** 16.

Pickett, S. T. A., M. L. Cadenasso, J. M. Grove, C. H. Nilon, R. V. Pouyat, W. C. Zipperer, and R. Costanza, 2001: Urban Ecological Systems: Linking Terrestrial Ecological, Physical, and Socioeconomic Components of Metropolitan Areas. *Annual Review of Ecology and Systematics*, 32**,** 127-157.

Price, A. G. and D. E. Carlyle-Moses, 2003: Measurement and modelling of growing-season canopy water fluxes in a mature mixed deciduous forest stand, southern Ontario, Canada. *Agricultural and Forest Meteorology*, 119**,** 69-85.

Renger, M., M. Bohne, M. Facklam, T. Harrach, W. Riek, W. Schäfer, G. Wessolek, and S. Zacharias, Eds., 2009: *Ergebnisse und Vorschläge der DBG-Arbeitsgruppe „Kennwerte des Bodengefüges“ zur Schätzung bodenphysikalischer Kennwerte*. Vol. 40. *Bodenphysikalische Kennwerte und Berechnungsverfahren für die Praxis. Bodenökologie und Bodengenese*, TU Berlin.

Richards, L. A., 1948: Porous plate apparatus for measuring moisture retention and transmission by soil. *Soil Sci.*, 66**,** 105-110.

Robinson, D. A., C. S. Campbell, J. W. Hopmans, B. K. Hornbuckle, S. B. Jones, R. Knight, F. Ogden, J. Selker, and O. Wendroth, 2008: Soil moisture measurement for ecological and hydrological watershed-scale observatories: A review. *Vadose Zone J.*, 7**,** 358-389.

Robock, A. and K. Y. Vinnikov, 2000: The Global Soil Moisture Data Bank. *Bull. Amer. Meteor. Soc.*, 81**,** 1281.

Robock, A., M. Q. Mu, K. Vinnikov, I. V. Trofimova, and T. I. Adamenko, 2005: Forty-five years of observed soil moisture in the Ukraine: No summer desiccation (yet). *Geophys. Res. Lett.*, 32**,** 5.

Rotach, M. W. L., R. Vogt, C. Bernhofer, E. Batchvarova, A. Christen, A. Clappier, B. Feddersen, S. E. Gryning, G. Martucci, H. Mayer, V. Mitev, T. R. Oke, E. Parlow, H. Richner, M. Roth, Y. A. Roulet, D. Ruffieux, J. A. Salmond, M. Schatzmann, and J. A. Voogt, 2005: BUBBLE - An urban boundary layer meteorology project. *Theoretical and Applied Climatology*, 81**,** 231-261.

Roth, M., 2000: Review of atmospheric turbulence over cities. *Q. J. R. Meteorol. Soc.*, 126**,** 941-990.

Scheffer, F., 2002: *Lehrbuch der Bodenkunde*. 15 ed. Spektrum.

Schlünzen, K. H., P. Hoffmann, G. Rosenhagen, and W. Riecke, 2009: Long-term changes and regional differences in temperature and precipitation in the metropolitan area of Hamburg. *International Journal of Climatology*, 30**,** 1121-1136.

Schmid, H. P., 1997: Experimental design for flux measurements: matching scales of observations and fluxes. *Agricultural and Forest Meteorology*, 87**,** 179-200.

Schmid, H. P., H. A. Cleugh, C. S. B. Grimmond, and T. R. Oke, 1991: Spatial variability of energy fluxes in suburban terrain. *Boundary-Layer Meteorology*, 54**,** 249-276.

Seneviratne, S. I. and R. Stöckli, 2008: *The role of land-atmosphere interactions for climate variability in Europe*. Vol. 33, *Climate Variability and Extremes during the Past 100 Years*, Springer, 179-193 pp.

Seyfried, M. S. and M. D. Murdock, 2001: Response of a new soil water sensor to variable soil, water content, and temperature. *Soil Sci. Soc. Am. J.*, 65**,** 28-34.

Soylu, M. E., E. Istanbulluoglu, J. D. Lenters, and T. Wang, 2011: Quantifying the impact of groundwater depth on evapotranspiration in a semi-arid grassland region. *Hydrol. Earth Syst. Sci.*, 15**,** 787-806.

Spronken-Smith, R. A., 2002: Comparison of summer- and winter-time suburban energy fluxes in Christchurch, New Zealand. *International Journal of Climatology*, 22**,** 979-992.

Spronken-Smith, R. A. and T. R. Oke, 1998: The thermal regime of urban parks in two cities with different summer climates. *Int. J. Remote Sens.*, 19**,** 2085-2104.

Starr, J. L. and I. C. Palineanu, 2002: Methods for measurement of soil water content: Capacitance devices. *Methods of soil analysis: Physical methods*, J. H. Dane and G. C. Topp, Eds., Soil Science Society of America, 463-474.

Statistisches Amt für Hamburg und Schleswig-Holstein, 2011: Statistische Berichte - Bodenflächen in Hamburg und Schleswig-Holstein am 31.12.2010 nach Art der tatsächlichen Nutzung.

Stewart, I. D. and T. R. Oke, 2012: „Local climate zones" for urban temperature studies. *Bull. Amer. Meteor. Soc.*

Stull, R. B., 1988: *An Introduction to Boundary Layer Meteorology*. Kluwer Academic Pub.

Svensson, M. K. and I. Eliasson, 2002: Diurnal air temperatures in built-up areas in relation to urban planning. *Landsc. Urban Plan.*, 61**,** 37-54.

UMS GmbH, 2009: User Manual T4/T4e Pressure Transducer Tensiometer. Version 06/2009. UMS GmbH.

Unger, J., 1996: Heat island intensity with different meteorological conditions in a medium-sized town: Szeged, Hungary. *Theoretical and Applied Climatology*, 54**,** 147-151.

Upmanis, H., I. Eliasson, and S. Lindqvist, 1998: The influence of green areas on nocturnal temperatures in a high latitude city (Goteborg, Sweden). *International Journal of Climatology*, 18**,** 681-700.

van Genuchten, M. T., 1980: A closed form equation for predicting the hydraulic conductivity of unsaturated soils. *Soil Sci. Soc. Am. J.*, 44**,** 892-898.

Ventura, F., O. Facini, S. Piana, and P. Rossi, 2010: Soil Moisture Measurements: Comparison of Instrumentation Performances. *J. Irrig. Drainage Eng. - ASCE*, 136**,** 81-89.

von Storch, H. and M. Claussen, 2010: *Klimabericht für die Metropolregion Hamburg*. Springer.

Voogt, J. A., 2003: Urban Heat Island. *Encyclopedia of Global Environmental Change Volume 3: Causes and Consequences of Global Environmental Change*, I. Douglas, Ed., John Wiley & Sons, 660-666.

Wang, J., T. A. Endreny, and D. J. Nowak, 2008: Mechanistic simulation of tree effects in an urban water balance model. *J. Am. Water Resour. Assoc.*, 44**,** 75-85.

Webb, E. K., G. I. Pearman, and R. Leuning, 1980: Correction of flux measurements for density effects due to heat and water-vapor transfer. *Q. J. R. Meteorol. Soc.*, 106**,** 85-100.

Wessolek, G. and M. Facklam, 1997: Site characteristics and hydrology of sealed areas. *Zeitschrift für Pflanzenernährung und Bodenkunde*, 160**,** 41-46.

Wessolek, G., R. Plagge, F. J. Leij, and M. T. van Genuchten, 1994: Analysing problems in describing field and laboratory measured soil hydraulic properties. *Geoderma*, 64**,** 93-110.

Western, A. W., R. B. Grayson, and G. Bloschl, 2002: Scaling of soil moisture: A hydrologic perspective. *Annu. Rev. Earth Planet. Sci.*, 30**,** 149-180.

Wetzel, P. J. and J. T. Chang, 1987: Concerning the Relationship between Evapotranspiration and Soil Moisture. *Journal of Climate and Applied Meteorology*, 26**,** 18-27.

Yeh, P. J. F. and J. S. Famiglietti, 2009: Regional Groundwater Evapotranspiration in Illinois. *J. Hydrometeor.*, 10**,** 464-478.

Zacharias, S., H. Bogena, L. Samaniego, M. Mauder, R. Fuss, T. Putz, M. Frenzel, M. Schwank, C. Baessler, K. Butterbach-Bahl, O. Bens, E. Borg, A. Brauer, P. Dietrich, I. Hajnsek, G. Helle, R. Kiese, H. Kunstmann, S. Klotz, J. C. Munch, H. Papen, E. Priesack, H. P. Schmid, R. Steinbrecher, U. Rosenbaum, G. Teutsch, and H. Vereecken, 2011: A Network of Terrestrial Environmental Observatories in Germany. *Vadose Zone J.*, 10**,** 955-973.

Appendix A - Maps

The following maps were created by using the Software ArcGIS ArcMap 9.3. The information on land use, soil texture and groundwater table depth was provided by Freie und Hansestadt Hamburg (2008, 2012a, 2010b).

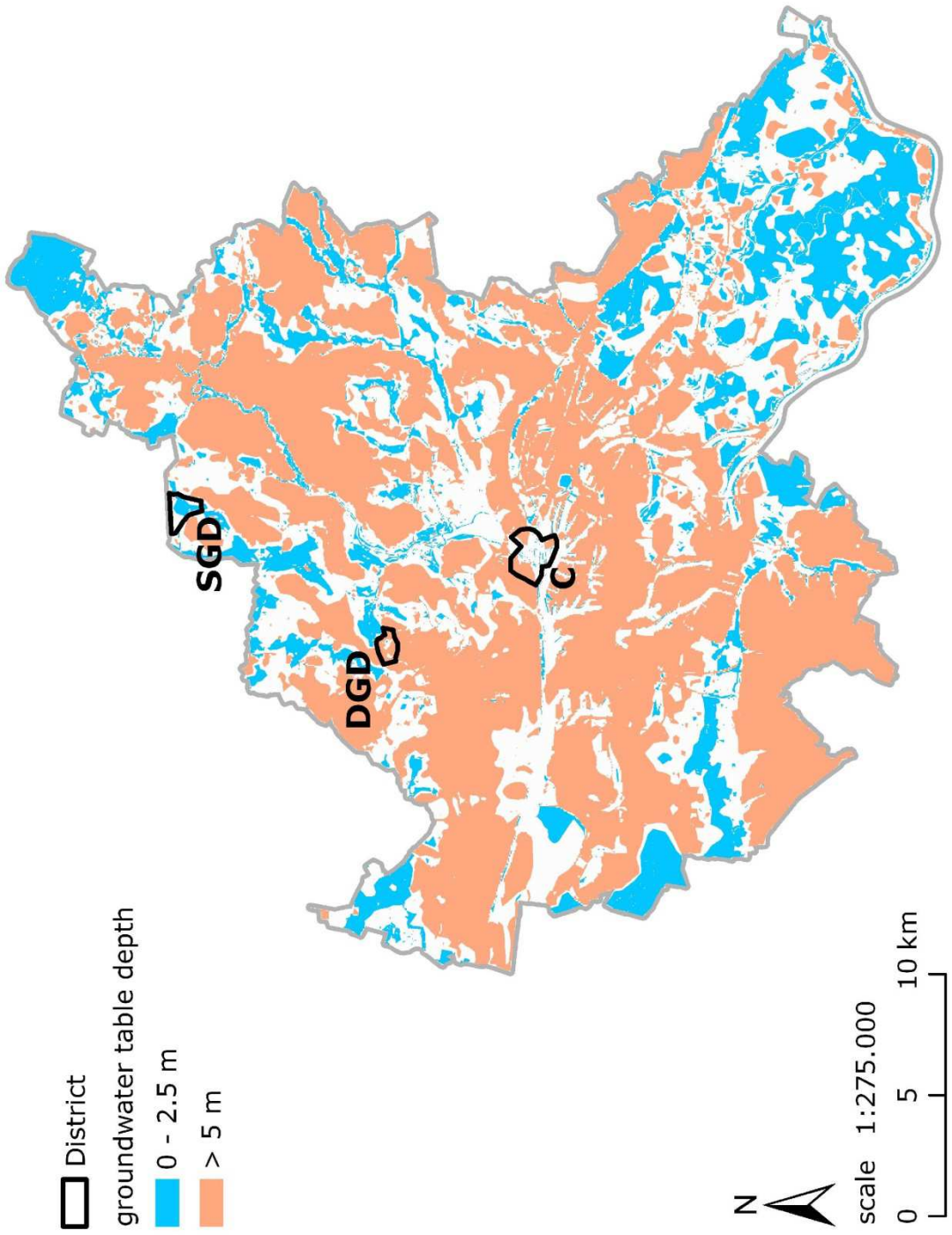

Figure A.1 Mean groundwater table depth in Hamburg (hydrological year 1995) and location of districts (Freie und Hansestadt Hamburg, 2010a). SGD = shallow groundwater table district, DGD = deep groundwater table district, C = inner city.

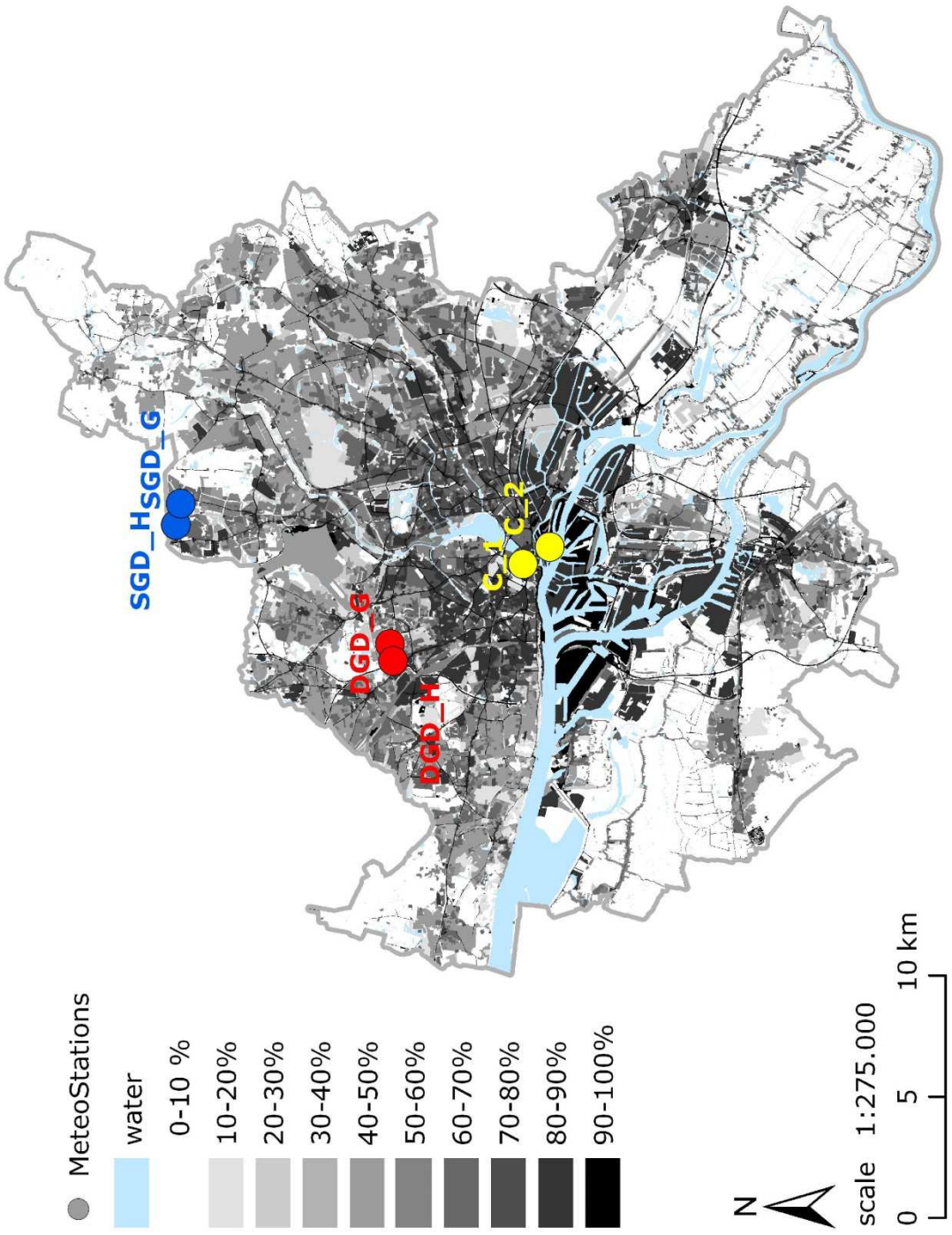

Figure A.2 Surface sealing in Hamburg (2008) (Freie und Hansestadt Hamburg, 2008) and location of MeteoStations. SGD = shallow groundwater table district, DGD = deep groundwater table district, C = inner city, H = housing area, G = green space.

Figure A.3 Pedological mapping of SGD green space: prevailing soil texture within the upper 30 cm and estimated capillary rise [mm/d] according to Ad-hoc Arbeitsgruppe Boden (2005) (aerial picture: Google Earth, ©2009 GeoBasis-DE/DKG and image ©2013 AeroWest).

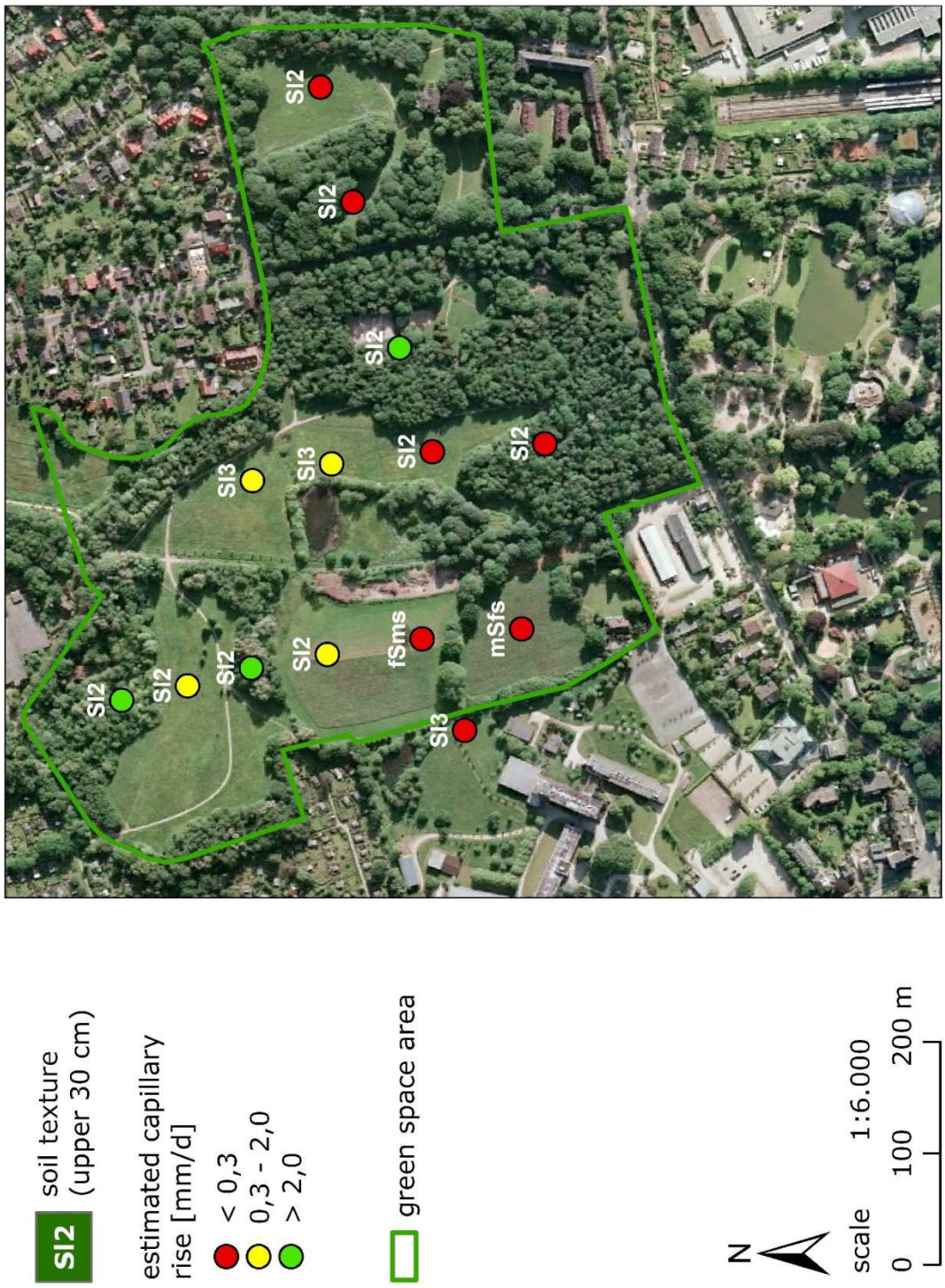

Figure A.4 Pedological mapping of DGD green space: prevailing soil texture within the upper 30 cm and estimated capillary rise [mm/d] according to Ad-hoc Arbeitsgruppe Boden (2005) (aerial picture: Google Earth, ©2013 AeroWest).

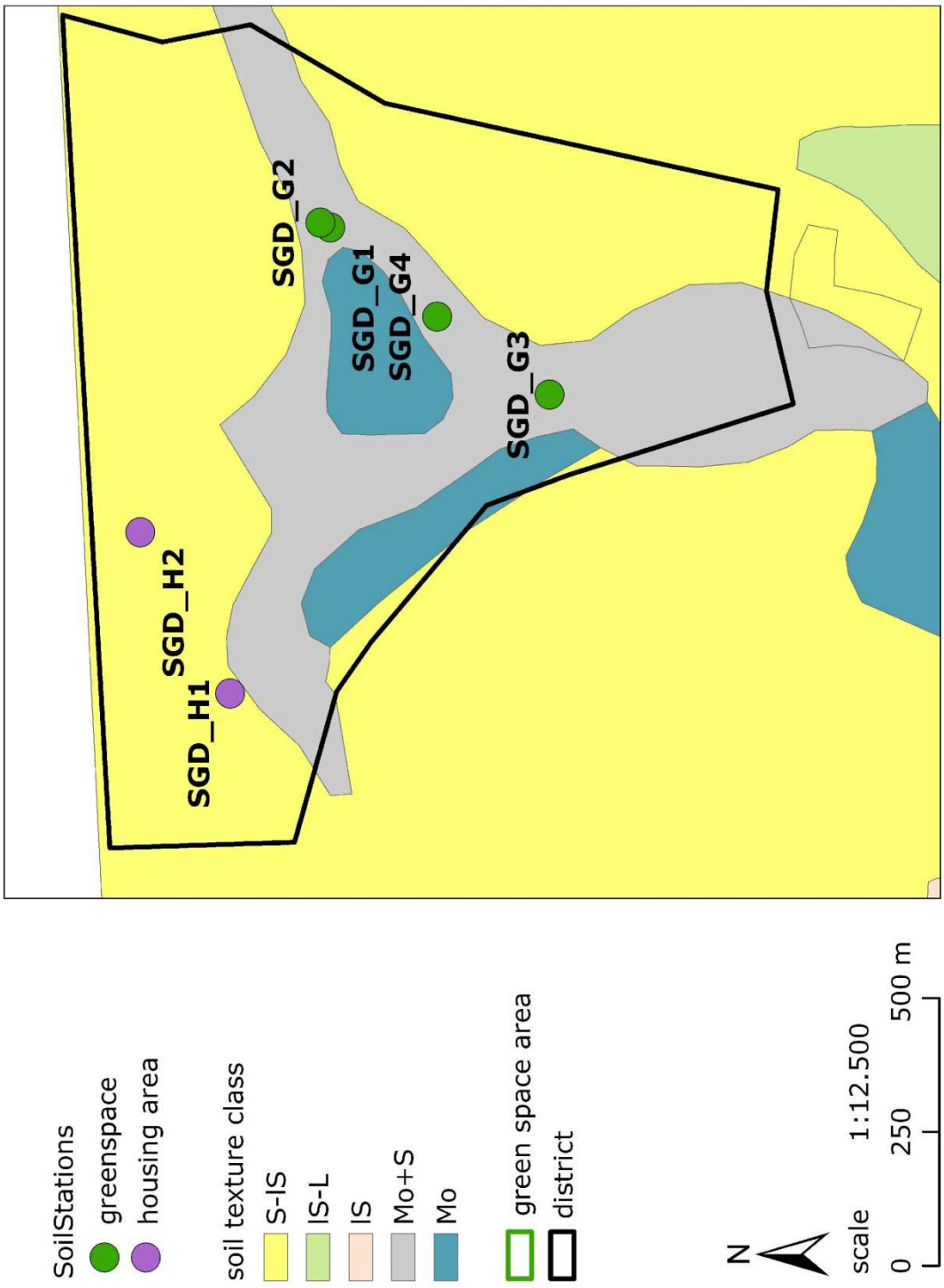

Figure A.5 Prevailing soil texture at SGD (Freie und Hansestadt Hamburg, 2010b) and location of SoilStations.

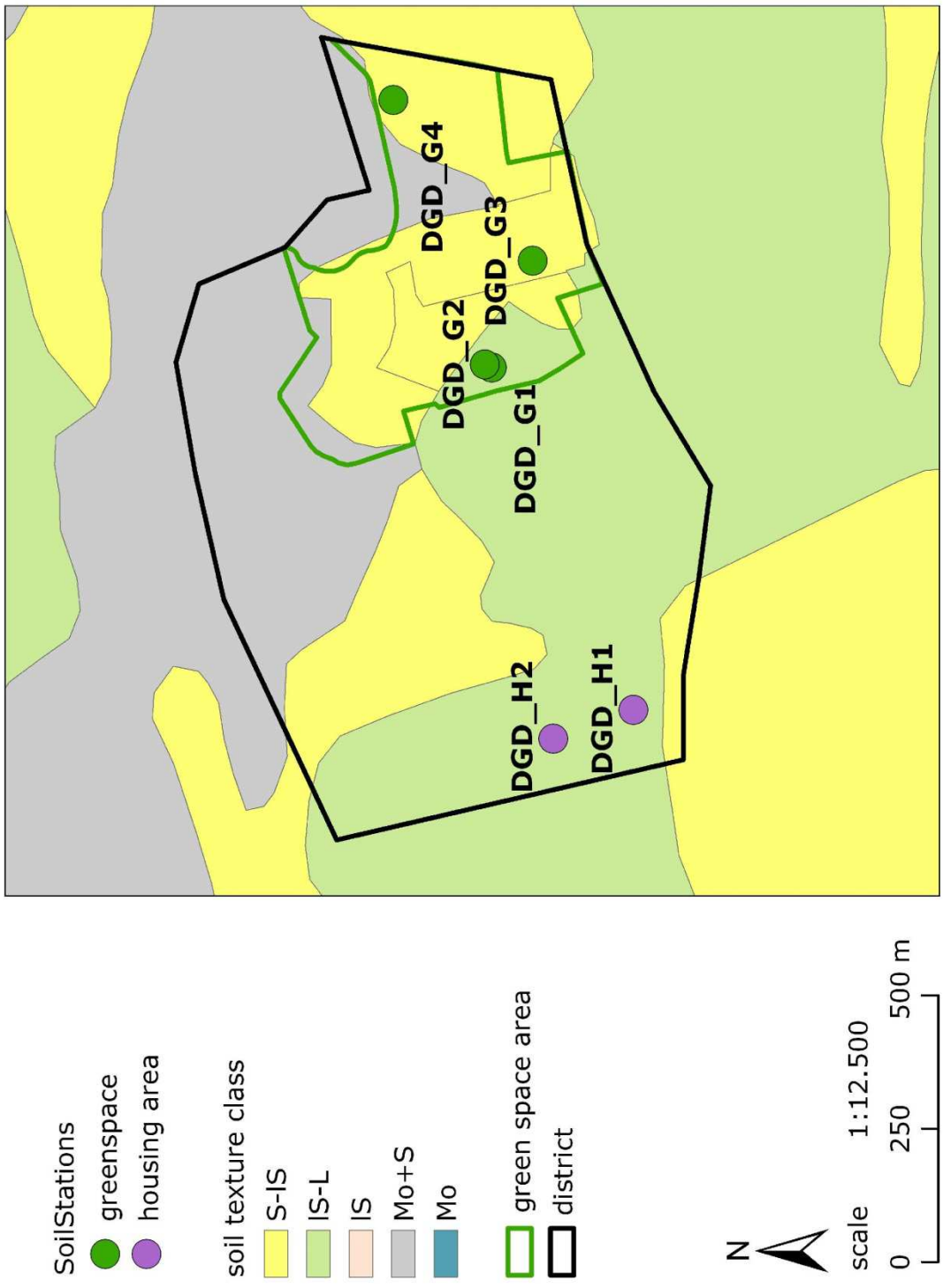

Figure A.6 Prevailing soil texture at DGD (Freie und Hansestadt Hamburg, 2010b) and location of SoilStations.

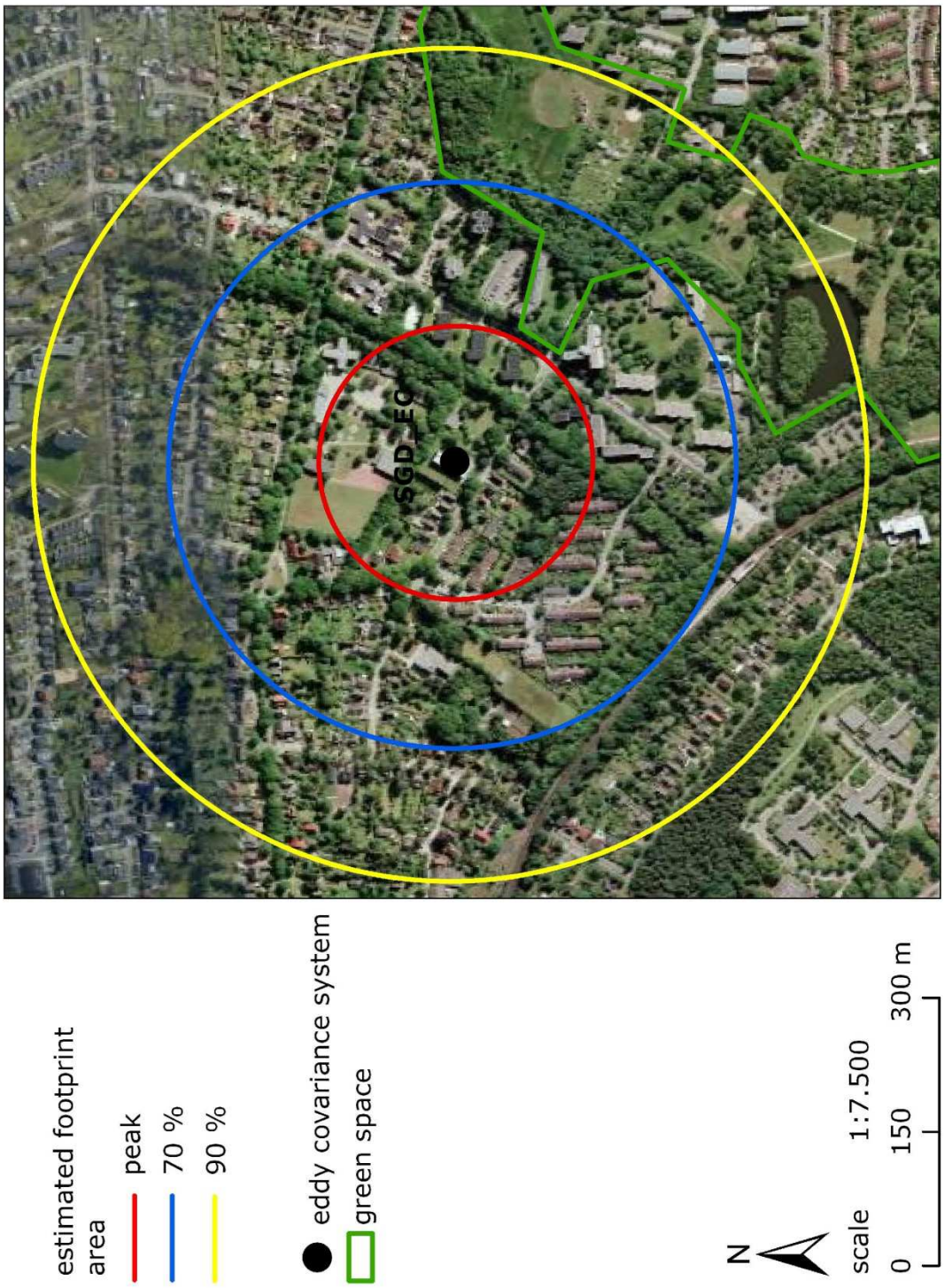

Figure A.7 Eddy covariance system location at SGD district; estimated footprint area: peak, 70 % and 90 %, calculated according to Kljun et al. (2004) (aerial picture: Google Earth, ©2009 GeoBasis-DE/DKG and image ©2013 AeroWest).

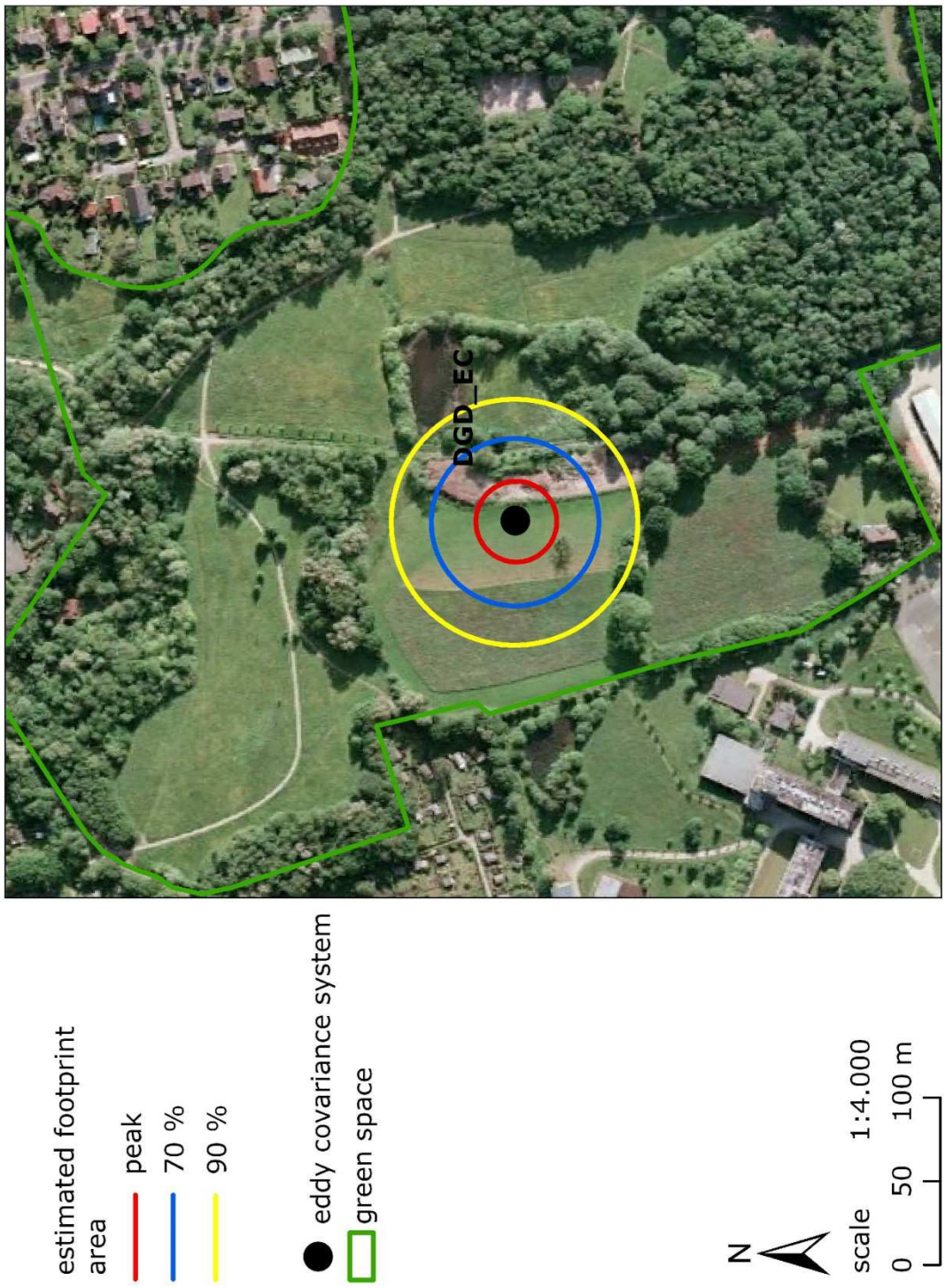

Figure A.8 Eddy covariance system location at DGD green space; estimated footprint area: peak, 70 % and 90 %, calculated according to Kljun et al. (2004) (aerial picture: Google Earth, ©2013 AeroWest).

Appendix B - Soil description

During the instrumentation of the SoilStations a complete pedological description of the soil profiles was carried out according to Ad-Hoc Arbeitsgruppe Boden (2005), including the sequence of the various soil layers and horizons and the classification of soil types following the German classification. In the following the completed form sheets are provided in German, as this is the language of the pedological mapping instructions and the form sheet.

Coordinates have been recorded with higher resolution than given in the form sheets. Soil texture data is given as specified in laboratory analyses.

Aufnahmeformblatt für bodenkundliche Profilaufnahmen nach KA 5

Standort SGD_G1

Titeldaten	TK-Nr.	Projekt	Profil-Nr.	Datum	Bearbeiter	Rechtswert	Hochwert	Höhe über NN	Aufschl.Art / Probenahme 55	Bemerkungen 55
	2326	HUSCO	4	18.11.2010	Sandoval	3567XXX	5950XXX	22,7 m	GG, P	-

Aufnahme-situation	Neigung 57,58	Exposition 59	Wölbung 59	Reliefformtyp 63	Mikrorelief 69	Lage im Relief 69	Bodenab-/-auftrag 69	Nutzungsart 71	Vegetation 73	Witterung 74	anthropogene Veränderungen 74	Bodenorganismen 76	Bemerkungen 79
	N0.1	-	WS0	T	RE	Z	-	G	GR	WT4	DO	Lu,an	-

Horizontdaten

Nr	Ober-/ Unter grenze 79	Horizont-symbol 83	**Pedogene und biogene Merkmale**								**Merkmale der Substratzusammensetzung**							
			Bodenfarbe 108	Humus-gehalt 110	Hydromor-phie-merkmale 112	Boden-feuchte 114	sonstige Merk-male 114	Gefüge-form und Größe 117,121	Hohl-räume (Risse, Poren Röhren) 123	Lagerungs-dichte Zersetz-ungsstufe 124	Durch-wurzel-ungs-inten-sität 129	Substratart 131,188	Substrat-genese 135	Gesamtbodenart 140			Carbo-nat-gehalt 168	Boden-aus-gangs-gestein 172	Strati-graphie 187
														Boden art/ Torfart 141,148, 157	Grob-boden-fraktionen/ Anteils-klassen 148	Summe Skelett (%) 150			
1	0-10	nHv	swbn	h6	-	feu 5	-	kru	-	Ld1	Wg 1 Wf 2	og-Hn	og	Su2	-	-	-	Hn	qh
2	10-28	nHw	swbn	h5	eh, fl, f2	feu 5	-	koh	-	Ld1	Wg1 Wf 2	og-Hn	og	Us	-	-	-	Hn	qh
3	28-32	II Gho	bn	h1	eh, fl, f2	feu 6	-	ein	-	Ld1	Wf 2	fg-ss (Sgf)	fg	Su2	-	-	-	Sgf	qp
4	32+	Gr	hoc	-	-	feu 6	-	ein	-	Ld1	Wf 1	fg-ss (Sgf)	fg	Su2	-	-	-	Sgf	qp

Bodenform

Bodensystematische Einheit 190 GHn Niedermoorgley	**Substratsystematische Einheit** 132,289,296 og – (Hn-qh) \ fg-ss (Sgf-qp)	
Humusform 298 AMO	Wasserstand u GOF 310 0,36 m	Bemerkungen 320 tieferes Profil nicht grabbar aufgrund GW-Stand

Figure B.1 Pedological description of soil profile at SGD_G1.

Aufnahmeformblatt für bodenkundliche Profilaufnahmen nach KA 5

Standort SGD_G2

Titeldaten	TK-Nr.	Projekt	Profil-Nr.	Datum	Bearbeiter	Rechtswert	Hochwert	Höhe über NN	Aufschl.Art / Probenahme 55	Bemerkungen 55
	2326	HUSCO	5	18.11.2010	Sandoval	3567XXX	5950XXX	22,8 m	GG, P	

Aufnahme-situation	Neigung 57,58	Exposition 59	Wölbung 59	Reliefformtyp 63	Mikrorelief 69	Lage im Relief 69	Bodenab-/ -auftrag 69	Nutzungsart 71	Vegetation 73	Witterung 74	anthropogene Veränderungen 74	Bodenorganismen 76	Bemerkungen 79
	N0.1	-	WS0	T	RE	Z	-	GE	LW,MO	WT4	-	Lu,an	-

Horizontdaten

Nr	Ober-/ Unter grenze 79	Horizont-symbol 83	Pedogene und biogene Merkmale									Merkmale der Substratzusammensetzung							
			Bodenfarbe 108	Humus-gehalt 110	Hydromor-phie-merkmale 112	Boden-feuchte 114	sonstige Merk-male 114	Gefüge-form und Größe 117,121	Hohl-räume (Risse, Poren Röhren) 123	Lagerungs-dichte Zersetz-ungsstufe 124	Durch-wurzel-ungs-intensität 129	Substratart 131,188	Substrat-genese 135	Gesamtbodenart 140			Carbo-nat-gehalt 168	Boden-aus-gangs-gestein 172	Strati-graphie 187
														Boden art/ Torfart 141,148, 157	Grob-boden-fraktionen/ Anteils-klassen 148	Summe Skelett (%) 150			
1	0-20	nHv	swbn	h5	-	feu 5	-	kru	-	Ld1	Wf 2	og-Hn	og	Su2	-	-	-	Hn	qh
2	20-30	nHw	droswbn	h6	eh, fl, f2	feu 5	-	koh	-	Ld1	Wf 2	og-Hn	og	Sl2	-	-	-	Hn	qh
3	30+	II Gr	grlioc	h4	-	feu 6	-	ein	-	Ld1	Wf 1	fg-ss (Sgf)	fg	Us	-	-	-	Sgf	qp

Bodenform

Bodensystematische Einheit 190	**Substratsystematische Einheit** 132,289,296	
KV Erdniedermoor	og - (Hn-qh) / fg-ss (Sgf-qp)	
Humusform 298	Wasserstand u GOF 310	Bemerkungen 320
AMO	0,4 m	tieferes Profil nicht grabbar aufgrund GW-Stand

Figure B.2 Pedological description of soil profile at SGD_G2.

Aufnahmeformblatt für bodenkundliche Profilaufnahmen nach KA 5

Standort SGD_G3

Titeldaten	TK-Nr.	Projekt	Profil-Nr.	Datum	Bearbeiter	Rechtswert	Hochwert	Höhe über NN	Aufschl.Art / Probenahme 55	Bemerkungen 55
	2326	HUSCO	12	09.03.11	Sandoval	3567XXX	5949XXX	21,2 m	GS, P	-

Aufnahme-situation	Neigung 57,58	Exposition 59	Wölbung 59	Reliefformtyp 63	Mikrorelief 69	Lage im Relief 69	Bodenab-/-auftrag 69	Nutzungsart 71	Vegetation 73	Witterung 74	anthropogene Veränderungen 74	Bodenorganismen 76	Bemerkungen 79
	N 0.1	N	WS 0	T	RE	Z	AY (?)	NP	WI	WT 3	-	Lu	-

Horizontdaten

Nr	Ober-/ Unter grenze 79	Horizont-symbol 83	**Pedogene und biogene Merkmale**								**Merkmale der Substratzusammensetzung**							
			Bodenfarbe 108	Humus-gehalt 110	Hydromor-phie-merkmale 112	Boden-feuchte 114	sonstige Merk-male 114	Gefüge-form und Größe 117,121	Hohl-räume (Risse, Poren Röhren) 123	Lagerungs-dichte Zersetz-ungsstufe 124	Durch-wurzel-ungs-inten-sität 129	Substratart 131,188	Substrat-genese 135	Gesamtbodenart 140			Carbo-nat-gehalt 168	Boden-aus-gangs-gestein 172	Strati-graphie 187
														Boden art/ Torfart 141,148, 157	Grob-boden-fraktionen/ Anteils-klassen 148	Summe Skelett (%) 150			
1	0-15, z	jAh	dbn	h3	-	feu 3	-	kru	-	Ld1	Wf 2 Wg 1	oj-ls(Sgf)	oj	mSgs	-	-	-	K	qh
2	15-80	jilCv	horlioc	h2	eh,fl,f1	feu 3	-	ein	-	Ld2	-	oj-(zk2)ss(Sgf	oj	gSms	gG 2, gGr 1	2 %	-	K	qh
3	80-110	jGo	dgrlibn	-	eh,fl,f3 rg,fl,f3	feu 5	-	ein	-	Ld3	-	oj-(k2)ss(Sgf)	oj	gSms	gG 2	2 %	-	K	qh
4	110+	lljGor	bhliocgr	-	eh,fl,f2 rg,fl,f7	feu 6	-	ein	-	Ld2	-	oj-(k2)ss(Sgf)	oj	gSms	gG 2	2 %	-	K	qh

Bodenform

Bodensystematische Einheit 190	**Substratsystematische Einheit** 132,289,296	Bemerkungen 320
Gley-Regosol GG-RQ	oj - (k2) ss (K - qh) // oj - (k2) ll (K – qh)	
Humusform 298	Wasserstand u GOF 310	
MU	ca. 1,20 m	Material verm. aufgeschoben; Oberboden tlw. gefroren

Figure B.3 Pedological description of soil profile at SGD_G3.

Aufnahmeformblatt für bodenkundliche Profilaufnahmen nach KA 5

Standort SGD_G4

Titeldaten	TK-Nr.	Projekt	Profil-Nr.	Datum	Bearbeiter	Rechtswert	Hochwert	Höhe über NN	Aufschl.Art / Probenahme 55	Bemerkungen 55
	2326	HUSCO	13	09.03.11	Sandoval	3567XXX	5949XXX	21,9 m	GG,P	-

Aufnahme-situation	Neigung 57,58	Exposition 59	Wölbung 59	Reliefformtyp 63	Mikrorelief 69	Lage im Relief 69	Bodenab-/ -auftrag 69	Nutzungsart 71	Vegetation 73	Witterung 74	anthropogene Veränderungen 74	Bodenorganismen 76	Bemerkungen 79
	N 0.1	W	WS 0	T	RE	Z	-	G	Wl	WT 3	-	Lu	-

Horizontdaten

Nr	Ober-/ Unter grenze 79	Horizont-symbol 83	Pedogene und biogene Merkmale									Merkmale der Substratzusammensetzung							
			Bodenfarbe 108	Humus-gehalt 110	Hydromorphie-merkmale 112	Boden-feuchte 114	sonstige Merk-male 114	Gefüge-form und Größe 117,121	Hohl-räume (Risse, Poren Röhren) 123	Lagerungs-dichte Zersetz-ungsstufe 124	Durch-wurzel-ungs-intensität 129	Substratart 131,188	Substrat-genese 135	Gesamtbodenart 140			Carbo-nat-gehalt 168	Boden-aus-gangs-gestein 172	Strati-graphie 187
														Boden art/ Torfart 141,148, 157	Grob-boden-fraktionen/ Anteils-klassen 148	Summe Skelett (%) 150			
1	0-30,v	jAh	swbn	h4	-	feu 3	-	kru	-	Ld1	Wf 2 Wg1	oj-ss(Sgf)	oj	Su2	-	-	-	K	qh
2	30-65	jilCv	hoc	h2	eh,fl,f3 rg,fl,f1	feu 3	-	ein	-	Ld1	-	oj-ss(Sgf)	oj	Su2	gG 1	1 %	-	K	qh
3	65+	jGro	orlidoc	-	ed,fl,f5 rg,fl,f5	feu 5	-	ein	-	Ld2	-	oj-ss(Sgf)	oj	gSms	gG 1	1 %	-	K	qh

Bodenform

Bodensystematische Einheit 190	**Substratsystematische Einheit** 132,289,296	
Gley-Regosol GG-RQ	oj - ss (K - qh)	
Humusform 298	Wasserstand u GOF 310	Bemerkungen 320
MU	ca. 85 cm	Material vermutlich aufgeschoben

Figure B.4 Pedological description of soil profile at SGD_G4.

Aufnahmeformblatt für bodenkundliche Profilaufnahmen nach KA 5

Standort SGD_H1

Titeldaten	TK-Nr.	Projekt	Profil-Nr.	Datum	Bearbeiter	Rechtswert	Hochwert	Höhe über NN	Aufschl.Art / Probenahme 55	Bemerkungen 55
	2326	HUSCO	6	19.11.2010	Sandoval	3566XXX	5950XXX	25,5 m	GS, P	-

Aufnahme-situation	Neigung 57,58	Exposition 59	Wölbung 59	Reliefformtyp 63	Mikrorelief 69	Lage im Relief 69	Bodenab-/-auftrag 69	Nutzungsart 71	Vegetation 73	Witterung 74	anthropogene Veränderungen 74	Bodenorganismen 76	Bemerkungen 79
	N0.1	-	WS0	H	RE	M	AY	NG	SV	WT4	-	Lu,an	-

Horizontdaten

Nr	Ober-/ Unter grenze 79	Horizont-symbol 83	**Pedogene und biogene Merkmale**								**Merkmale der Substratzusammensetzung**							
			Bodenfarbe 108	Humus-gehalt 110	Hydromor-phie-merkmale 112	Boden-feuchte 114	sonstige Merk-male 114	Gefüge-form und Größe 117,121	Hohl-räume (Risse, Poren Röhren) 123	Lagerungs-dichte Zersetz-ungsstufe 124	Durch-wurzel-ungs-inten-sität 129	Substratart 131,188	Substrat-genese 135	Gesamtbodenart 140			Carbo-nat-gehalt 168	Boden-aus-gangs-gestein 172	Strati-graphie 187
														Boden art/ Torfart 141,148, 157	Grob-boden-fraktionen/ Anteils-klassen 148	Summe Skelett (%) 150			
1	0-30	jAh1-M	swbn	h4	-	feu 3	-	sub	-	Ld1	Wg 1 Wf 4	oj-ss (Sgf6, Ybz2)	oj	Su2	mGr 2 gGr 1	5 %	-	K, Ybz2	qh
2	30-45	jAh2-M	swbn	h5	-	feu 4	-	sub	-	Ld1	Wg 1 Wf 3	oj-ss (Sgf6, Ybz2)	oj	Su2	mGr 2 gGr 2	5 %	-	K, Ybz2	qh
3	45-55	ll fAeh	hgr	h3, bae	-	feu 3	Sgb	sub	-	Ld2	Wf 2	fg-ss (Sgf)	fg	mSfs	mG 2	2 %	-	Sgf	qp
4	55-115	fBhs	dorro	h1, fl	-	feu 3	Oe, Hu	sub	-	Ld3	Wg 1	fg-ss (Sgf)	fg	mS	G 2	5 %	-	Sgf	qp
5	115+	iC	hoc	-	-	feu 2	-	ein	-	Ld3	Wg 1	fg-ss (Sgf)	fg	fSms	-	-	-	Sgf	qp

Bodenform

Bodensystematische Einheit 190	**Substratsystematische Einheit** 132,289,296	
Kolluvisol über gekapptem Podsol YK/ePP	oj-ss (K, Ybz-qh) / fg-ss (Sgf-qp)	
Humusform 298	Wasserstand u GOF 310	Bemerkungen 320
MU	-	-

Figure B.5 Pedological description of soil profile at SGD_H1.

Aufnahmeformblatt für bodenkundliche Profilaufnahmen nach KA 5

Standort SGD_H2

Titeldaten	TK-Nr.	Projekt	Profil-Nr.	Datum	Bearbeiter	Rechtswert	Hochwert	Höhe über NN	Aufschl.Art / Probenahme 55	Bemerkungen 55
	2326	HUSCO	7	24.11.2010	Sandoval	3567XXX	5950XXX	25,4m	GS, P	-

Aufnahme-situation	Neigung 57,58	Exposition 59	Wölbung 59	Reliefformtyp 63	Mikrorelief 69	Lage im Relief 69	Bodenab-/ -auftrag 69	Nutzungsart 71	Vegetation 73	Witterung 74	anthropogene Veränderungen 74	Bodenorganismen 76	Bemerkungen 79
	N0.1	-	WS0	H	RE	M	-	NG	SV	WT4	-	Lu,an	-

Horizontdaten

Nr	Ober-/ Unter grenze 79	Horizont-symbol 83	**Pedogene und biogene Merkmale**									**Merkmale der Substratzusammensetzung**								
			Bodenfarbe 108	Humus-gehalt 110	Hydromorphie-merkmale 112	Boden-feuchte 114	sonstige Merk-male 114	Gefüge-form und Größe 117,121	Hohl-räume (Risse, Poren Röhren) 123	Lagerungs-dichte Zersetz-ungsstufe 124	Durch-wurzel-ungs-intensität 129	Substratart 131,188	Substrat-genese 135	Gesamtbodenart 140			Carbo-nat-gehalt 168	Boden-aus-gangs-gestein 172	Strati-graphie 187
														Boden art/ Torfart 141,148, 157	Grob-boden-fraktionen/ Anteils-klassen 148	Summe Skelett (%) 150			
1	0-50	jAh-M	swbn	h4	-	feu 3	-	subpol	-	Ld1	Wg 1 Wf 5	oj-ss (Sgf)	oj	Su2	-	-	-	K	qh
2	50-115	II iC	hoc	-	-	feu 3	-	ein	-	Ld3	Wg 2	fg-ss (Sgf)	fg	Su2	-	-	-	Sgf	qp
3	115+	Go	gelioc	-	eh, fl, f5 ed, bae,	feu 3	-	ein	-	Ld2	-	fg-ss (Sgf)	fg	mSfs	mG 2	3 %	-	Sgf	qp

Bodenform

Bodensystematische Einheit 190	**Substratsystematische Einheit** 132,289,296	
gYK flach vergleyter Kolluvisol	oj-ss (K) / fg-ss (Sgf-qp)	
Humusform 298	Wasserstand u GOF 310	Bemerkungen 320
MU	-	-

Figure B.6 Pedological description of soil profile at SGD_H2.

Aufnahmeformblatt für bodenkundliche Profilaufnahmen nach KA 5

Standort DGD_G1

Titeldaten	TK-Nr.	Projekt	Profil-Nr.	Datum	Bearbeiter	Rechtswert	Hochwert	Höhe über NN	Aufschl.Art / Probenahme 55	Bemerkungen 55
	2325	HUSCO	2	17.11.2010	Sandoval	3562XXX	5941XXX	14,7 m	GS+BP, P	-

Aufnahme-situation	Neigung 57,58	Exposition 59	Wölbung 59	Reliefformtyp 63	Mikrorelief 69	Lage im Relief 69	Bodenab-/-auftrag 69	Nutzungsart 71	Vegetation 73	Witterung 74	anthropogene Veränderungen 74	Bodenorganismen 76	Bemerkungen 79
	N0.1	-	WS0	T	RE	Z	AY	GE	GR	WT3	-	Lu,an	-

Horizontdaten

Nr	Ober-/ Unter grenze 79	Horizont-symbol 83	**Pedogene und biogene Merkmale**							**Merkmale der Substratzusammensetzung**								
			Bodenfarbe 108	Humus-gehalt 110	Hydromor-phie-merkmale 112	Boden-feuchte 114	sonstige Merk-male 114	Gefüge-form und Größe 117,121	Hohl-räume (Risse, Poren Röhren) 123	Lagerungs-dichte Zersetz-ungsstufe 124	Durch-wurzel-ungs-inten-sität 129	Substratart 131,188	Substrat-genese 135	Gesamtbodenart 140			Carbo-nat-gehalt 168	Boden-aus-gangs-gestein 172	Strati-graphie 187
														Boden art/ Torfart 141,148, 157	Grob-boden-fraktionen/ Anteils-klassen 148	Summe Skelett (%) 150			
1	0-15	jAh	dbn	h4	-	feu 3	-	sub-kru	Rre, f3	Ld1	Wf 6	oj-ls (K, Yb)	oj	Sl4	Gr 2	5%	-	K, Yb2	qh
2	15-35	M	orlidbn	h4	-	feu 3	-	sub	Rre, f2	Ld1	Wg 1 Wf 5	oj-ls (K, Yb)	oj	Sl2	Gr 2	5%	-	K, Yb2	qh
3	35-52	II Sw	or	h2	eh, dif, f6	feu 3	-	sub	Rre, f2	Ld3	Wf 2	gm-ll (Lg)	gm	Sl4	fGr 2, mGr 2	8%	-	Lg	qp
4	52-95	Go-Sd	grlioc	h1, bae	eh, bae, f4	feu 3	-	sub	Rre, f2	Ld4	Wg 1 Wf 2	gm-ll (Lg)	gm	Sl4	fGr 2	3%	-	Lg	qp
5	95-130	III Gor	grlioc	h1, bae	eh, bae, f3	feu 4	-	sub	Rre, f1	Ld4	Wf 1	gm-ls (Sg)	gm	Sl3	fG 2	3%	-	Sg	qp
6	130-185	Gr	gr	-	eh, bae, f2	feu 5	-	koh	-	Ld4	-	gm-ls (Mg)	gm	mSfs	fG 2	3%	c4	Mg	qp
7	185+	Gr	buligr	-	eh, bae, f2	feu 5	-	sub	-	Ld 4	-	gm-sl (Mg)	gm	Sl4	-	-	c4	Mg	qp

Bodenform

Bodensystematische Einheit 190	**Substratsystematische Einheit** 132,289,296	
GG-SS Gley-Pseudogley	oj-ls (K, Yb-qh) / gm-ll (Lg-qp) // gm-ls (Mg-qp)	
Humusform 298	Wasserstand u GOF 310	Bemerkungen 320
MU	1,6 m ?	evtl. gespanntes Grundwasser?

Figure B.7 Pedological description of soil profile at DGD_G1.

Aufnahmeformblatt für bodenkundliche Profilaufnahmen nach KA 5

Standort DGD_G2

Titeldaten	TK-Nr.	Projekt	Profil-Nr.	Datum	Bearbeiter	Rechtswert	Hochwert	Höhe über NN	Aufschl.Art / Probenahme 55	Bemerkungen 55
	2325	HUSCO	3	17.11.2010	Sandoval	3562XXX	5941XXX	14,0 m	GS+BP, P	-

Aufnahme-situation	Neigung 57,58	Exposition 59	Wölbung 59	Reliefformtyp 63	Mikrorelief 69	Lage im Relief 69	Bodenab-/ -auftrag 69	Nutzungsart 71	Vegetation 73	Witterung 74	anthropogene Veränderungen 74	Bodenorganismen 76	Bemerkungen 79
	N0.1	-	WS0	T	RH	K	AY	GE	LW/GR	WT3	-	Lu,an	-

Horizontdaten

Nr	Ober-/ Unter grenze 79	Horizont-symbol 83	Pedogene und biogene Merkmale									Merkmale der Substratzusammensetzung							
			Bodenfarbe 108	Humus-gehalt 110	Hydromor-phie-merkmale 112	Boden-feuchte 114	sonstige Merk-male 114	Gefüge-form und Größe 117,121	Hohl-räume (Risse, Poren Röhren) 123	Lagerungs-dichte Zersetz-ungsstufe 124	Durch-wurzel-ungs-intensität 129	Substratart 131,188	Substrat-genese 135	Gesamtbodenart 140			Carbo-nat-gehalt 168	Boden-aus-gangs-gestein 172	Strati-graphie 187
														Boden art/ Torfart 141,148, 157	Grob-boden-fraktionen/ Anteils-klassen 148	Summe Skelett (%) 150			
1	0-15	jAh	dbn	h4	-	feu 3	-	sub	Rre, f2	Ld1	Wf 5	oj-ls (K, Yb)	oj	Sl3	Gr 2	2%	-	K, Yb2	qh
2	15-50	M1	brlioc	h3	eh, fl, f2 rb, fl, f1	feu 2	-	sub	Rre, f2	Ld2	Wf 5	oj-ls (K, Yb)	oj	Sl3	fx 3 Gr 2	25%	-	K, Yb4	qh
3	50-110	M2	dbn	h3	eh, fl, f2	feu 2	-	sub	Rre, f1	Ld1	Wg 2 Wf 3	oj-ls (K, Yb)	oj	Sl3	gGr2	5%	-	K, Yb2	qh
4	110+	II Gro	gr	-	eh, bae, f3	feu 3	-	sub	-	Ld4	Wg 1	gm-ls (Sg)	gm	Sl3	gGr2	3%	c3	Mg	qp

Bodenform

Bodensystematische Einheit 190	**Substratsystematische Einheit** 132,289,296	
KK Kolluvisol	oj-ls (K, Ybz-qh) // gm-ls (Mg-qp)	
Humusform 298	Wasserstand u GOF 310	Bemerkungen 320
MU	-	-

Figure B.8 Pedological description of soil profile at DGD_G2.

Aufnahmeformblatt für bodenkundliche Profilaufnahmen nach KA 5

Standort DGD_G3

Titeldaten	TK-Nr.	Projekt	Profil-Nr.	Datum	Bearbeiter	Rechtswert	Hochwert	Höhe über NN	Aufschl.Art / Probenahme 55	Bemerkungen 55
	2325	HUSCO	8	02.03.11	Sandoval	3562XXX	5941XXX	19,5 m	GS, P	-

Aufnahme-situation	Neigung 57,58	Exposition 59	Wölbung 59	Reliefformtyp 63	Mikrorelief 69	Lage im Relief 69	Bodenab-/-auftrag 69	Nutzungsart 71	Vegetation 73	Witterung 74	anthropogene Veränderungen 74	Bodenorganismen 76	Bemerkungen 79
	N2	NW	WS 2	H	RW	O	AY	F	LW	WT 3	-	Lu	-

Horizontdaten

Nr	Ober-/ Unter grenze 79	Horizont-symbol 83	**Pedogene und biogene Merkmale**								**Merkmale der Substratzusammensetzung**								
			Bodenfarbe 108	Humus-gehalt 110	Hydromor-phie-merkmale 112	Boden-feuchte 114	sonstige Merk-male 114	Gefüge-form und Größe 117,121	Hohl-räume (Risse, Poren Röhren) 123	Lagerungs-dichte Zersetz-ungsstufe 124	Durch-wurzel-ungs-inten-sität 129	Substratart 131,188	Substrat-genese 135	Gesamtbodenart 140			Carbo-nat-gehalt 168	Boden-aus-gangs-gestein 172	Strati-graphie 187
														Boden art/ Torfart 141,148, 157	Grob-boden-fraktionen/ Anteils-klassen 148	Summe Skelett (%) 150			
1	0-25, t	jAh	dbn	h4	-	feu 3	-	subpo l	-	Ld1	Wf 5, Wg 3	oj-ss(Sf)	oj	Sl2	-	-	c0	K	qh
2	25-45	M-yjCv	hgrlibn	h1	-	feu 4	-	subop l	-	Ld3	Wf3, Wg1	oj-(zz2)ss(Sf6	oj	Sl3	mGr 3, gGr 2	15 %	c0	K, Yb2	qh
3	45-65	II eSw	orlioc	-	eh,fl,f3 ed,fl,f1	feu 4	C	kit	-	Ld3	-	oj-(zz2)fl(Mg6	oj	Sl4	mGr3, gGr 2	15 %	c3	K, Yb2	qh
4	65-90	III eSd	gr	-	ed,fl,f1 rg,fl,f3	feu 5	C	kit	-	Ld4	-	gm-(zz2)fl(Mg)	gm	Sl3	mGr1, mG1	2 %	c3	Mg	qp
5	90+	eSwd	gr	-	eh,fl,f3 rg,fl,f3	feu 4	C	kit	-	Ld4	-	gm-(zz2)fl(Mg)	gm	Sl4	mGr1, mG1	2 %	c3	Mg	qp

Bodenform

Bodensystematische Einheit 190	**Substratsystematische Einheit** 132,289,296	
Pseudogley-Pararendzina SS-RZ	oj - ss (K-qh) / oj - (zz2) fl (K,Yb2 - qh) / gm - (zz2) fl (Mg - qp)	
Humusform 298	Wasserstand u GOF 310	Bemerkungen 320
MU	-	-

Figure B.9 Pedological description of soil profile at DGD_G3.

Aufnahmeformblatt für bodenkundliche Profilaufnahmen nach KA 5

Standort DGD_G4

Titeldaten	TK-Nr.	Projekt	Profil-Nr.	Datum	Bearbeiter	Rechtswert	Hochwert	Höhe über NN	Aufschl.Art / Probenahme 55	Bemerkungen 55
	2325	HUSCO	10	03.03.11	Sandoval	3562XXX	5941XXX	15,5	GS, P	-

Aufnahme-situation	Neigung 57,58	Exposition 59	Wölbung 59	Reliefformtyp 63	Mikrorelief 69	Lage im Relief 69	Bodenab-/ -auftrag 69	Nutzungsart 71	Vegetation 73	Witterung 74	anthropogene Veränderungen 74	Bodenorganismen 76	Bemerkungen 79
	N1.2	NE	WS 1	H	RE	M	-	NP	WI	WT 3	-	Lu	-

Horizontdaten

Nr	Ober-/ Unter grenze 79	Horizont-symbol 83	Pedogene und biogene Merkmale									Merkmale der Substratzusammensetzung							
			Bodenfarbe 108	Humus-gehalt 110	Hydromor-phie-merkmale 112	Boden-feuchte 114	sonstige Merk-male 114	Gefüge-form und Größe 117,121	Hohl-räume (Risse, Poren Röhren) 123	Lagerungs-dichte Zersetz-ungsstufe 124	Durch-wurzel-ungs-intensität 129	Substratart 131,188	Substrat-genese 135	Gesamtbodenart 140			Carbo-nat-gehalt 168	Boden-aus-gangs-gestein 172	Strati-graphie 187
														Boden art/ Torfart 141,148, 157	Grob-boden-fraktionen/ Anteils-klassen 148	Summe Skelett (%) 150			
1	0-40, k	jAh-M	dbn	h3	-	feu 2	-	ein	-	Ld1-2	Wf 3, Wg 1	oj-(zz2)ls(Sf6,	oj	mSgs	gGr1, fX2	5 %	c 0	K, Yb1	qh
2	40-50	II Al	hbn	h1	-	feu 2	-	ein	-	Ld2	-	a-ss(sa)	a	gSms	-	-	c 0	Sa	qp
3	50+	lCv-Bbt	hoc	-	-	feu 2	T, bae	ein	-	Ld3	-	a-ss(sa)	a	gSms	-	-	c 0	Sa	qp

Bodenform

Bodensystematische Einheit 190	**Substratsystematische Einheit** 132,289,296	
Bänderparabraunerde LLd	oj - (zz2) ls (K,Yb1-qh) / a - ss (sa-qp)	
Humusform 298	Wasserstand u GOF 310	Bemerkungen 320
MU	-	angelehnt an Gutachten (DBF)

Figure B.10 Pedological description of soil profile at DGD_G4.

Aufnahmeformblatt für bodenkundliche Profilaufnahmen nach KA 5

Standort DGD_H1

Titeldaten	TK-Nr.	Projekt	Profil-Nr.	Datum	Bearbeiter	Rechtswert	Hochwert	Höhe über NN	Aufschl.Art / Probenahme 55	Bemerkungen 55
	2425	HUSCO	1	16.11.2010	Sandoval	3561XXX	5941XXX	19,0 m	GS, P	

Aufnahme-situation	Neigung 57,58	Exposition 59	Wölbung 59	Reliefformtyp 63	Mikrorelief 69	Lage im Relief 69	Bodenab-/-auftrag 69	Nutzungsart 71	Vegetation 73	Witterung 74	anthropogene Veränderungen 74	Bodenorganismen 76	Bemerkungen 79
	N0.1	-	WS0	T	RE	Z	AY	NG	SV	WT3	-	Lu,an	-

Horizontdaten

Nr	Ober-/ Unter grenze 79	Horizont-symbol 83	**Pedogene und biogene Merkmale**								**Merkmale der Substratzusammensetzung**							
			Bodenfarbe 108	Humus-gehalt 110	Hydromor-phie-merkmale 112	Boden-feuchte 114	sonstige Merk-male 114	Gefüge-form und Größe 117,121	Hohl-räume (Risse, Poren Röhren) 123	Lagerungs-dichte Zersetz-ungsstufe 124	Durch-wurzel-ungs-inten-sität 129	Substratart 131,188	Substrat-genese 135	Gesamtbodenart 140			Carbo-nat-gehalt 168	Boden-aus-gangs-gestein 172	Strati-graphie 187
														Boden art/ Torfart 141,148, 157	Grob-boden-fraktionen/ Anteils-klassen 148	Summe Skelett (%) 150			
1	0-20	jAh	grlidbn	h3	-	feu 5	-	sub-kru	-	Ld1	Wf 5	oj-ls (Sf6, Ybz2)	oj	Su2	mGr 2, mG 2	5-10%	c0	K, Ybz2	qh
2	20-40	M	grlibn	h3	-	feu 5	-	sub	-	Ld2	Wf 4	oj-ls (Sf6, Ybz2)	oj	Su2	mGr 2, gGr 2	5-10%	c0	K, Ybz2	qh
3	40-70	II Bv	docbn	h2	-	feu 4	-	sub	-	Ld2	Wf 3	fg-ls (Sf)	fg	Su2	mGr 4, gG 2	30%	c0	Sf	qp
4	70-85	Sw-Bv	hocbn	h1, bae	eh, fl, f1	feu 4	-	ein-sub	-	Ld3	Wf 1	fg-ls (Sf)	fg	Su2	gG 3	15%	c0	Sf	qp
5	85-105	Sw	hocbn	h1, bae	ed, fl, f6	feu 4	-	ein	-	Ld3	Wf 1	fg-ls (Sf)	fg	Su2	G 3	15%	c0	Sf	qp
6	105-160	III Sd	hoc/rolior	-	ed, fl, f4 rg, fl, f4	feu 3	-	sub	-	Ld4	Wf 0	gm-ll (Lg)	gm	Ls3 + Linsen Lts	G 1	1%	c0	Lg	qp

Bodenform

Bodensystematische Einheit 190	**Substratsystematische Einheit** 132,289,296	
sBB-YK pseudovergleyter Braunerde-Kolluvisol	oj-ls (K, Ybz-qh) / fg-ls (Sf-qp) // gm-ll (Lg-qp)	
Humusform 298	Wasserstand u GOF 310	Bemerkungen 320
MU	-	-

Figure B.11 Pedological description of soil profile at DGD_H1.

Aufnahmeformblatt für bodenkundliche Profilaufnahmen nach KA 5

Standort DGD_H2

Titeldaten	TK-Nr.	Projekt	Profil-Nr.	Datum	Bearbeiter	Rechtswert	Hochwert	Höhe über NN	Aufschl.Art / Probenahme 55	Bemerkungen 55
	2325	HUSCO	11	04.03.11	Sandoval	3561XXX	5941XXX	19 m	GS, P	-

Aufnahme-situation	Neigung 57,58	Exposition 59	Wölbung 59	Reliefformtyp 63	Mikrorelief 69	Lage im Relief 69	Bodenab-/ -auftrag 69	Nutzungsart 71	Vegetation 73	Witterung 74	anthropogene Veränderungen 74	Bodenorganismen 76	Bemerkungen 79
	N 0.1	S	WS 0	T	RE	Z	AY	N	SV	WT 3	-	Lu	-

Horizontdaten

Nr	Ober-/ Untergrenze 79	Horizont-symbol 83	Pedogene und biogene Merkmale									Merkmale der Substratzusammensetzung							
			Bodenfarbe 108	Humus-gehalt 110	Hydromorphie-merkmale 112	Boden-feuchte 114	sonstige Merk-male 114	Gefüge-form und Größe 117,121	Hohl-räume (Risse, Poren Röhren) 123	Lagerungs-dichte Zersetz-ungsstufe 124	Durch-wurzel-ungs-intensität 129	Substratart 131,188	Substrat-genese 135	Gesamtbodenart 140			Carbo-nat-gehalt 168	Boden-aus-gangs-gestein 172	Strati-graphie 187
														Boden art/ Torfart 141,148, 157	Grob-boden-fraktionen/ Anteils-klassen 148	Summe Skelett (%) 150			
1	0-15, z	jAeh	swbn	h4	-	feu 3	-	subpol	-	Ld1	Wf2	oj-ls(Sf)	oj	mSgs	-	-	-	K	qh
2	15-55	M-Sw	gr +hgr(fl) +dgr(fl)	h2	eh,fl,f2	feu 4	-	kit	-	Ld4	-	oj-(zz3)tl(Lg6,	oj	Sl2	mGr 3	10 %	-	K, Ybz 2	qh
3	55-110	II Sd	rolioc	-	ed,fl,f3 rg,fl,f3	feu 4	-	kit	-	Ld5	-	gm-(zz2)ll(Lg)	gm	Ls4	mGr 2	5 %	-	Lg	qp
4	110+	III ilC	hoc	-	ed,fl,f1	feu 3	-	ein	-	Ld2	-	fg-ss(Sgf)	fg	Su2	-	-	-	Sgf	qp

Bodenform

Bodensystematische Einheit 190	**Substratsystematische Einheit** 132,289,296	
Pseudogley-Kolluvisol SS-YK	oj - ls (K - qh) / oj - (zz3) tl (K,Ybz2 - qh) / gm - (zz2) ll (Lg - qp) //fg - ss(Sgf -qp)	
Humusform 298	Wasserstand u GOF 310	Bemerkungen 320
MU	-	Schutt evtl. von Kleingartenkolonie

Figure B.12 Pedological description of soil profile at DGD_H2.

Table B.1a) Laboratory analysis results for disturbed soil samples of SGD sites. pH measured in $CaCl_2$, el. cond. = electrical conductivity, C/N = ratio of carbon and nitrogen, C = total content of carbon.

profile	depth [cm]	pH	el. cond. [µS]	C/N	C [%]
SGD_G1	5	4.2	106	14.2	14.9
	10	4.0	60	14.9	10.1
	40	4.0	68	19.6	5.0
SGD_G2	5	4.3	86	16.7	8.8
	10	4.4	83	17.4	11.3
	40	4.9	70	17.8	4.9
SGD_G3	5	4.6	63	12.5	3.1
	10	4.3	32	12.7	2.1
	40	5.1	19	14.9	0.4
	80	4.5	26	15.3	0.4
SGD_G4	5	4.8	64	13.4	3.8
	10	4.6	48	14.0	3.6
	40	4.9	26	15.8	2.0
	80	5.3	14	17.4	0.1
SGD_H1	5	5.2	30	18.3	4.7
	10	5.2	28	21.2	5.7
	40	4.5	21	23.1	5.9
	80	4.2	12	22.4	0.6
	160	4.6	6	77.6	0.1
SGD_H2	5	5.3	23	16.6	4.6
	10	5.5	24	18.4	4.7
	40	5.8	22	21.5	3.1
	80	6.0	11	19.8	0.2
	160	5.5	6	23.7	0.1

Table B.1b) Laboratory analysis results for disturbed soil samples of DGD sites. pH measured in CaCl2, el. cond. = electrical conductivity, C/N = ratio of carbon and nitrogen, C = total content of carbon.

profile	depth [cm]	pH	el. cond. [µS]	C/N	C [%]
DGD_G1	5	5.1	57	11.4	6.2
	10	5.3	57	10.7	4.5
	40	5.9	27	11.9	0.8
	80	6.0	17	9.9	0.1
	160	7.2	22	11.9	0.0
DGD_G2	5	5.3	62	14.2	3.5
	10	5.2	38	14.1	1.9
	40	7.0	125	16.9	1.9
	80	5.4	42	10.4	2.3
	160	7.3	71	16.0	0.3
DGD_G3	5	5.5	93	12.0	4.0
	10	5.4	82	12.1	3.8
	40	7.5	123	21.5	1.3
	80	7.7	316	95.1	1.6
DGD_G4	5	4.4	60	13.2	3.7
	10	4.4	28	12.4	2.0
	40	4.7	16	13.5	0.8
	80	4.8	9	13.4	0.1
	160	5.0	10	14.8	0.1
DGD_H1	5	4.4	26	14.1	2.4
	10	4.6	30	14.4	2.4
	40	3.9	18	12.7	1.2
	80	4.4	13	11.5	0.3
	160	4.0	38	6.0	0.1
DGD_H2	5	4.6	73	16.8	5.7
	10	4.4	60	20.5	5.0
	40	6.4	37	13.0	0.7
	80	5.4	53	7.0	0.2
	160	5.7	17	8.8	0.0

Table B.2a) Laboratory analysis results for disturbed and undisturbed soil samples of SGD sites. Particle size distribution, as determined with Köhn analysis method. Pore size distribution, as determined with drainage branch of retention curve.

profile	depth [cm]	clay [%]	silt [%]	sand [%]	macro pores (> 10 µm)	medium-sized pores (10 µm - 0.2 µm) [%]	micro pores (< 0.2 µm) [%]
SGD_G1	5	10.13	20.68	69.20	25.32	17.93	26.25
	10	8.33	20.73	70.91	20.28	31.80	18.32
	40	7.45	58.84	33.75	17.54	32.56	15.70
SGD_G2	5	5.72	26.28	67.94	13.46	33.98	21.96
	10	6.71	25.16	68.08	17.47	18.71	29.62
	40	6.32	43.49	50.14	16.24	45.77	10.99
SGD_G3	5	2.56	4.10	93.33	30.64	20.40	7.36
	10	2.43	4.63	92.91	26.93	11.80	6.67
	40	2.13	7.87	90.04	31.72	5.80	2.98
	80	2.10	8.00	89.89	26.34	8.92	3.64
SGD_G4	5	6.12	12.72	81.12	28.18	20.31	10.42
	10	3.78	11.24	84.95	28.91	16.83	11.06
	40	2.85	5.95	91.18	16.06	24.59	7.05
	80	0.97	1.46	97.53	28.95	10.49	1.75
SGD_H1	5	2.60	10.60	86.77	27.46	14.93	12.31
	10	2.85	9.92	87.25	30.01	16.65	9.35
	40	2.48	10.86	86.69	22.53	19.12	13.05
	80	3.50	10.06	86.46	31.80	3.48	3.61
	160	0.23	1.23	98.53	31.55	5.11	0.54
SGD_H2	5	5.33	12.54	82.09	22.24	19.89	13.37
	10	3.15	10.67	86.13	30.44	12.88	12.08
	40	3.66	14.42	81.97	38.90	9.33	7.97
	80	2.69	11.96	85.35	28.61	6.65	3.04
	160	0.97	1.21	97.85	35.60	4.48	1.93

Table B.2b) Laboratory analysis results for disturbed and undisturbed soil samples of DGD sites. Particle size distribution, as determined with Köhn analysis method. Pore size distribution, as determined with drainage branch of retention curve ('-' = no valuable data).

profile	depth [cm]	clay [%]	silt [%]	sand [%]	macro pores (> 10 µm) [%]	medium-sized pores (10 µm - 0.2 µm) [%]	micro pores (< 0.2 µm) [%]
DGD_G1	5	12.23	17.06	70.69	27.65	27.44	13.11
	10	12.87	16.90	70.21	13.18	23.63	17.99
	40	19.01	16.60	64.42	6.46	10.59	20.75
	80	12.30	20.10	67.60	8.99	2.58	19.34
	160	1.98	2.69	95.31	7.60	18.29	2.01
DGD_G2	5	9.40	16.08	74.54	17.61	23.84	13.15
	10	10.65	17.80	71.55	14.53	14.56	12.31
	40	11.56	15.98	72.49	20.73	10.77	12.40
	80	11.73	16.69	71.58	26.78	11.31	12.92
	160	10.37	16.56	73.11	8.70	9.54	9.26
DGD_G3	5	6.68	13.11	80.21	16.62	26.97	14.80
	10	9.31	14.88	75.80	21.66	23.21	12.83
	40	9.10	19.30	71.58	11.76	7.80	19.43
	80	19.98	30.23	50.81	10.75	1.99	20.06
DGD_G4	5	3.42	4.37	92.98	28.18	22.08	9.04
	10	9.51	17.74	72.77	35.44	13.60	7.16
	40	4.76	7.07	88.15	27.18	9.74	5.18
	80	2.09	1.21	96.73	34.40	3.94	2.25
	160	2.10	1.73	96.13	42.83	2.86	2.00
DGD_H1	5	5.47	17.48	77.11	18.08	16.81	12.81
	10	6.31	18.73	74.92	21.71	14.89	12.20
	40	7.10	17.08	75.79	27.33	9.01	9.57
	80	3.46	16.68	79.84	27.13	6.37	6.50
	160	20.39	31.35	48.28	5.29	2.75	28.26
DGD_H2	5	4.54	9.15	86.33	17.90	18.29	17.21
	10	5.09	10.38	84.57	24.51	13.27	16.52
	40	6.35	17.13	76.52	18.32	4.81	13.38
	80	27.73	28.71	43.56	-	-	-
	160	3.39	10.43	86.20	32.80	10.90	4.40

Appendix C - Water retention curves

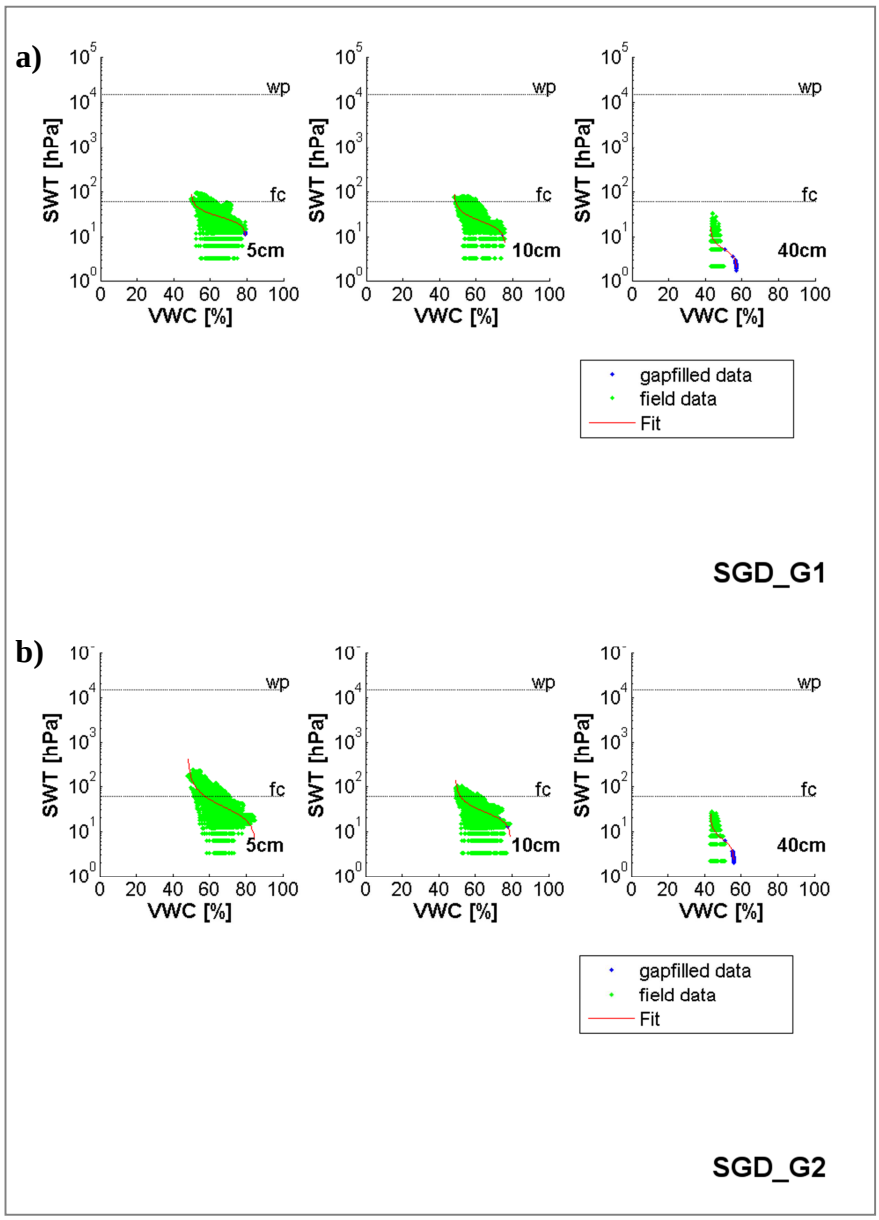

Figure C.1 Water retention curves of field data of 2011 and 2012 and fitted (van Genuchten, 1980) curve for all SoilStation profiles, incl. reconstructed soil water tension (*SWT*) data (missing data up to 850 hPa, blue data points). (*VWC* = volumetric water content, wp = permanent wilting point, fc = field capacity) **a)** SGD_G1, **b)** SGD_G2.

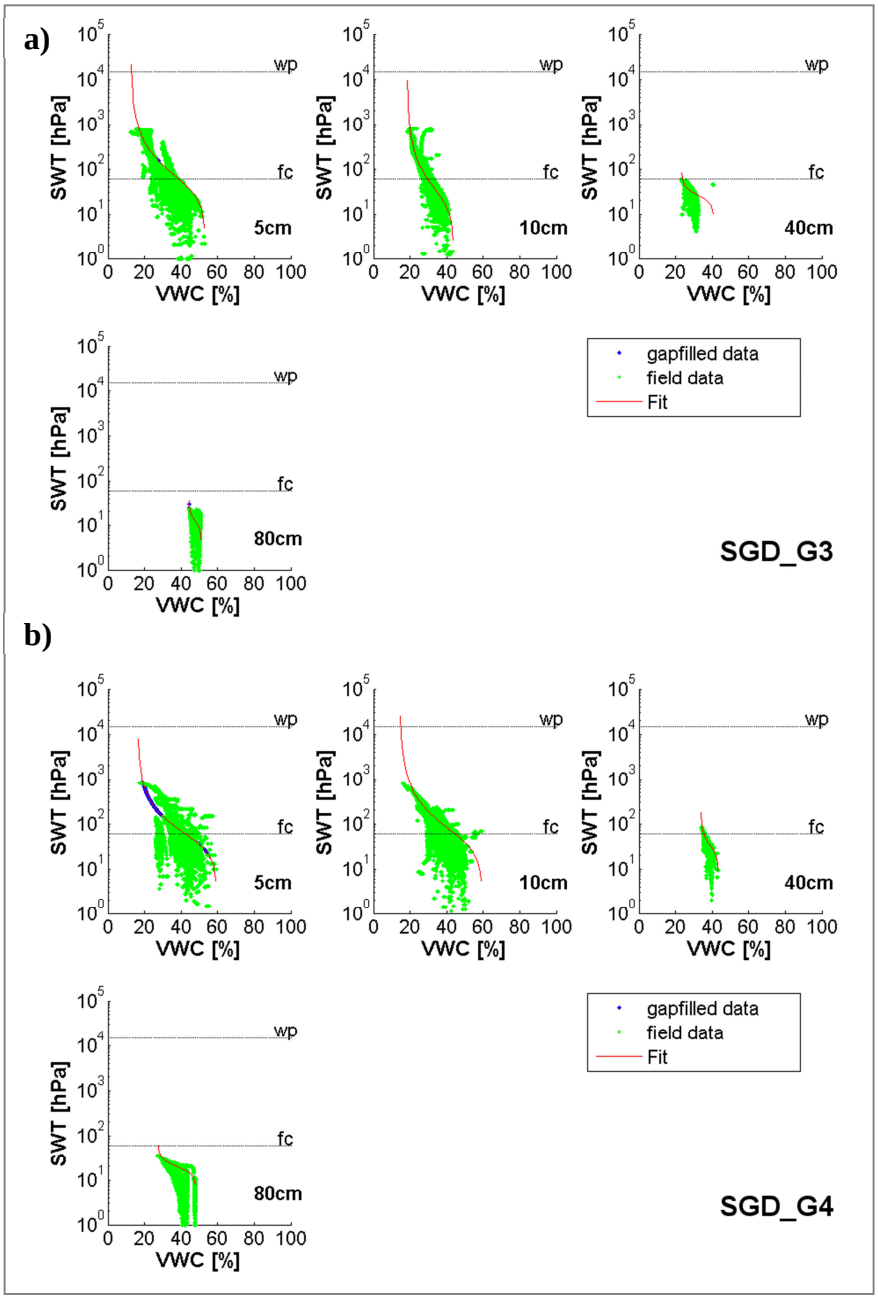

Figure C.2 Water retention curves of field data of 2011 and 2012 and fitted (van Genuchten, 1980) curve for all SoilStation profiles, incl. reconstructed soil water tension (*SWT*) data (missing data up to 850 hPa, blue data points). (*VWC* = volumetric water content, wp = permanent wilting point, fc = field capacity) **a)** SGD_G3, **b)** SGD_G4.

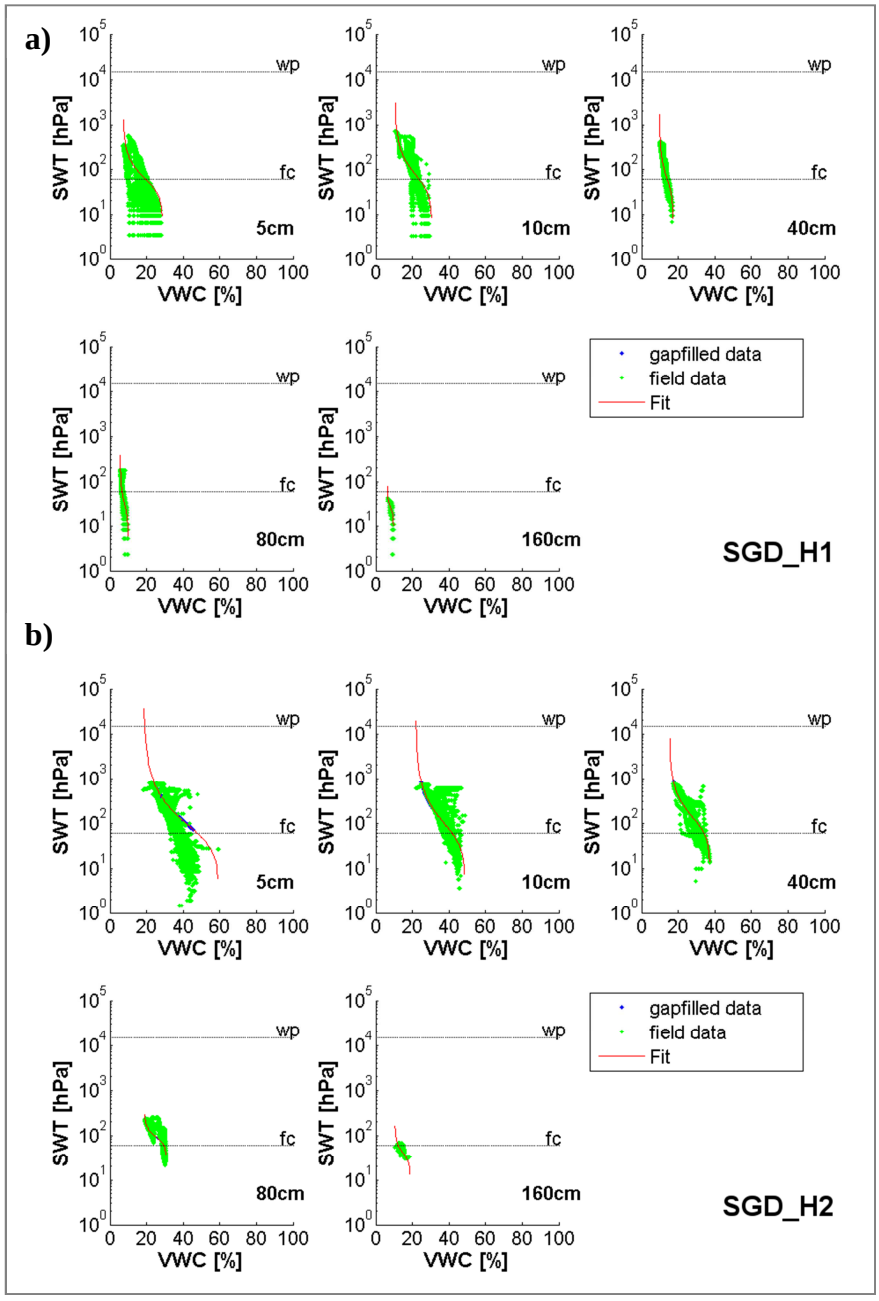

Figure C.3 Water retention curves of field data of 2011 and 2012 and fitted (van Genuchten, 1980) curve for all SoilStation profiles, incl. reconstructed soil water tension (*SWT*) data (missing data up to 850 hPa, blue data points). (*VWC* = volumetric water content, wp = permanent wilting point, fc = field capacity) **a)** SGD_H1, **b)** SGD_H2.

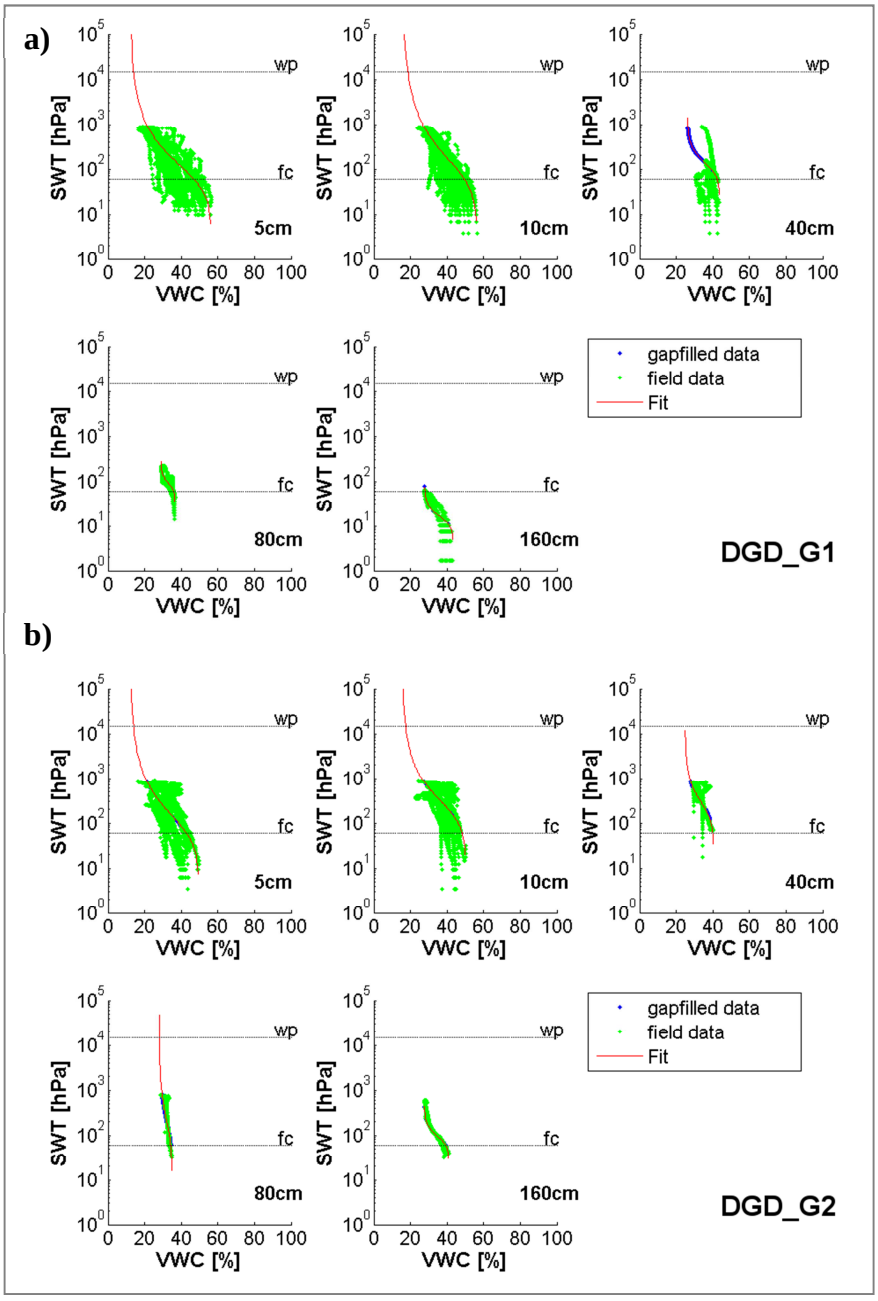

Figure C.4 Water retention curves of field data of 2011 and 2012 and fitted (van Genuchten, 1980) curve for all SoilStation profiles, incl. reconstructed soil water tension (*SWT*) data (missing data up to 850 hPa, blue data points). (*VWC* = volumetric water content, wp = permanent wilting point, fc = field capacity) **a)** DGD_G1, **b)** DGD_G2.

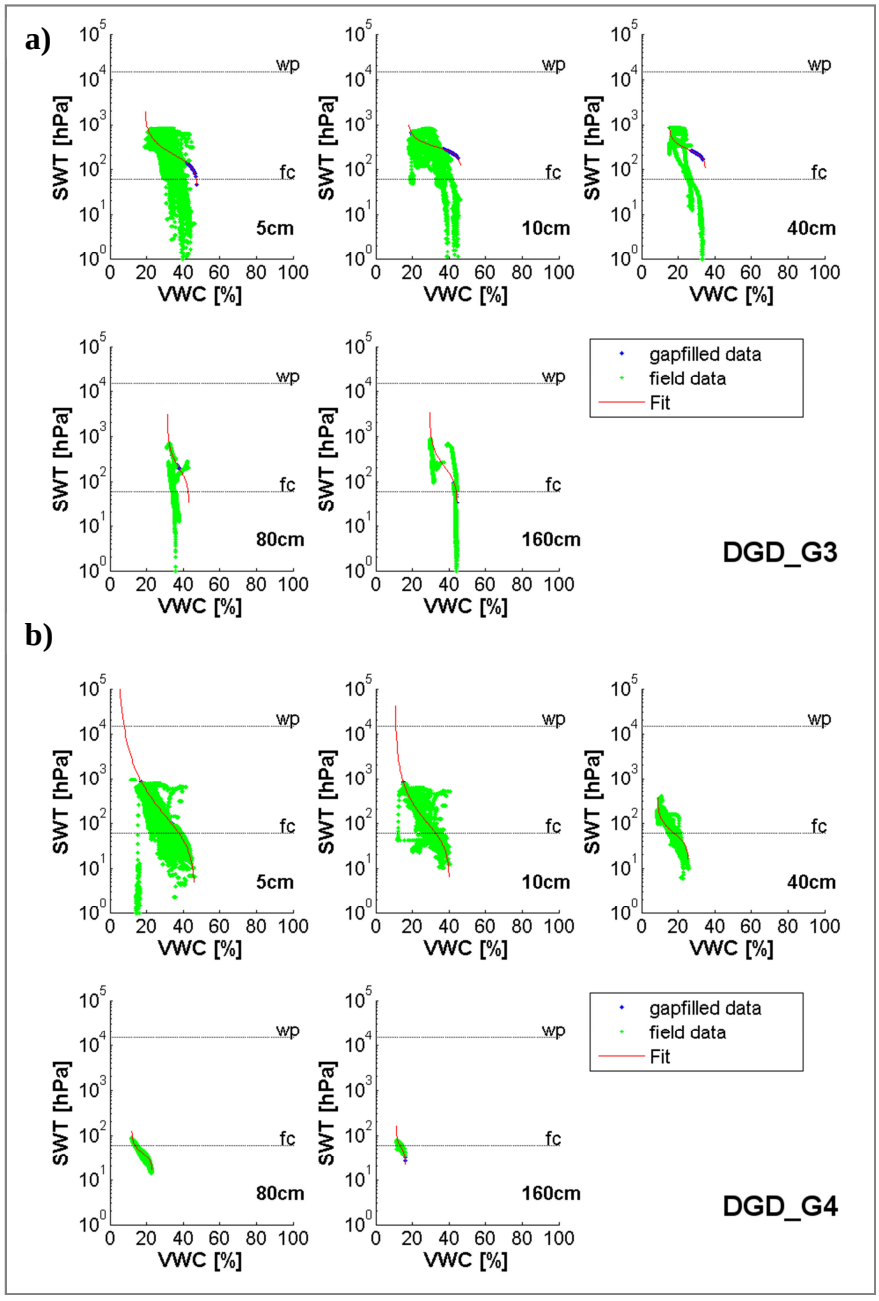

Figure C.5 Water retention curves of field data of 2011 and 2012 and fitted (van Genuchten, 1980) curve for all SoilStation profiles, incl. reconstructed soil water tension (*SWT*) data (missing data up to 850 hPa, blue data points). (*VWC* = volumetric water content, wp = permanent wilting point, fc = field capacity) **a)** DGD_G3, **b)** DGD_G4.

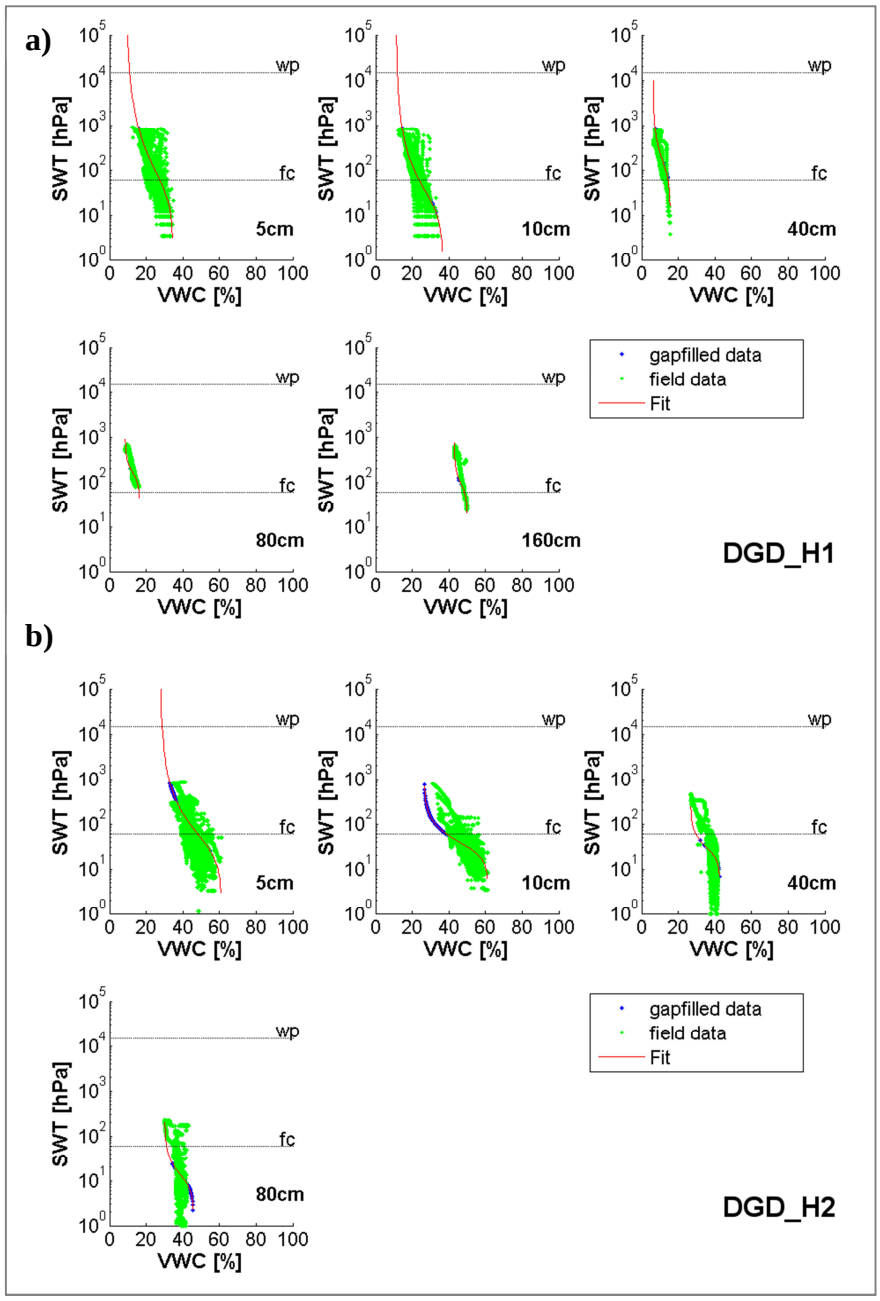

Figure C.6 Water retention curves of field data of 2011 and 2012 and fitted (van Genuchten, 1980) curve for all SoilStation profiles, incl. reconstructed soil water tension (*SWT*) data (missing data up to 850 hPa, blue data points). (*VWC* = volumetric water content, wp = permanent wilting point, fc = field capacity) **a)** DGD_H1, **b)** DGD_H2.

Acknowledgement

This work would not have been possible without the support of several individuals who contributed in different ways:

Foremost, my advisors Prof. Dr. Annette Eschenbach and Prof. Dr. Felix Ament continuously guided me during my Ph.D. study and research. They provided valuable support not only with their knowledge, but also with their patience, motivation and enthusiasm. Prof. Dr. Lars Kutzbach and Dr. Alexander Gröngröft shared plenty of ideas and were great help during in-depth discussions. The extensive laboratory and field work would not have been that successful without the support of the laboratory assistants, technicians and engineers of the Institute of Soil Science and the Meteorological Institute's Elektroniklabor. The collection of the enormous amount of data was only possible with the work and assistance of several student research assistants. The working groups "Synthesis of Observations and Models", "Soil Protection and Soil Technology" and "Regional Hydrology in Terrestrial Systems" gave food for thought concerning technical and scientific issues and the collaboration with the CliSAP research unit D4 members was certainly productive.

As a member of the graduate school SICSS I benefited from numerous educational courses and an excellent research network. The Chair of my Advisory Panel Dr. Stephan Bakan accompanied and encouraged the progression of my Ph.D. work.

The data used in this study were collected within the project Hamburg Urban Soil Climate Observatory (HUSCO). The project is supported through the Cluster of Excellence 'CliSAP' (EXC177), University of Hamburg, funded through the German Science Foundation (DFG). Furthermore, financial support was granted by the Freie und Hansestadt Hamburg, Leitstelle Klimaschutz. Several landowners allowed us to deploy and run our measurements stations on their ground: Hagenbecks Tierpark, Vattenfall Europe Wärme AG, HafenCity Hamburg GmbH, ISUF e.V., Nord-IMMO Management GmbH & Co. KG, DFMG Deutsche Funkturm GmbH, the Gymnasium Albrecht Thaer and the city of Hamburg (Bezirksamt Eimsbüttel and Hamburg-Nord), and the Thoms, Hansen and Hurtig families. Additional data was provided by the German Meteorological Service (DWD), Hamburger Wasserwerke GmbH and Behörde für Stadtentwicklung und Umwelt, Abteilung Bodenschutz/Altlasten and Gewässerschutz.

Aside from the working environment, my parents supported me in every imaginable way. My husband Christian deserves the utmost appreciation for his untiring patience and encouragement.

Thank you.

Declaration on oath

I hereby declare, on oath, that I have written the present dissertation by my own and have not used other than the acknowledged resources and aids.

Hamburg, March 2013

(Sarah Wiesner)